

https://dspace.org/

Inhibition of MCF-7 cell-line proliferation using broadband electric fields

Malan, Keagan Ryan

2018

https://hdl.handle.net/10539/26371

Malan, Keagan Ryan (2018) Inhibition of MCF-7 cell-line proliferation using broadband electric fields, University of the Witwatersrand, Johannesburg, https://hdl.handle.net/10539/26371

Downloaded from a DSpace repository. https://dspace.org/



UNIVERSITY OF THE
WITWATERSRAND,
JOHANNESBURG

INHIBITION OF MCF-7 CELL-LINE PROLIFERATION USING BROADBAND ELECTRIC FIELDS

Keagan Ryan Malan

A dissertation submitted to the Faculty of Engineering and the Built Environment, University of the Witwatersrand, in fulfilment of the requirements for the degree of Master of Science in Engineering.

Johannesburg, 2018

Declaration

I declare that this dissertation is my own work. It is being submitted for the degree of Master of Science in Engineering to the University of the Witwatersrand, Johannesburg. It has not been submitted before for any degree or examination to any other university.

_____

Keagan Ryan Malan

_____ day of _____ year _____

day *month* *year*

Abstract

The aim of this research was to determine whether the efficacy of Tumour Treating Field therapy could be improved using broadband electric fields instead of the single-frequency treatment currently being used. A customised, low-impedance experimental set-up was designed, simulated, constructed and used to deliver the broadband electric fields to cultured cells from the MCF-7 cell-line in an *in vitro* environment. The experimental set-up used a Nunc Lab-Tek Chamber Slide system that had been adapted using four 3D-printed parts and a customised gasket. Enamelled copper wires with bare diameters of 0.100 mm were used to deliver the electric fields in cell cultures containing both two wires and eight wires. Each wire was located 1 mm away from adjacent wires in the cell culture. The simulations were performed using FEKO and showed that a 2 V excitation placed on adjacent wires resulted in a minimum electric field intensity of approximately 4 V/cm between the wires. This matched analytical predictions within 36 %. Treatment was performed for 24 hours and the results were quantified with a resazurin-based dye assay. The results showed that, with the voltages used, there were no significant and repeatable differences between the broadband treatment and the optimal single-frequency treatment. However, as the results from both of these treatments were similar to those of the untreated controls, it is suspected that the voltages used were too low to generate the electric field intensities required to inhibit the proliferation of the MCF-7 cells. Future work can be done in repeating these experiments using higher voltages, in repeating them for other cell-lines, and in characterising the frequencies of sensitivity for other cell-lines and their non-cancerous counterparts.

Acknowledgements

I would like to thank the National Research Foundation of South Africa (NRF) and the German Academic Exchange Service (DAAD) for funding this research with the DAAD-NRF Joint Scholarship Program (reference: SFH14071977385 and SFD13071621692). The research performed would not have been possible without this funding.

I would also like to extend my gratitude to my supervisors Professor David Rubin, Professor Michiel Postema and Doctor Marietha Nel, who never gave up on me and, in their diversity, provided the guidance and assistance needed to conduct this cross-discipline research. A special mention must be made of Doctor Marietha Nel whom I got to work with closely in the laboratory and who, after countless failed experiments, was a beacon of light and inspiration in times of deep disillusionment.

I owe my thanks too to my current employer, Doctor Dirk Koekemoer from eMoyo, for granting me the leave I required to finish this research and for allowing me to print out my prototypes on the company's 3D printer. This really helped move the research forward at the required pace and reminded me of how fortunate I am to have an employer that cares so much about his employees.

Throughout my academic career, my parents and siblings have been extremely supportive and they too deserve my thanks. Jacques, Brenda, Jason and Amy, I am indebted to you and would never have been exposed to the opportunities that came my way without your continued input, love and support.

Lastly, I would like to thank my girlfriend, Kirsten, for keeping me sane and for looking after me during the final stages of the research, when I needed it most.

Contents

1 Introduction and Problem Description **1**

1.1 Introduction 1

1.1.1 Cancer statistics and predictions 1

1.1.2 Cancer treatment 2

1.2 Problem description 2

1.2.1 Aim of the research 4

1.2.2 Research question 4

1.2.3 Research objectives 4

1.2.4 Organisation of the dissertation 5

2 Background **6**

2.1 Tumour Treating Fields 6

2.1.1 Fundamentals 6

2.1.2 Mechanisms of action 6

2.1.3 Frequency dependence 8

2.1.4 Mitotic axis alignment 10

2.1.5 Broadband extension 11

2.2 Broadband signals 11

2.2.1 Summing two sinusoids . . . 12
2.2.2 Summing many sinusoids . . . 13
2.2.3 Discreet sinusoids . . . 14
2.2.4 Methods of generating broadband signals . . . 16
2.3 Biological experiments . . . 16
2.3.1 Cell-lines . . . 17
2.4 Spectrophotometry . . . 17
2.4.1 Beer's Law . . . 18
2.4.2 Cell proliferation assays . . . 19

3 Electric Field Theory **21**
3.1 Electromagnetic fundamentals . . . 21
3.2 Quasistatics . . . 23
3.3 Dielectrics . . . 25
3.3.1 Fundamentals . . . 25
3.3.2 Lossy dielectrics . . . 27
3.4 Electric field produced by a wire . . . 28

4 Design **30**
4.1 Design of culture plate . . . 30
4.1.1 Important design inputs . . . 30
4.1.1.1 Overview . . . 30
4.1.1.2 Explanations . . . 31
4.1.2 Design overview . . . 32
4.1.2.1 Culture surface . . . 32

4.1.2.2 Electrodes . . . 32
4.1.2.3 Well-structure . . . 33
4.1.3 Chosen design . . . 34
4.2 Design of jig to seal the culture plate . . . 35
4.2.1 Wire Guider . . . 36
4.2.2 Slide Platform . . . 37
4.2.3 Clamp Brace . . . 37
4.2.4 Lid Spacer . . . 38
4.3 Design of quantification technique . . . 39
4.3.1 Choice of cell-line . . . 39
4.3.2 Choice of quantification technique . . . 40
4.3.2.1 Alamar Blue identified as resazurin . . . 40
4.3.2.2 Resazurin concentration for MCF-7 growth . . . 41

5 Simulations **43**

5.1 Simulation details . . . 43
5.1.1 Software package and solver settings . . . 43
5.1.2 Geometry . . . 43
5.1.3 Materials . . . 45
5.1.4 Excitations . . . 46
5.1.5 Near-field request . . . 46
5.2 Simulation results . . . 47
5.2.1 Two wires . . . 47
5.2.2 Eight wires . . . 47
5.3 Comparison with analytical predictions . . . 48
5.3.1 Analytical predictions . . . 48
5.3.2 Comparison . . . 50

6 Methodology **56**

6.1 Preparation for experiments 56

6.1.1 3D printed jig 56

6.1.2 Customised gasket 56

6.1.3 Threading of wires 58

6.1.4 Clamping and sealing 58

6.1.5 Sterilisation 60

6.1.6 Cell culture technique 61

6.1.7 Cell proliferation dye preparation 62

6.1.8 Creation and loading of broadband signal 63

6.2 Experimental procedure 66

6.3 Quantification of results 66

7 Results **71**

7.1 Nomenclature 71

7.2 Sets of results 72

7.2.1 Positive controls 72

7.2.2 Multiple pairs of wires 73

7.2.3 Broadband treatment 73

7.3 Summary and analysis 75

8 Ultrasound **80**

8.1 Introduction 80

8.2 Preliminary experiments 81

8.3 Preliminary results 84

8.4 Discussion 84

9 Discussion **85**

9.1 Research aim and objectives 85

9.2 Complications with the experimental set-up 86

9.3 Scrutiny of the methodology and results 87

9.4 Extensions 88

10 Conclusions and Future Work **90**

10.1 Conclusions 90

10.2 Recommendations for future work 90

List of Figures

1.2.1 Sensitivity distribution of cells and cell populations. 3

1.2.2 Treatment of the cancerous cell population. 4

2.1.1 Behaviour of dipoles in electric fields. 8

2.1.2 Alignment of tubulin subunits in an electric field. 9

2.1.3 Converging of tubulin subunits towards a higher electric field density. 9

2.2.1 Superposition of two closely-spaced sinusoids (initially in-phase). 12

2.2.2 Superposition of two closely-spaced sinusoids (initially out-of-phase). 13

2.2.3 Summation of 100 sinusoids (all in-phase at $t = 0$). 15

4.1.1 Nunc Lab-Tek Chamber Slide. 34

4.2.1 Wire Guider. 36

4.2.2 Slide Platform. 37

4.2.3 Clamp Brace. 38

4.2.4 Lid Spacer. 39

5.1.1 Geometry used for the 2-wire simulations. 44

5.1.2 Geometry used for the 8-wire simulations. 44

5.1.3 Close-up of the wire geometry. 45

5.2.1 Simulation results for a single pair of insulated wires in culture medium. . . 48

5.2.2 Simulation results for a single pair of insulated wires in culture medium (axes adapted). 49

5.2.3 Simulation results for a single pair of insulated wires in culture medium (axes further adapted). 50

5.2.4 Simulation results for four pairs of insulated wires in culture medium. . . . 51

5.2.5 Simulation results for four pairs of insulated wires in culture medium (axes adapted). 52

5.2.6 Simulation results for four pairs of insulated wires in culture medium (axes further adapted). 53

5.3.1 Analytical predictions for electric field intensity and electric potential. . . . 54

5.3.2 Analytical predictions for the electric field intensity (axes adapted). 55

6.1.1 3D-printed parts. From left to right: Slide Platform, Wire Guider, Clamp Brace and Lid Spacer. 57

6.1.2 Customised gasket (left) next to original gasket (right). 57

6.1.3 Threaded wires for a 8-wire set-up (left) and a 2-wire set-up (right). 59

6.1.4 Sealed assembly. 60

6.1.5 Wires visible in the sealed assembly. 61

6.1.6 Time-domain of the broadband signal. 63

6.1.7 Single-sided FFT of the broadband signal. 64

6.1.8 Power spectral density of the broadband signal. 65

6.2.1 Laboratory set-up. 67

6.2.2 Inside of the incubator. 67

6.3.1 Sealed assembly. 68

6.3.2 96-well plate with aliquots. 69

6.3.3 The spectrophotometer that was used. 70

7.2.1 Reduction of the dye for the positive controls, where greater deviations between controls are evident for Experiment Set 2 when compared with Experiment Set 1. 72

7.2.2 Normalised inhibition of proliferation for the positive controls, where Experiment Set 2 shows large uncertainties and large deviations between the various controls. 73

7.2.3 Reduction of the dye in the test comparing the efficacies of treatment using 2 wires and 8 wires, where Experiment Set 1 shows very similar reductions but Experiment Set 2 shows a lowered reduction for the 8-wire treatment. . . . 74

7.2.4 Normalised inhibition of proliferation for the cells undergoing treatment using 2 wires and 8 wires. The 2-wire treatment for Experiment Set 2 appears to stimulate cell proliferation instead of inhibiting it. 74

7.2.5 Reduction of the dye in the test comparing the efficacies of single-frequency treatment and broadband treatment. The experiment sets display opposite trends with Experiment Set 2 showing an increase in reduction for the broadband treatment. 75

7.2.6 Normalised inhibition of proliferation for the cells undergoing single-frequency treatment and broadband treatment. The broadband treatment in Experiment Set 2 appears to be stimulating cell proliferation instead of inhibiting it. 75

7.3.1 Percent reduction data showing large uncertainties in both experiment sets. 76

7.3.2 Normalised inhibition of proliferation data showing large uncertainties and no convincing trends between experiment sets. 76

8.2.1 Transducer clamped to the underside of a 24-well cell culture plate. 81

8.2.2 Ultrasonic treatment set-up with clamped transducers. 82

8.2.3 Ultrasonic treatment set-up in a water-bath. 83

List of Tables

2.1 Phases of clinical human trials. 17

4.1 Comparison of ideal insulated and uninsulated electrodes. 33

4.2 Details of Nunc Lab-Tek Chamber Slides. 34

4.3 Wire parameters. 35

5.1 Geometry used for the simulations. 45

5.2 Materials used in the simulations. 45

5.3 Excitations used in the simulations. 46

5.4 Number of points in the near-field request. 46

6.1 Parameters of the broadband signal. 64

7.1 Percent reduction data showing large uncertainties for the two experiment sets. 77

7.2 Normalised inhibition of proliferation data showing large uncertainties for the two experiment sets. 78

7.3 Welch's t-tests performed on Experiment Set 1, showing a significant difference between broadband versus single-frequency treatment. 78

7.4 Welch's t-tests performed on Experiment Set 2, showing no significant difference between any of the comparisons. 78

Chapter 1

Introduction and Problem Description

1.1 Introduction

1.1.1 Cancer statistics and predictions

Cancer is a ubiquitous problem in society, crossing all racial, cultural, social and economic boundaries. In 2015 it was estimated to be responsible for 8.8 million deaths, making it the second leading cause of death due to non-communicable diseases, trumped only by cardiovascular diseases which resulted in an estimated 17.9 million deaths [1]. In 2030, cancer mortalities are expected to reach 11.5 million, accounting for more than 5 % of the total estimated deaths [2].

The prevalence and incidence data are also cause for concern: in 2015 it was estimated that there were 90.5 million people living with cancer, of whom 18.6 million were new cases for that year [3]. Assuming a global population of 7.3 billion at the time that the data was collected, this translates to a prevalence of 1240 cases/100 000 people and an incidence of 255 cases/100 000 people. The number of new cases each year already exceeds the predictions for 2020 which were estimated to be 16.5 million by Bray and Møller [4] and 15.5 million by Mathers and Loncar [2].

The age-standardised death rate of cancer is decreasing (down by 10 % between 2005 and 2015) [1] resulting in an increasing age-specific rate of prevalence (up by 12.4 % between 2005 and 2015) [3]. This indicates that people are living longer with the disease, which is a testament to the advancements made in the field of cancer treatment.

1.1.2 Cancer treatment

The conventional forms of cancer treatment have many drawbacks such as severe side-effects and the radiation of healthy tissue. Although much research has been performed in developing methods to reduce the severity of the adverse effects and to mitigate the risks, there is great potential in the development of other forms of treatment that do not have these inherent problems.

Treatment using Tumour Treating Fields (TTFs) shows promise in certain tumours where it has similar efficacy to chemotherapy treatment, but with the patient experiencing a better quality-of-life [5, 6]. Additionally, when used in conjunction with chemotherapy, TTF treatment has been shown to increase the efficacy and sensitivity of the chemotherapy without any additional toxicity [7].

The TTFs used are low-intensity (1–3 V/cm), intermediate frequency (100–300 kHz), alternating electric fields which were given their name after the discovery that they disrupt specific processes in the cell-division cycle and lead to an inhibitory effect on the proliferation of tumour cells [8].

1.2 Problem description

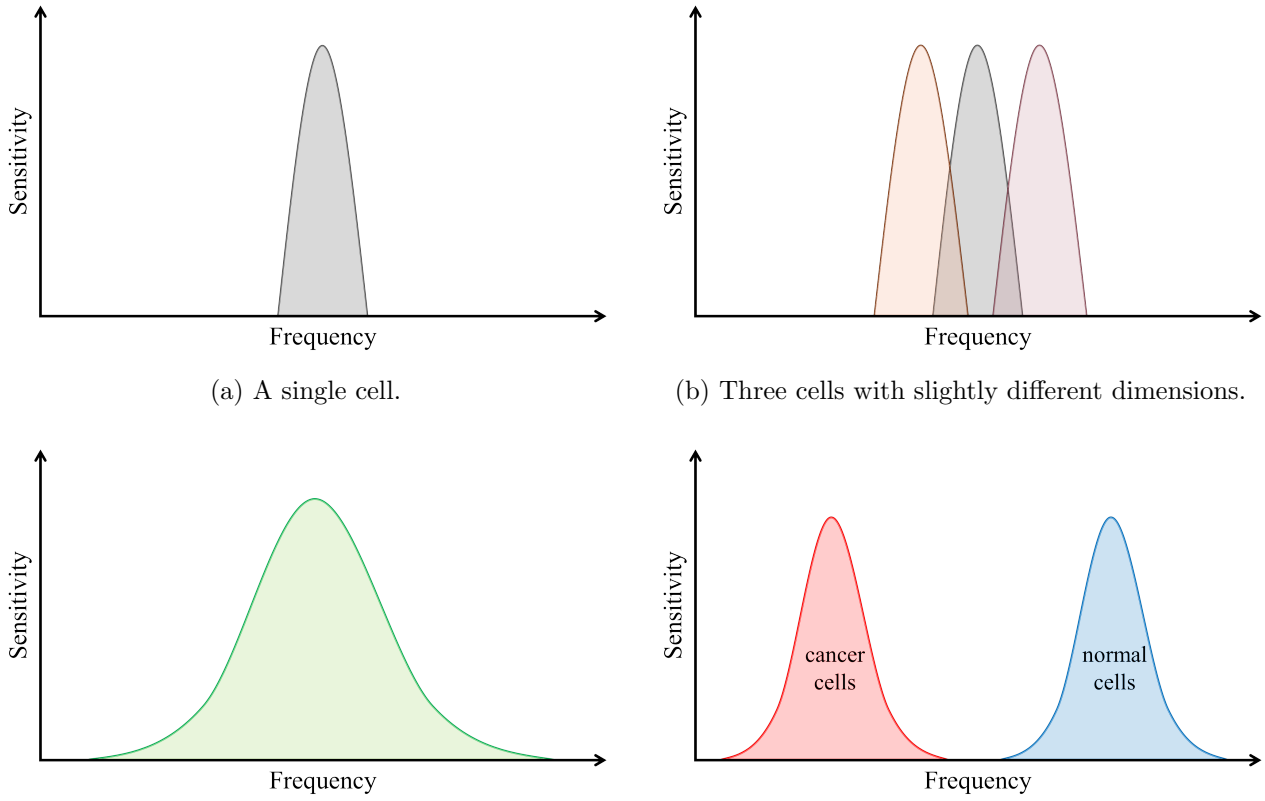
Given the burden that cancer places on both patients and the medical system, there is a need to develop efficient and effective treatment modalities to combat this disease. In particular, treatment must:

- Be able to discriminate between tissues
- Be able to discriminate between normal and cancerous cells of the same tissue
- Be performed non-invasively
- Be effective and lead to better survival rates

The conventional cancer treatments typically do not meet these criteria. For example, the discrimination between normal and cancerous cells of the same tissue poses problems for radiation therapy, chemotherapy and surgery alike, with the resultant complications being said to be "necessary side effects" of the treatment. However, treatment using TTFs meets all of the above criteria and has been shown to have reasonable success in both experimental and clinical trials [6, 9, 10, 11].

Importantly, it may be possible to further improve the efficacy of the treatment, thereby making it an even more attractive alternative to conventional treatment modalities. Treatment is currently only being performed using a single frequency of excitation for each tissue type, but it is proposed that the efficacy of the treatment can be improved by using multiple frequencies simultaneously for the treatment of the same tissue. However, this simultaneous, multiple-frequency (broadband) treatment has not been experimentally tested before and as a result, the possible improvements in treatment efficacy are presently unknown.

The motivation for the proposed broadband treatment is as follows. If a single cell has a narrow band of sensitivity as shown in Figure 1.2.1a, and cells are of slightly different dimensions leading to different sensitivities, as shown in Figure 1.2.1b, then a population of cells should have a broader band of sensitivity, as depicted in Figure 1.2.1c. As the physical and electrical properties of cancer cells are different to that of normal cells [12], it is inferred that a cancerous and normal cell population should have different bands of sensitivity, as shown in Figure 1.2.1d.



(a) A single cell.

(b) Three cells with slightly different dimensions.

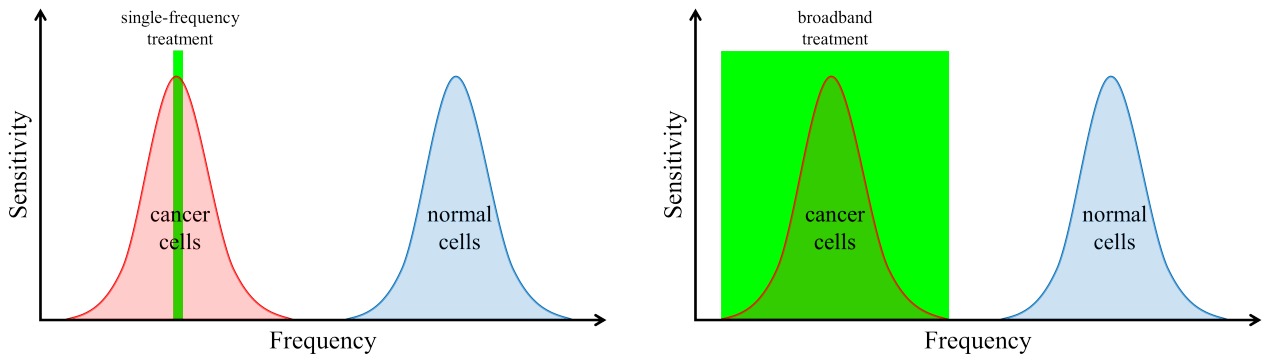
(c) A population of cells.

(d) Cancerous and normal cell populations.

Figure 1.2.1: Sensitivity distribution of cells and cell populations.

Therefore, without damaging normal cells in the vicinity of the treatment, single-frequency treatment should target a small proportion of the cancer cells (Figure 1.2.2a), whereas broad-

band treatment should target a larger proportion of the cancer cells (Figure 1.2.2b).



(a) Single frequency treatment.

(b) Broadband treatment.

Figure 1.2.2: Treatment of the cancerous cell population.

1.2.1 Aim of the research

Investigation into why no broadband treatment is currently being performed showed that fairly large voltages were required to perform this type of treatment due to the high permittivity and conductivity of biological materials [13]. The aim of this research was therefore to assess the viability of cancer treatment using broadband electric fields, and if viable, to implement it and compare it to the current single-frequency treatment. It was proposed that the voltages required for broadband treatment could be lowered by constructing and using a customised, low-impedance experimental set-up.

1.2.2 Research question

This research attempted to answer the question:

> "Can the efficacy of TTF treatment be improved by using broadband electric fields?"

1.2.3 Research objectives

The objectives of the research were to:

- Treat a cell-line with single-frequency TTF treatment at the optimal treatment-frequency for that cell-line
- Treat the same cell-line with a comparable form of broadband TTF treatment
- Compare the results obtained using these two treatment techniques

1.2.4 Organisation of the dissertation

The rest of this dissertation is organised as follows. Chapter 2 contains a brief background of concepts used in the research and Chapter 3 explains the electric field theory behind the experiments. This is followed by the design of the experimental set-up in Chapter 4 and the simulation of the experimental set-up in Chapter 5.

The experimental methodology used, and the results obtained therefrom are then presented in Chapters 6 and 7 respectively. Chapter 8 details an extension of the research into the field of ultrasound, Chapter 9 contains a discussion of matters pertaining to the research, and conclusions are formulated in Chapter 10.

Chapter 2

Background

This chapter introduces phenomena and concepts that underpin the research presented in this dissertation.

Tumour Treating Fields and their mechanisms of action are described in Section 2.1, followed by an explanation of broadband signals in Section 2.2. The different categories of biological experiments are then discussed in Section 2.3, and an overview of spectrophotometry and its use in cell proliferation assays is presented in Section 2.4.

2.1 Tumour Treating Fields

2.1.1 Fundamentals

As mentioned previously, TTFs are alternating electric fields which have an intensity in the range of 1–3 V/cm and a frequency in the range of 100–300 kHz [5]. Importantly, TTFs are different from other physical modalities such as ionizing radiation and heating, in that they disrupt specific processes in the mitotic (cell-division) cycle, leading to apoptosis (programmed cell death) rather than necrosis (death due to trauma) [5, 8, 14]. Interestingly however, TTF treatment is also highly selective, inhibiting the proliferation of tumour cells but not that of normal cells [5].

2.1.2 Mechanisms of action

In order to understand the mechanisms of action of TTFs, it is important to understand the behaviour of dipoles in electric fields. When placed in a uniform electric field, an electric

dipole experiences a torque that attempts to align the electric dipole moment with the field [15]. Therefore, in a uniform alternating electric field, dipoles remain stationary but oscillate or rotate at the frequency of the field.

However, in a non-uniform alternating electric field, dipoles experience a net force as well as a torque. Therefore, dipoles move towards the region of higher field density, whilst oscillating or rotating at the frequency of the alternating field. These phenomena are illustrated in Figure 2.1.1.

There are two proposed mechanisms of action for TTFs, each acting in a different phase of the mitotic cycle [5, 8, 9]:

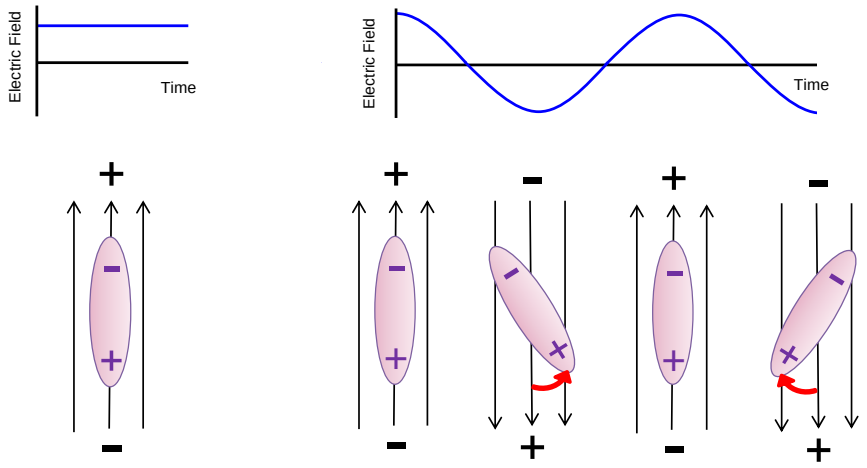
1. *Metaphase*

   In metaphase, the highly polarised tubulin subunits align to form tubulin polymers known as microtubules. These microtubules then arrange themselves spatially in the cell to form the mitotic spindle [16]. The TTFs disrupt the alignment of the tubulin subunits needed for polymerisation, as well as the microtubule alignment needed for the correct formation of the spindle. This leads to mitotic arrest, followed by apoptosis. Figure 2.1.2 illustrates this effect.

2. *Anaphase/Telophase*

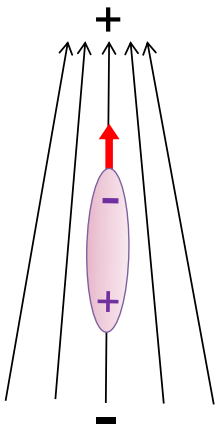
   During cytokinesis, a cleavage furrow forms near the old metaphase plate. This furrow is caused by a contractile ring of actin microfilaments which pinches the dividing cell into an hourglass shape [16]. When TTFs are present in the cell, there is a higher field density at the furrow, which causes movement of all dipoles and charges towards the furrow. This leads to a piling-up of the intracellular macromolecules and organelles. Cleavage cannot be completed and apoptosis occurs. This movement of dipoles towards the cleavage furrow is illustrated in Figure 2.1.3.

For a more comprehensive explanation of the mechanisms involved, including detailed mathematical modelling of both the cell and sub-cellular structures, the reader is referred to the research performed by Tuszynski *et al.* [17].



(a) Dipole in a uniform DC field.

(b) Dipole in an AC field.



(c) Dipole in a converging DC field.

Figure 2.1.1: Behaviour of dipoles in electric fields.

2.1.3 Frequency dependence

Currently, tumours are being treated using a single, apparently optimal frequency that is specific to the type of tumour. At this optimal frequency, the torque acting on the intracellular tubulin subunits is at a maximum [18]. Appendix A of [18] shows that the optimal frequency is proportional to the membrane thickness and the conductivity of the cytoplasm, but is inversely proportional to the cell radius. Plots of the simulation results from this

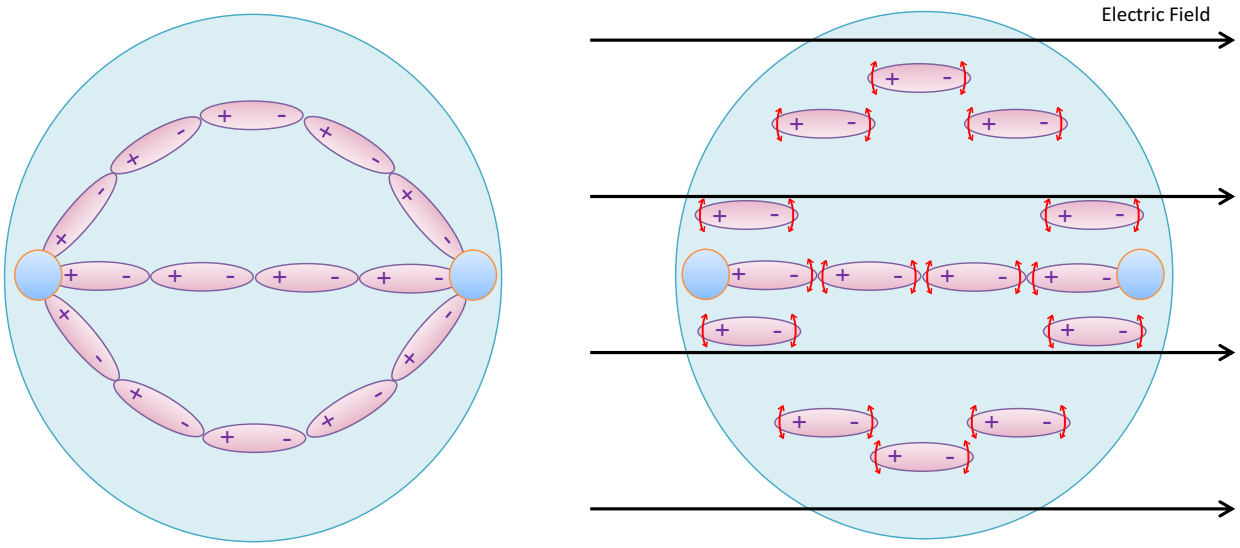


Figure 2.1.2: Alignment of tubulin subunits in an electric field.

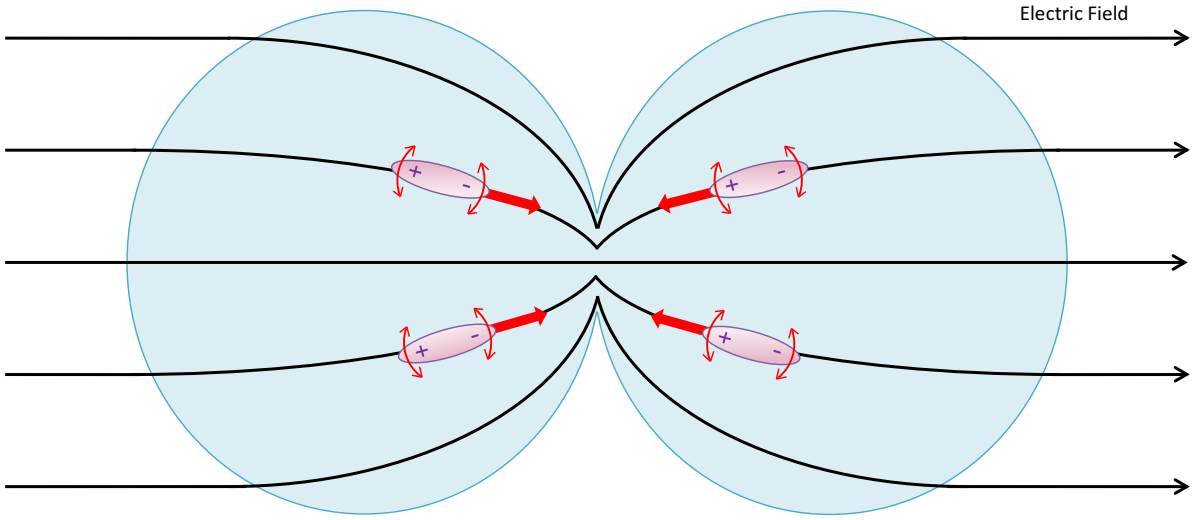


Figure 2.1.3: Converging of tubulin subunits towards a higher electric field density.

analysis can be seen in Figure 7 of the same appendix of [18].

It has been shown that the physical and electrical parameters of cancer cells differ significantly from that of their normal counterparts [12, 19]. These differences lead to higher electric field intensities in the cancer cells when the same field is applied [20]. Therefore, cancer cells and normal cells experience mitotic interference at different frequencies, leading to the selectivity mentioned previously [8].

The extent of the differences between normal and cancerous cells can be quite large. Hondroulis *et al.* reported whole-cell resistances for cancerous, adenocarcinoma cells (SKOV3) being more than double those of normal, endothelial cells (HUVEC) [12]. Ermolina *et al.* showed that these differences are present for lymphocytes too, with the membrane conductivities of normal cells being up to five times larger than those of cancerous cells [19]. Bajaj *et al.* further support this by noting that there are large electrostatic and hydrophobic differences between the cell-membrane surfaces of normal, immortalised breast cells (MCF10A), cancerous, non-metastatic cells (MCF-7) and cancerous, metastatic cells (MDA-MB-231) [21]. In the research by Bajaj *et al.*, these differences were used to displace fluorophores, which allowed for the detection of fluorescences that differed by more than two-fold between the three types of cells [21].

It should also be noted that in the study by Hondroulis *et al.*, the resistance of the normal, endothelial cells (HUVEC) changed only marginally ($\approx 25\,\%$) when subjected to TTF treatment, whereas the resistance of the cancerous, adenocarcinoma cells changed significantly ($\approx 250\,\%$) under the same conditions [12].

Complex models that can be used to analytically predict the range of sensitive frequencies for a particular cell-line have been proposed [17, 22]. However, the dimensions and electrical properties of various parts of the cell and its surroundings (in particular the extracellular space, cytoplasm and membrane) need to be known as they are used as inputs for the models [17, 22].

It may also be possible that some form of mechanical resonance exists at the optimal frequencies proposed. This idea is elaborated on in Chapter 8, where treatment using ultrasound is discussed.

2.1.4 Mitotic axis alignment

It has been shown that TTFs are more effective when the direction of the field is aligned with the axis of the cell division [8]. However, in a population of cells the axes of cell division are randomly orientated [18]. Previous authors have attempted to overcome this by sequentially switching the field direction every second, alternating between two perpendicular directions [7].

It is proposed that instead of changing the field direction, the axes of cell division should be rotated so that they are aligned with the field. This can be performed using a small DC electric field ($\approx 1.5\,\mathrm{V/cm}$) [23].

It has also been shown that small DC electric fields ($\approx 2\,\mathrm{V/cm}$) arrest the cell cycle of vascular endothelial cells at the G_1/S transition [24]. Although it is unknown if the same effect is present in other cell types, vascular endothelial cells are key to angiogenesis and

the inhibition of their proliferation may have great significance in treating tumours [24]. However, there is a concern that if the cell cycles of the tumour cells are also arrested at the G_1/S transition, the cells won't reach mitosis and will therefore be immune to the TTF treatment which is only effective on dividing cells.

2.1.5 Broadband extension

Confirming their theoretical hypotheses, Kirson *et al.* showed that a cultured population of tumour cells responds to TTF treatment at many frequencies (see Figure 2C from [8]). They plotted the efficacy of the treatment as a function of the frequencies used, and an optimal frequency (corresponding to the frequency with the highest efficacy) was then chosen for treatment. However, it is proposed that far better efficacies can be achieved if treatment is performed using the simultaneous application of all of the frequencies that the tumour cells are sensitive to.

Treatment using many frequencies simultaneously is called broadband treatment. An explanation of this term, and the methods of creating signals for broadband treatment, is provided below. It should be noted that one of the concerns with using broadband treatment is that the frequency-dependent selectivity mentioned in Section 2.1.3 may be diminished, allowing for the TTFs to damage normal cells along with cancer cells.

2.2 Broadband signals

In a spectrum of frequencies, a specific range is called a band. For example, in the electromagnetic spectrum, the band of frequencies comprising visible light is between 4.2×10^{14} Hz and 7.9×10^{14} Hz [25]. The width of the band is appropriately called the bandwidth and is an indication of how many frequencies are present in the band. As such, white light is composed of the full band of visible light and therefore has a broader bandwidth than light of a single colour [15].

An example of these terms being used in medicine is provided by the Broadband Light (BBL) treatment used by dermatologists: in this treatment, the skin is subjected to light with wavelengths of between 560 nm and 1200 nm, corresponding to the frequency band in the electromagnetic spectrum of between 2.5×10^{14} Hz and 5.4×10^{14} Hz [26].

As sinusoids in the time domain correlate to single frequencies in the frequency domain [27], a signal containing a band of frequencies can be obtained through the summation of sinusoids in the time domain. Given below is a summary of the mathematics that underpins this summation.

2.2.1 Summing two sinusoids

The theory behind the summation of two sinusoids is based on the well-known trigonometric identity seen in Equation 2.2.1.

$$cos\,(\alpha) + cos\,(\beta) \quad = \quad 2cos\left(\frac{\alpha+\beta}{2}\right) cos\left(\frac{\alpha-\beta}{2}\right) \tag{2.2.1}$$

Figure 2.2.1 shows the sum of two sinusoids with frequencies $f_1 = 100\,\text{kHz}$ and $f_2 = 110\,\text{kHz}$. Both sinusoids had unity amplitude and the phases (θ_1 and θ_2) were chosen such that at $t = 0$ they were in-phase ($\theta_1 = \theta_2 = 0$).

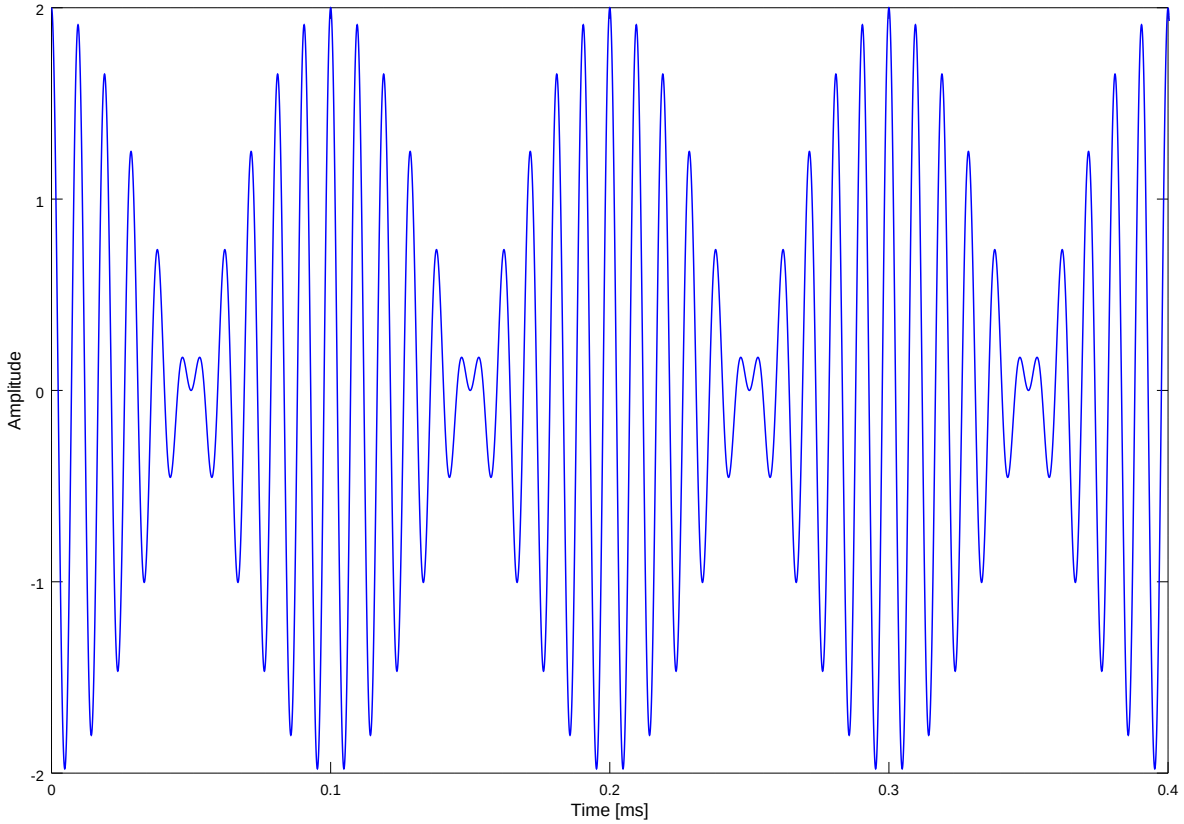


Figure 2.2.1: Superposition of two closely-spaced sinusoids (initially in-phase).

Following the above equations, the high-frequency oscillations in Figure 2.2.1 occur at a frequency of $\frac{f_1+f_2}{2} = 105\,\text{kHz}$. One would expect the low-frequency amplitude modulation to be evident at a frequency of $\frac{|f_1-f_2|}{2} = 5\,\text{kHz}$, however, the modulation occurs twice per

cycle (in both the positive and negative portions of the low-frequency modulating signal), causing a "beat" frequency given by $|f_1 - f_2| = 10\,\text{kHz}$ [15]. Note that this relationship is true whether frequency or angular frequency is used, as they are just scaled versions of each other.

Figure 2.2.2 shows the sum of the same two sinusoids used in Figure 2.2.1, but in this case the phases were selected so that at $t = 0$, the sinusoids were out-of-phase ($\theta_1 = 0$, and $\theta_2 = \pi$). Note that changing the phase of the sinusoids causes a delay in the resultant signal, but does not affect any of its other characteristics.

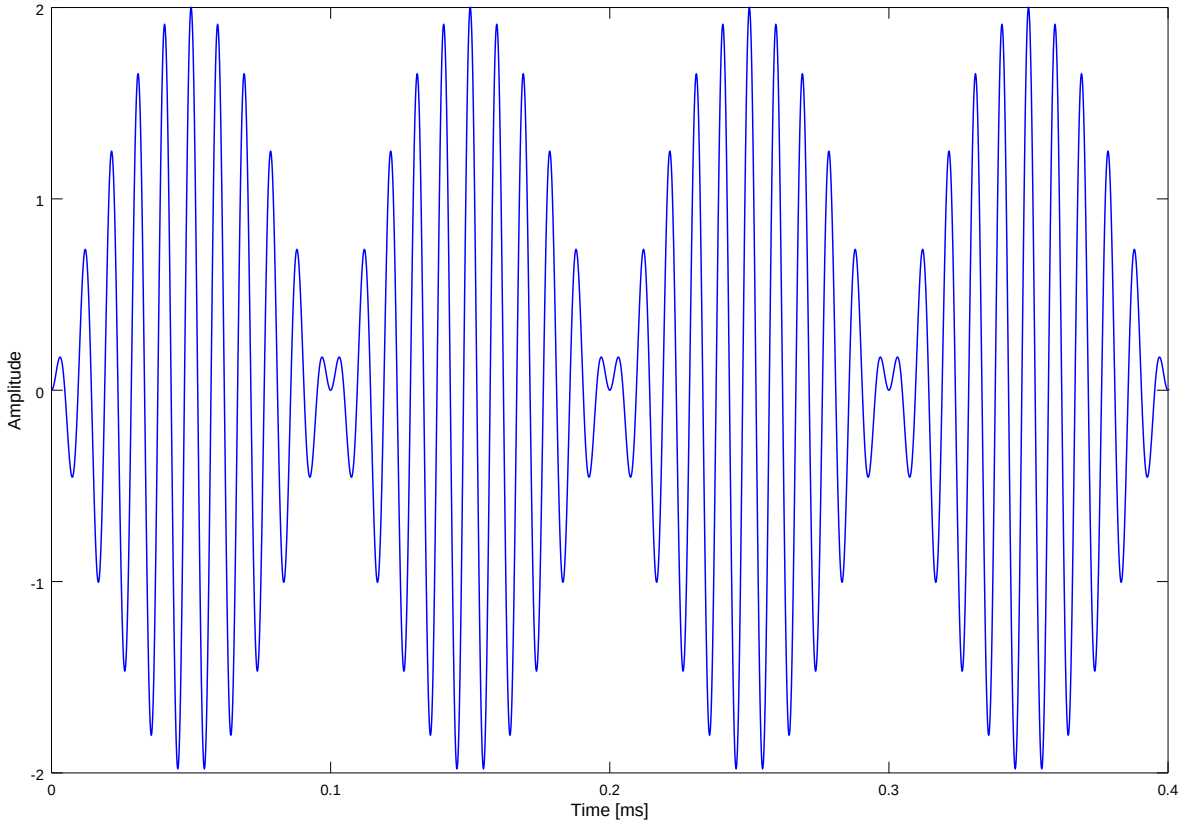


Figure 2.2.2: Superposition of two closely-spaced sinusoids (initially out-of-phase).

2.2.2 Summing many sinusoids

Summing many closely-spaced, in-phase sinusoids results in a sine cardinal (sinc) function that has a peak amplitude at $t = 0$. If the amplitude of the sinusoids being summed are all the same, the magnitude of the peak can be calculated using Equation 2.2.2.

$$\begin{aligned} |Acos(\omega_1 t) + Acos(\omega_2 t) + \ldots + Acos(\omega_N t)| \Big|_{t=0} &= |Acos(0) + Acos(0) + \ldots + Acos(0)| \\ &= A + A + \ldots + A \\ &= AN \end{aligned} \tag{2.2.2}$$

where

A = amplitude of each sinusoid
ω_i = angular frequency of the i^{th} sinusoid
t = time
N = number of sinusoids being summed

Figure 2.2.3 shows a sinc function that was generated by summing 100 sinusoids that all had an amplitude of 1 V and were all in-phase at $t = 0$. Note that the sinusoids that were summed were discreet and the resulting signal had a finite period, leading to the periodicity seen in the figure.

2.2.3 Discreet sinusoids

Using the same nomenclature as above, consider a continuous-time sinusoid $f(t) = Acos(\omega t + \theta)$. If this signal is sampled with a sampling period of T, then the signal becomes

$$f(kT) = Acos(k\omega T + \theta) \tag{2.2.3}$$

where k is an index and $f(kT)$ is the k^{th} sample of the function.

This equation is sometimes written in different notation as

$$f[k] = Acos(k\Omega + \theta) \tag{2.2.4}$$

where $\Omega = \omega T$ and is called the angular frequency of the discreet sinusoid.

The overall period of the signal is given by $N_0 T$ with N_0 being the number of samples in the signal and T being the sampling period used in the sampling of the signal [27].

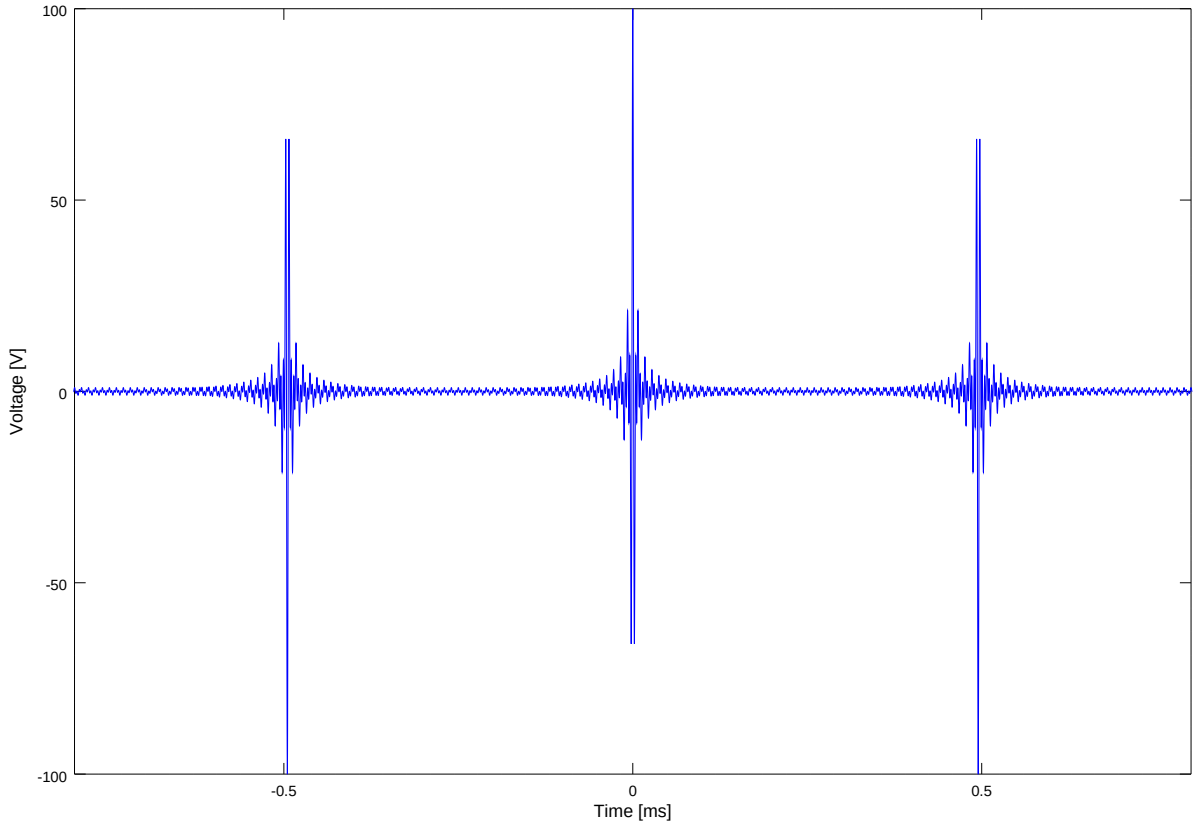


Figure 2.2.3: Summation of 100 sinusoids (all in-phase at $t = 0$).

If several of these sinusoids, each with a unique phase, are summed in a frequency band from the first frequency Ω_0, to the last frequency $\Omega_0 + (N-1)\,\Delta\Omega$, the resulting signal can be obtained by a simple summation in the discreet-time domain [27]:

$$f[k] \quad = \quad \sum_{i=0}^{N-1} A cos\left[k\left(\Omega_0 + i\Delta\Omega\right) + \theta_i\right]$$

where

k = sample index
$f[k]$ = k^{th} sample of the overall function
N = number of sinusoids in the summation
A = amplitude of each individual sinusoid
Ω_0 = first frequency in the band
$\Delta\Omega$ = spacing between frequencies in the band
i = sinusoid index
θ_i = phase of the i^{th} sinusoid

A further discussion of discreet sinusoids is given in Chapter 6 where the creation and implementation of the broadband signal used for the treatment is detailed.

2.2.4 Methods of generating broadband signals

The waveforms in Figures 2.2.1, 2.2.2 and 2.2.3 were obtained by summing discreet sinusoids in the time domain. It should be noted that the same waveforms can be obtained by performing an Inverse Fourier Transform (IFT) on the band of frequencies in the frequency domain. The formation of the sinc pattern in Figure 2.2.3 can also be predicted using the IFT: a group of closely spaced sinusoids of the same amplitude form a rectangular pulse function in the frequency domain, and the IFT of a rectangular pulse function is a sinc function, for both analogue [27] and discreet signals [28].

Another method of creating a broadband signal is to bandpass filter white noise [28]. In theory, white noise contains the full spectrum of frequencies so that after filtering, only the desired band remains [28].

It should be noted too that there are frequency modulation techniques such as frequency-shift keying (FSK) that utilise a spread spectrum, however, the frequencies in the spectrum are applied sequentially and not simultaneously [27] and are therefore not suitable for use in this research.

2.3 Biological experiments

Biological experiments are typically initiated in an *in vitro* environment such as petri-dishes, test tubes, cell-culture chambers or any other artificial labware. The advantage of *in vitro* experiments is that the cells are beyond the influences of the organism as a whole and aren't subjected to byproducts produced by other cells [29].

Once proof of concept has been performed in the *in vitro* environment, the next step is to perform the same experiment in an *in vivo* environment to see if the same results are

obtained (see [30] as an example). These *in vivo* experiments typically progress from animal trials to human trials, when deemed safe to do so (see [18] for this progression with the TTF treatment research).

Human trials are then broken down by the FDA into phases [31], which are summarised in Table 2.1.

Table 2.1: Phases of clinical human trials.

	Number of patients	**Length of study**	**Purpose**
Phase I	20 - 100	Several months	Identify dosage and side effects
Phase II	100 - 300	Several months to 2 years	Evaluate efficacy and side effects
Phase III	300 - 3000	1 to 4 years	Further evaluate efficacy and monitor side effects
Phase IV	3000+	4+ years	Post-market safety monitoring

2.3.1 Cell-lines

The first case of cell culturing was in 1907 when scientists cultured nerve cells in order to ascertain whether a nerve fibre was the outgrowth of a single cell or the fusion of many cells [14]. These days, cell culture is commonplace in the biological sciences, with cultures either being prepared directly from the tissue of an organism (primary cultures) or with primary cells being repeatedly subcultured (passaged) as secondary cultures [14].

As most primary cells in culture stop dividing after a finite number of cell divisions, the cells need to be immortalised so that repetitive subculturing can occur [14]. This process usually involves ensuring that the telomeres don't shorten (by introducing a gene that is involved in the production of telomerase) and through inactivating certain protective mechanisms (by introducing certain cancer-promoting oncogenes) [14]. Immortal cells can also be generated directly from cancer cells and are then called transformed cells [14].

Once immortalisation is achieved, the cells can be subcultured repetitively as a cell-line [14]. For *in vitro* experiments, specific cell-lines are generally used. These cell-lines are standardised, commercially available stocks of specific and well-established cells that have undergone rigorous characterisation and which have well-known origins [14]. Such cell-lines enable researchers from all over the globe to experiment on cells of the same type and origin, thereby allowing for the accurate comparison of scientific research [14]. One of the largest repositories of cells lines is maintained by the American Type Culture Collection (ATCC) (see [32]).

2.4 Spectrophotometry

Spectroscopic methods, such as spectrophotometry, can be used to calculate the concentrations of substances in a solution [33].

A spectrometer operates as follows [33]: the light from a light source is passed through a series of lenses, slits or collimators before being split into light of a single wavelength by a monochromator. This monochromatic light is then passed through the sample and a comparison of the incident light intensity and the detected light intensity is used to calculate the absorbance that the sample has on that specific wavelength of light.

2.4.1 Beer's Law

Beer's Law (also called the Beer-Lambert Law or the Beer-Lambert-Bouguer Law) states that, for each wavelength of light, there is a linear relationship between the concentration of a substance and its absorbance [33]. Equation 2.4.1 represents this relationship [34]:

$$A = \varepsilon c l \tag{2.4.1}$$

where

A = absorbance
ε = molar absorptivity coefficient (also called the molar extinction coefficient)
c = concentration of the substance
l = path-length of the light

It is important to note that the molar absorptivity coefficient is a function of wavelength and its profile is unique for each substance.

Usually, there are several substances in a solution, each with their own concentrations and each contributing some absorbance to the total absorbance [35]. Assuming the path-length for all of the substances is the same, this situation is represented by Equation 2.4.2.

$$\begin{aligned} A_{total} &= A_1 + A_2 + \ldots + A_N \\ &= \varepsilon_1 c_1 l + \varepsilon_2 c_2 l + \ldots + \varepsilon_N c_N l \\ &= \sum_{i=1}^{N} \varepsilon_i c_i l \\ &= l \sum_{i=1}^{N} \varepsilon_i c_i \end{aligned} \tag{2.4.2}$$

Note that this equation holds true for each wavelength of light. Usually, the absorbance is measured, the molar absorptivity coefficient and path-length are known, and the concentrations are hence determined. However, it must be emphasised that to solve for the concentrations of N substances in a solution, the total absorbance at N wavelengths needs to be measured so that simultaneous equations can be created and all of the unknown concentrations can be evaluated.

2.4.2 Cell proliferation assays

There are many cell proliferation assays that utilise Beer's Law to estimate concentrations from absorbance data [34]. An example of this is the Alamar Blue assay which uses a dye (identified as resazurin) which has a reduced and an oxidised form [34, 36]. Metabolic activity chemically reduces the dye, converting it from resazurin, which is deep blue in colour, to resorufin, which has a pink hue [34]. The concentrations of these two forms are calculated by measuring the absorbances of the solution at two separate wavelengths (usually using a microplate reader [34]) and applying Beer's Law to the data obtained.

The equations given in the protocol, however, are independent of path-length as the protocol specifies that the volume of fluid pipetted into the wells must be the same [37]. An overview of the calculations underpinning the protocol is given below.

The absorbance of the dye solution is first measured at a wavelength λ_1, providing an equation of the form

$$C_{red}\varepsilon_{red(\lambda_1)} + C_{ox}\varepsilon_{ox(\lambda_1)} = A_{\lambda_1} \tag{2.4.3}$$

where

C_{red} = concentration of the reduced form of the dye solution
C_{ox} = concentration of the oxidised form of the dye solution
$\varepsilon_{red(\lambda_1)}$ = molar absortivity coefficient of the reduced form of the dye solution at λ_1
$\varepsilon_{ox(\lambda_1)}$ = molar absortivity coefficient of the oxidised form of the dye solution at λ_1
A_{λ_1} = absorbance of the dye solution at λ_1

The absorbance is then measured at a separate wavelength λ_2, providing another equation of the form

$$C_{red}\varepsilon_{red(\lambda_2)} + C_{ox}\varepsilon_{ox(\lambda_2)} = A_{\lambda_2} \tag{2.4.4}$$

where C_{red} and C_{ox} are defined as above and where

$\varepsilon_{red(\lambda_2)}$ = molar absortivity coefficient of the reduced form of the dye solution at λ_2
$\varepsilon_{ox(\lambda_2)}$ = molar absortivity coefficient of the oxidised form of the dye solution at λ_2
A_{λ_2} = absorbance of the dye solution at λ_2

These two equations are solved simultaneously for the unknown concentrations, yielding

$$C_{red} = \frac{\varepsilon_{ox(\lambda_2)} A_{\lambda_1} - \varepsilon_{ox(\lambda_1)} A_{\lambda_2}}{\varepsilon_{red(\lambda_1)} \varepsilon_{ox(\lambda_2)} - \varepsilon_{ox(\lambda_1)} \varepsilon_{red(\lambda_2)}} \tag{2.4.5}$$

$$C_{ox} = \frac{\varepsilon_{red(\lambda_1)} A_{\lambda_2} - \varepsilon_{red(\lambda_2)} A_{\lambda_1}}{\varepsilon_{red(\lambda_1)} \varepsilon_{ox(\lambda_2)} - \varepsilon_{ox(\lambda_1)} \varepsilon_{red(\lambda_2)}} \tag{2.4.6}$$

These concentrations are then used to infer metabolic activity, and therefore cell proliferation and viability [37]. It must be emphasised, however, that appropriate controls need to be used in this process as it is actually the ratio of concentrations in the test wells compared to the control wells that allows for the calculation of the cell proliferation in the test wells to be determined relative to the cell proliferation in the control wells [37].

This assay is therefore a relative assay, not giving an absolute value for cell proliferation, but rather a percentage increase or decrease relative to the cell proliferation of the control.

Chapter 3

Electric Field Theory

This chapter details the electromagnetic theory that is relevant to this research.

The fundamental equations underpinning electromagnetic theory are described in Section 3.1, followed by the simplifications which can be made for quasistatic and electrostatic fields in Section 3.2. A discussion on dielectrics then ensues in Section 3.3, and the chapter is concluded with an analysis of the electric field produced by a wire in Section 3.4.

Where possible, the differential form of equations is given instead of the integral form.

3.1 Electromagnetic fundamentals

The fundamentals of electromagnetic theory is based upon a set of six equations [25]: Lorentz's force equation (Equation 3.1.1), the equation of continuity (Equation 3.1.2), and Maxwell's equations (Equations 3.1.3 to 3.1.6). Together, these equations can be used to predict and explain all electromagnetic phenomena on the macroscopic scale [25].

$$\boldsymbol{F} = q\left(\boldsymbol{E} + \boldsymbol{u} \times \boldsymbol{B}\right) \tag{3.1.1}$$

$$\boldsymbol{\nabla} \cdot \boldsymbol{J} = -\frac{\partial \rho}{\partial t} \tag{3.1.2}$$

$$\boldsymbol{\nabla} \times \boldsymbol{E} = -\frac{\partial \boldsymbol{B}}{\partial t} \tag{3.1.3}$$

$$\boldsymbol{\nabla} \times \boldsymbol{H} = \boldsymbol{J} + \frac{\partial \boldsymbol{D}}{\partial t} \tag{3.1.4}$$

$$\boldsymbol{\nabla} \cdot \boldsymbol{D} = \rho \tag{3.1.5}$$

$$\boldsymbol{\nabla} \cdot \boldsymbol{B} = 0 \tag{3.1.6}$$

where

$\nabla\cdot$	= divergence operator
$\nabla\times$	= curl operator
$\frac{\partial}{\partial t}$	= operator for the partial derivative with respect to time
ρ	= volume density of free charges
q	= charge
$\boldsymbol{u}$	= velocity vector
$\boldsymbol{J}$	= volume density of free currents
$\boldsymbol{F}$	= electromagnetic force
$\boldsymbol{E}$	= electric field intensity
$\boldsymbol{H}$	= magnetic field intensity
$\boldsymbol{D}$	= electric flux density
$\boldsymbol{B}$	= magnetic flux density

Lorenz's force equation describes the electromagnetic force that a charge q undergoes when placed in an electromagnetic field, the equation of continuity dictates that charge must be conserved, and Maxwell's equations explain the interactions between electric and magnetic fields and their respective flux densities [25]. Note that in these equations, $\boldsymbol{J}$ comprises both convection current ($\rho\boldsymbol{u}$) and conduction current ($\sigma\boldsymbol{E}$), where σ represents conductivity and the other symbols are as defined above.

For linear and isotropic media, the link between the flux densities and their respective intensities is given by the vector constitutive relations which are shown in Equations 3.1.7 and 3.1.8, for the electric and magnetic quantities respectively [25].

$$\boldsymbol{D} = \varepsilon\boldsymbol{E} \tag{3.1.7}$$

$$\boldsymbol{B} = \mu\boldsymbol{H} \tag{3.1.8}$$

where

ε = permittivity
μ = permeability

Maxwell's equations can be rewritten using the constitutive relations in order to obtain

$$\boldsymbol{\nabla} \times \boldsymbol{E} = -\frac{\partial \mu \boldsymbol{H}}{\partial t} \tag{3.1.9}$$

$$\boldsymbol{\nabla} \times \boldsymbol{H} = \boldsymbol{J} + \frac{\partial \varepsilon \boldsymbol{E}}{\partial t} \tag{3.1.10}$$

$$\boldsymbol{\nabla} \cdot \varepsilon \boldsymbol{E} = \rho \tag{3.1.11}$$

$$\boldsymbol{\nabla} \cdot \mu \boldsymbol{H} = 0 \tag{3.1.12}$$

In this form, it can be seen that $\boldsymbol{E}$ and $\boldsymbol{H}$ are coupled in Equations 3.1.9 and 3.1.10. This coupling is produced by the magnetic induction predicted by Faraday's Law and the displacement current density predicted by the generalisation of Ampere's Circuital Law, with these phenomena being represented by the time-derivative terms in Equations 3.1.9 and 3.1.10 respectively [38].

3.2 Quasistatics

If the geometry of the system under scrutiny has dimensions much smaller than the wavelength of the electromagnetic wave and the currents vary slowly with time (i.e. they are of a low frequency), quasistatic assumptions can be made [25, 38]. This is tantamount to ignoring radiation effects and time-retardation effects resulting from the finite propagation velocity of electromagnetic waves [25].

Depending on whether the system is dominated by electric fields or magnetic fields, the system may then be analysed as either electroquasistatic, meaning that the magnetic induction term of Equation 3.1.9 may be neglected, or as magnetoquasistatic, meaning that the displacement current density term of Equation 3.1.10 may be neglected [38].

The condition for either the electroquasistatic or magnetoquasistatic assumption to be valid is given by Equation 3.2.1, but practically, Equation 3.2.2 is commonly used [25, 38].

$$L \ll \lambda \tag{3.2.1}$$

$$L < \frac{\lambda}{50} \tag{3.2.2}$$

where

L = spatial length
λ = wavelength of the electromagnetic wave in the medium of interest

As an example, consider a medium similar to water with relative permittivity and relative permeability defined as $\varepsilon_r = 80$ and $\mu_r = 1$, respectively, at the frequency of interest. The speed of an electromagnetic wave in this medium (given by Equation 3.2.3) evaluates to 3.35×10^7 m/s. Note that the relative permittivity ε_r and μ_r are both material-specific and frequency-dependent, and this speed would not necessarily be true in another medium or at another frequency.

$$v = \frac{1}{\sqrt{\varepsilon\mu}} = \frac{1}{\sqrt{\varepsilon_r\varepsilon_0\mu_r\mu_0}} \tag{3.2.3}$$

For a source with a frequency of 100 kHz, the wavelength of the electromagnetic wave (given by Equation 3.2.4) evaluates to 335 m.

$$\lambda = \frac{v}{f} \tag{3.2.4}$$

Using the condition in Equation 3.2.2, an electromagnetic wave of 100 kHz travelling in a medium similar to water may be considered to be quasistatic if the geometry of the system consists of dimensions, L, being less than 6.71 m. Therefore, in this situation, it may be assumed that the system does not radiate and that the time-delays due to the propagation of the electromagnetic wave are unimportant.

If the system is dominated by electric fields, an electroquasistatic assumption may be chosen and the magnetic induction caused by moving charges may be ignored. Equation 3.1.9 may then be simplified, resulting in the electric field being defined by its curl and divergence as

$$\boldsymbol{\nabla} \times \boldsymbol{E} = 0 \tag{3.2.5}$$
$$\boldsymbol{\nabla} \cdot \varepsilon \boldsymbol{E} = \rho \tag{3.2.6}$$

Equations 3.2.5 and 3.2.6 illustrate that the electric field in this situation is irrotational and diverges according to the permittivity of the medium through which it is travelling and the volume density of free charges therein.

Note that, although there are no time-derivatives in these equations, this does not mean that the electric field is time-independent. It simply means that the electric field at any instant in time can be determined from the values of its sources in that instant, irrespective of what the values of the sources were in the instant of time earlier. Essentially, each instant of time can be considered as a snapshot in which the electric field can be solved for if the value of the sources in the same snapshot are known [38].

The solution of the system may proceed by taking the divergence of Equation 3.1.10 and using Equation 3.2.6 to obtain Equation 3.2.7 [38].

$$\boldsymbol{\nabla \cdot J} + \frac{\partial \rho}{\partial t} = 0 \tag{3.2.7}$$

With $\boldsymbol{E}$ and $\boldsymbol{J}$ determined from Equations 3.2.6 and 3.2.7 respectively, $\boldsymbol{H}$ can be solved for through the substitution of $\boldsymbol{E}$ and $\boldsymbol{J}$ in Equation 3.1.10 [38]. However, generally $\boldsymbol{H}$ is not crucial to the electroquasistatic motion of charges and may be ignored [38].

If $\boldsymbol{H}$ is ignored, the problem is simplified to that of an electrostatic one. In fact, the fundamental postulates of electrostatics are given as Equations 3.2.5 and 3.2.6, and can be used to derive all other laws, relations and theorems pertaining to electrostatics [25].

3.3 Dielectrics

3.3.1 Fundamentals

The electromagnetic properties of media can be described using three constitutive parameters: permittivity (ε), permeability (μ) and conductivity (σ) [39]. For electrostatic analyses, the contributions from the magnetic field (dictated by μ) and from the flow of electrons (dictated by σ) are neglected and the only parameter of importance is the permittivity.

Non-conducting materials are termed dielectrics [15] and most are deemed to be simple media, meaning they are homogeneous, linear and isotropic as defined below [25]:

1. Homogeneous: the permittivity of the material is independent of position
2. Linear: the polarisation vector ($\boldsymbol{P}$) is directly proportional to the electric field intensity
3. Isotropic: the polarisation vector is directly proportional to the electric field intensity, independent of the direction of the field

For a dielectric, the electric flux density is a function of both the electric field intensity and the polarisation vector [25], as seen in Equation 3.3.1.

$$\boldsymbol{D} = \varepsilon_0 \boldsymbol{E} + \boldsymbol{P} \tag{3.3.1}$$

However, for linear and isotropic media, the polarisation vector is proportional to the electric field intensity [25]

$$\boldsymbol{P} = \varepsilon_0 \chi_e \boldsymbol{E} \tag{3.3.2}$$

which when substituted into Equation 3.3.1, yields

$$\begin{aligned} \boldsymbol{D} &= \varepsilon_0 \left(1 + \chi_e\right) \boldsymbol{E} \\ &= \varepsilon_0 \varepsilon_r \boldsymbol{E} \\ &= \varepsilon \boldsymbol{E} \end{aligned} \tag{3.3.3}$$

where

$$\varepsilon_r = 1 + \chi_e = \frac{\varepsilon}{\varepsilon_0} \tag{3.3.4}$$

and where

ε_r = relative permittivity
χ_e = electric susceptibility
ε = absolute permittivity
ε_0 = permittivity of free space

Thus it can be seen that the constitutive relation between the electric field intensity and the electric flux density holds for dielectrics, as long as the absolute permittivity of the dielectric is used.

3.3.2 Lossy dielectrics

A lossy dielectric material can be analysed with the same equations, except using a complex permittivity ε_c:

$$\varepsilon_c = \varepsilon' - j\varepsilon'' \tag{3.3.5}$$

where ε' represents the energy storage capability of the material and ε'' accounts for the ohmic and polarization losses in the material [25, 13]. Both of these quantities are generally functions of frequency [25]. In Equation 3.3.5, the expression for ε_c is given in real-imaginary form, however, it may also be represented in a modulus-argument form as

$$\varepsilon_c = |\varepsilon|\, e^{-j\delta} \tag{3.3.6}$$

where δ is termed the loss angle [25]. The loss tangent, $\tan\delta$, is another measure of the loss of the material and may be written as follows [25]:

$$\tan\delta = \frac{\varepsilon''}{\varepsilon'} \tag{3.3.7}$$

An alternative means of representing lossy dielectrics is to incorporate all of the loss into a conductivity parameter, σ, whilst leaving the permittivity of the material, ε, as a real number. In this formulation, ε represents only the energy storage capabilities of the material and σ accounts for all of the losses. To convert between the formulations, the following may be used [25]:

$$\sigma = \omega\varepsilon'' \tag{3.3.8}$$

Clearly, the loss tangent may now be written as:

$$\tan\delta = \frac{\sigma}{\omega\varepsilon} \tag{3.3.9}$$

remembering that ε in Equation 3.3.9 represents the same energy storage capability that ε' represented in Equation 3.3.7.

Using Equation 3.3.9, a medium is said to be a "good conductor" if $\sigma \gg \omega\varepsilon$, and is conversely said to be a "good insulator" if $\omega\varepsilon \gg \sigma$ [25]. Note that these conditions are frequency-dependent, meaning that a material can be a good insulator at one frequency but a good conductor at another.

It must also be noted that as soon as losses are incorporated into the system, electrostatic assumptions are no longer valid. However, electrostatic analyses may still render good approximations if the losses are small enough.

3.4 Electric field produced by a wire

Returning to electrostatics, the electric field intensity of an infinitely long and straight line charge consists of only a radial component, which is given by

$$\boldsymbol{E} = \boldsymbol{a_r} E_r = \boldsymbol{a_r} \frac{\rho_l}{2\pi\epsilon r} \tag{3.4.1}$$

where

$\boldsymbol{a_r}$ = unit vector in the radial direction from the source to the field point
ρ_l = line charge density
ε = permittivity of the medium surrounding the line charge
r = radial distance from the line charge

Although no physical line charge can be infinitely long, Equation 3.4.1 provides a good approximation for the electric field for points that are close to a long and straight line charge [25].

As $\boldsymbol{E}$ is a curl-free vector, it can be described as the gradient of a scalar field [25] which allows for the definition of the electric potential V, such that

$$\boldsymbol{E} = -\boldsymbol{\nabla}\, V \tag{3.4.2}$$

Clearly, if $\boldsymbol{E}$ is known, V can be calculated from integration of $\boldsymbol{E}$.

The potential difference between two points can also be obtained from integration. For example, the potential difference between two points located along the same radial line at $r = r_1$ and $r = r_2$ away from the line charge (with the electric field given by Equation 3.4.1), can be calculated as

$$\begin{aligned} V &= -\int_{r_1}^{r_2} \boldsymbol{E} dr \\ &- \int_{r_1}^{r_2} E_r \cdot (\boldsymbol{a_r} dr) \\ &= -\int_{r_1}^{r_2} \frac{\rho_l}{2\pi\epsilon r} \cdot (\boldsymbol{a_r} dr) \\ &= -\frac{\rho_l}{2\pi\epsilon} \ln\left(\frac{r_2}{r_1}\right) \\ &= \frac{\rho_l}{2\pi\epsilon} \ln\left(\frac{r_1}{r_2}\right) \end{aligned} \tag{3.4.3}$$

If multiple wires are present, the electric field at any point in space can be determined as the superposition of the electric fields generated by each wire [25].

Chapter 4

Design

This chapter details the design of all the components that were required to perform experiments, along with the decisions and trade-offs that needed to be made to achieve the final design.

The design of the culture plate and the jig to seal and hold the culture plate in place are described in Sections 4.1 and 4.2 respectively. The choice for the quantification technique chosen is then explained in Section 4.3.

4.1 Design of culture plate

4.1.1 Important design inputs

4.1.1.1 Overview

The cell culture set-up used by Kirson *et al.* for their *in vitro* tests (see [8]) was found to be too limited to perform the broadband experiments required for this research. Various adaptations needed to be made to overcome these limitations and the factors that were identified as having particular importance were:

1. The ability to generate the required electric fields with low voltages
2. The ability to run multiple tests simultaneously
3. The ability to see the cells through a microscope

4. The capacity to use reasonable working volumes

5. The ease, repeatability and inexpense of the construction

The reasons for the importance of each of these design inputs is explained in more detail below.

4.1.1.2 Explanations

The voltages used to generate the electric fields need to be as low as possible because this allows for more frequencies to be included in the broadband treatment. If the electrodes delivering the electric fields are considered to be a capacitor, then the design of the set-up should be made such that it has a high capacitance resulting in a low capacitive impedance according to Equation 4.1.1.

$$X_c = \frac{1}{j\omega C} \tag{4.1.1}$$

The ability to perform multiple tests simultaneously has many advantages in improving the efficiency and accuracy of the research. Firstly, it allows for different treatments to be performed simultaneously and be compared to a single control. Secondly, several cell-lines may be tested under the same conditions, if required. Lastly, biological systems can be temperamental and the ability to run multiple tests simultaneously allows for statistical analyses to be used which are important for having confidence in the results obtained [14]. For example, results can be written as $\bar{x} \pm \sigma$ where $\bar{x}$ is the mean and σ is the standard deviation. The standard deviation may then be compared to the uncertainty of the measurement and the validity of the results may be ascertained. In addition, outliers can be highlighted and the reasons for their presence can be investigated.

The ability for cells to be seen through a microscope allows for the morphology (and the morphological changes) of the cells to be analysed. Furthermore, various structures can be stained and photographed using molecular probes and fluorescence microscopy. In addition, live-cell imaging may be performed in order to divulge information about the mechanisms of action for the treatment.

Having large working volumes is important in order to avoid evaporation issues, and so that the supernate can be pipetted off several times if several measurements need to be taken. Evaporation can also be lowered by increasing the humidity in the incubator. However, if left unchecked, the evaporation of the medium can cause incorrect results due to lowered cellular metabolic activity and increased dye concentrations if colorimetric techniques are used [40].

The ease and inexpense of construction allows for a repeatable creation of the set-up, even by those with limited equipment and few resources. It should be noted that, although other

authors have recently recognised the need for standardising a cell culture platform for TTF treatment (for example, see [41] and [42]), the design inputs proposed in this dissertation are different as the ease and inexpense of construction features as a major constraint.

4.1.2 Design overview

The culture plate required for this research had three main components:

1. The culture surface
2. The electrodes
3. The well structure

In order to perform successful experiments, it was necessary that the combination of these components met the requirements of the design inputs described above. Each of these components is discussed below and the chosen design for the culture plate is detailed in Section 4.1.3.

4.1.2.1 Culture surface

In the original *in vitro* experiments by Kirson *et al.*, thin wires were fixed to the culture surface of 4-well cell culture chambers and the cells were cultured only between the wires [8]. When attempting to repeat their experiment, two major difficulties arose:

1. Drilling into the curved surface of the wells made the manufacture of the experimental set-up complex and lowered its repeatability.
2. When gluing wires down, it was difficult to get a good seal on the bottom of the dish without the glue encapsulating the wire, essentially forming another layer of insulation. If glue wasn't used, it was difficult to keep the wires in contact with the bottom of the dish where the cells adhered.

4.1.2.2 Electrodes

Electrode Insulation Electric fields may be delivered using either insulated or uninsulated electrodes. Essentially, the insulation prevents electrons from passing through it causing the current that is generated to be capacitive instead of conductive. The major consequences of this are summarised in Table 4.1 below [25]:

Table 4.1: Comparison of ideal insulated and uninsulated electrodes.

	Insulated	**Uninsulated**
Current induced	Displacement (capacitive)	Conductive
Predominant electromagnetic domain	Electrostatic	Electrodynamic
Governing equation	$\boldsymbol{J} = j\omega\epsilon\boldsymbol{E}$	$\boldsymbol{J} = \sigma\boldsymbol{E}$
Electron flow through dielectric?	No	Yes
Electrochemistry?	No	Yes
Losses	Polarisation (dielectric)	Polarisation (dielectric), ohmic and electrochemical

From the information in Table 4.1 it must be emphasised that although it may be tempting to use uninsulated wires to deliver electric fields, this must be avoided to ensure that the results aren't affected by ohmic heating or electrochemical interactions.

Kirson *et al.* confirmed this finding through their analysis of intracellular calcium concentrations of cell cultures (see Appendix B and Figure 6 of [18]), where a significant rise ($\approx 10\,\%$) in concentration was noted after just 10 minutes of electric field exposure through uninsulated electrodes. They concluded that, as a result of this, insulated electrodes should be used to avoid similar (and potentially hazardous) ionic changes.

Electrode placement The choice and placement of electrodes is essential in order to deliver the required electric fields. Of particular concern is that culture medium is not only a good dielectric ($\epsilon_r \approx 80$) [8] which makes it difficult to establish a strong electric field in it due to the large polarisation vector that is created (see Section 3.3), but it is also fairly conductive ($\sigma \approx 0.3\,\mathrm{S/m}$) [8] which essentially "shorts out" the field according to Ohm's Law, the point form of which is given as the governing equation of the uninsulated system in Table 4.1 [25].

Investigations into low-conductivity growth media showed that, although these media are generally used for bacterial cultures [43], they may also be used with human cell cultures without significant loss in cell viability or cell adhesion over short periods of time [44]. For this research, however, it was decided that the possible benefits of making and using custom culture media did not outweigh the possible sources of error that could be introduced by it.

4.1.2.3 Well-structure

As mentioned previously, the ability to perform multiple tests simultaneously is advantageous for both statistical purposes and for testing different cell-lines under the same conditions. Therefore, it was decided that a well-structure should be chosen that allows for simultaneous experiments to be performed easily and repeatably in triplicates or quadruplicates.

In addition, the well-structure needed to be large enough to house enough fluid to ensure that evaporation didn't affect the results but at the same time it needed to be small enough so that large quantities of dye and media didn't need to be expended in each experiment.

4.1.3 Chosen design

After several iterations of design and construction, it was decided that a standard chamber slide system should be used. The Nunc Lab-Tek Chamber Slides with catalogue number 177402 were chosen. This item is depicted in Figure 4.1.1 with its specifications provided in Table 4.2.

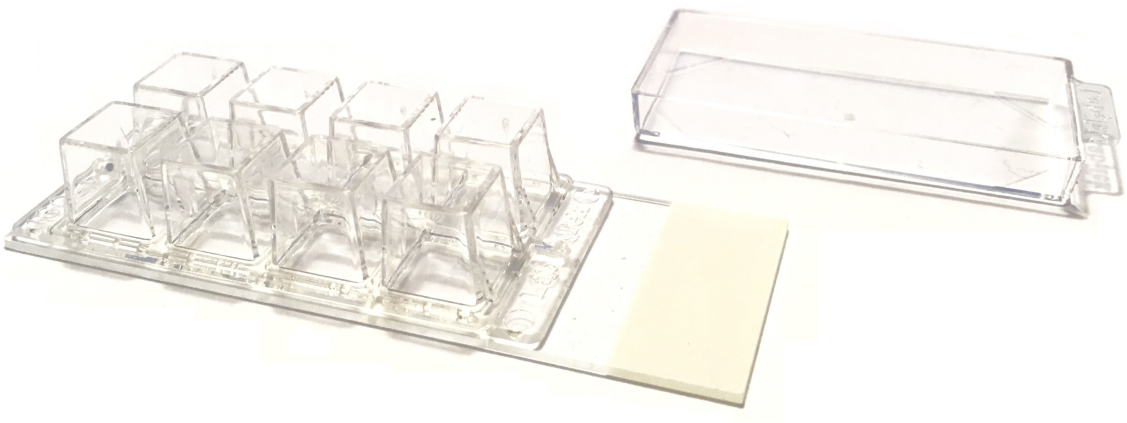


Figure 4.1.1: Nunc Lab-Tek Chamber Slide.

Table 4.2: Details of Nunc Lab-Tek Chamber Slides.

No. of wells	8
Shape of wells	Rectangular
Suggested working volume [ml/well]	0.2 - 0.4
Culture area [cm^2/well]	0.8

The advantage of using this chamber slide system over a standard multi-well system was that no modifications needed to be made to the structure, with the system still adhering to all of the design inputs outlined in Section 4.1.1:

- Insulated wires could be placed between the glass slide and the wells without the need for drilling or glueing.
- The wires could be far thinner than would be possible if drilling or glueing was to be performed.
- The wires could be placed any distance apart, and this distance could be adjusted from experiment to experiment.

- The cells could be viewed on a standard microscope.
- The working volume was large enough to prevent evaporation from affecting the results, and several aliquots could be taken from each well.
- Multiple tests could be run simultaneously with each chamber slide being able to provide quadruplicate wells for both the experiment and the control.
- The construction was simple, repeatable and inexpensive.

The wire that was chosen to be used was an enamelled copper wire with parameters detailed in Table 4.3. It was chosen as it was the thinnest wire that was strong enough to be handled without breaking whilst still being reasonably easy to work with.

Table 4.3: Wire parameters.

Parameter	**Value**	**Unit**
Bare diameter	0.100	mm
Outer diameter	0.119	mm
Insulation thickness	9.5	μm
Minimum breakdown voltage	900	V
Resistance	2.176	Ω/m

4.2 Design of jig to seal the culture plate

A 3D-printed jig consisting of four parts was created to:

- Hold the chamber slide system in place.
- Guide the wires so that they could be placed accurately across the chamber slide system's length.
- Ensure that a good seal was maintained between the glass slide and the well-structure.

The jig was designed in Autodesk Inventor Professional 2016 and its parts are shown in Figures 4.2.1 to 4.2.4. Each of the parts are briefly described below.

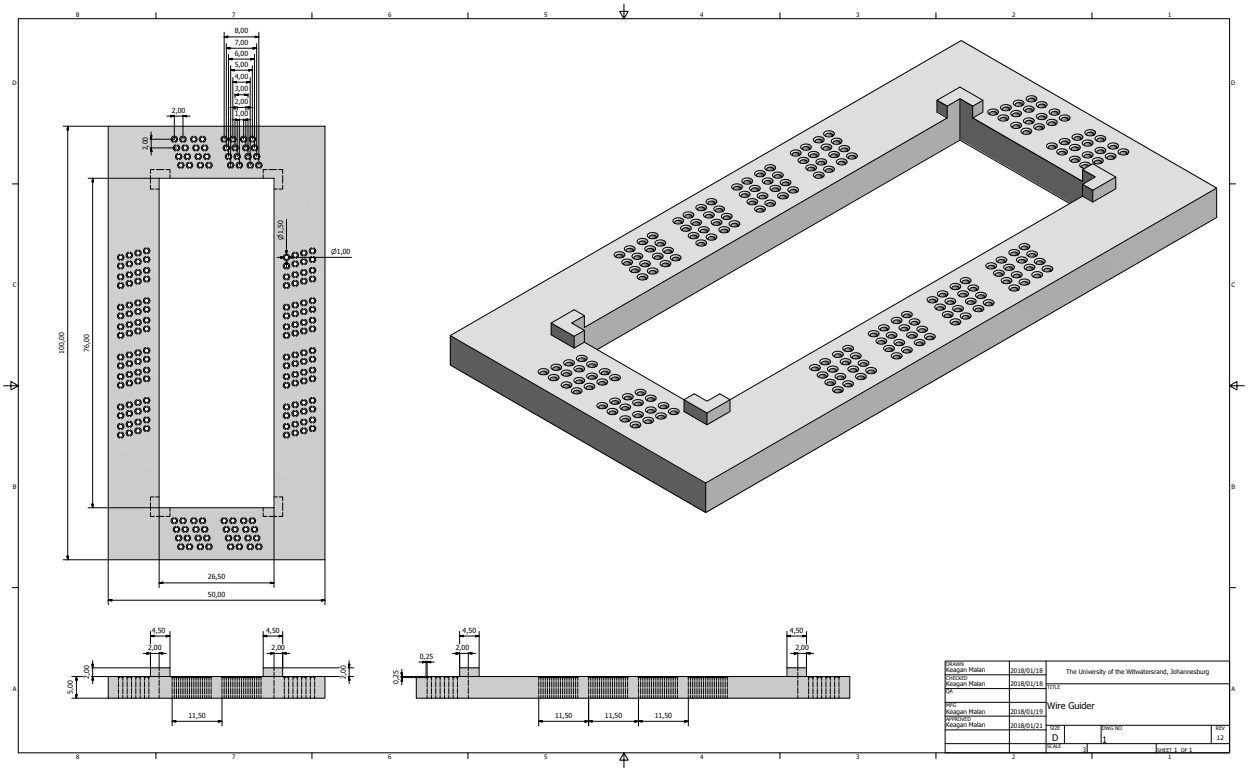


Figure 4.2.1: Wire Guider.

4.2.1 Wire Guider

The Wire Guider depicted in Figure 4.2.1 served the purpose of guiding the wires so that they could be held parallel at fixed distances apart. The rectangular cut-out in the centre was to allow for the slide to be inserted into place from below when the wires were strung across it.

There were several groups of holes arranged around the part. Each hole-group was designed to guide wires across the slide to the hole-group on the opposite side of the slide. The hole-groups were laid out such that their centre-lines passed through the centre-lines of the wells.

There were 16 holes in each hole-group: 8 to the left of the centre-line and 8 to the right of the centre-line. The holes were laid out so that, symmetrically about the centre line, the distance between "pairs" of wires ranged from 1 mm to 8 mm in increments of 1 mm. The holes were provided so that wires could be fed through and stretched taught over the slide. This allowed for the wires to be kept parallel at very precise distances apart.

Where dimensions are not given in Figure 4.2.1, congruency and symmetry with similar dimensioned features may be assumed.

4.2.2 Slide Platform

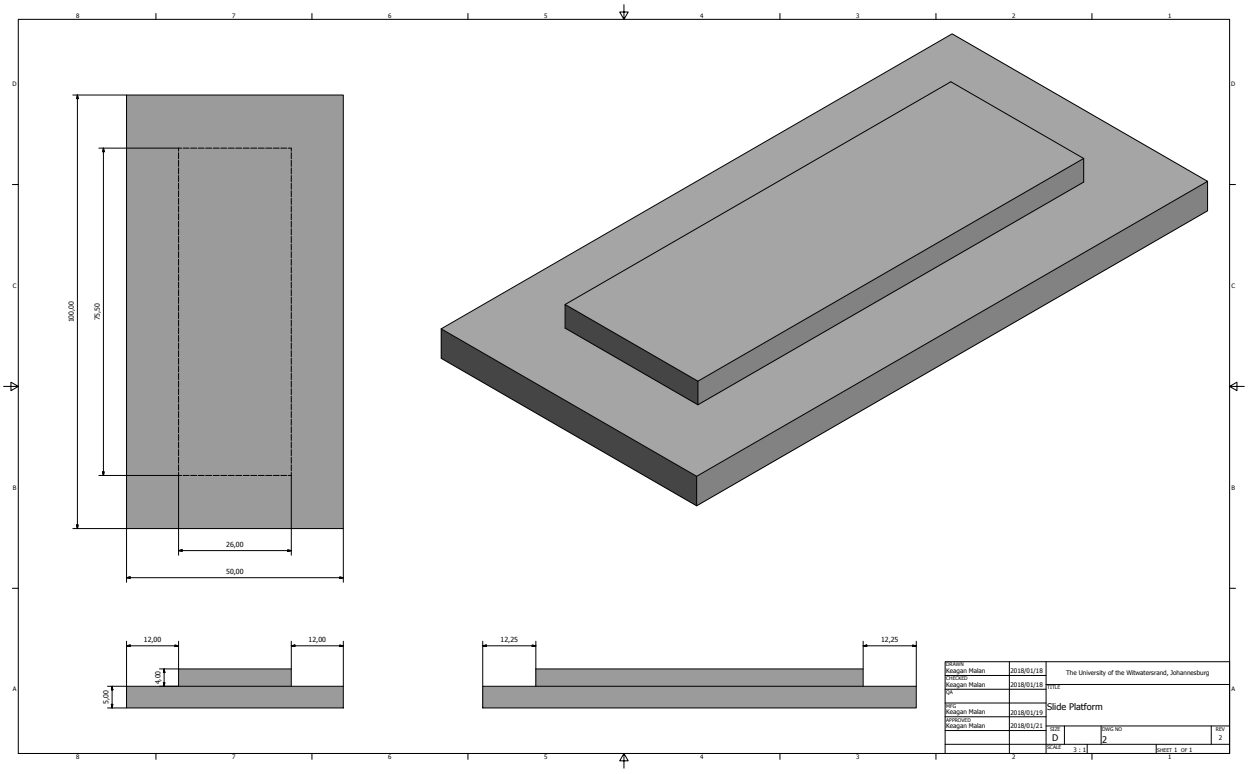


Figure 4.2.2: Slide Platform.

The purpose of the Slide Platform depicted in Figure 4.2.2 was to provide a platform for the glass slide to rest on. It was designed so that slides could be added or removed without disturbing the wires strung across the Wire Guider and it was dimensioned so that its raised portion fitted snugly into the central cut-out of the Wire Guider.

When a standard glass slide was placed on the Slide Platform and the assembly was raised into the Wire Guider, the top surface of the glass slide sat flush with the top surface of the Wire Guider. This ensured that the wires sat directly on the surface of the glass slide where the cell layer was located.

4.2.3 Clamp Brace

The Clamp Brace shown in Figure 4.2.3 was designed to be placed over the wells such that the top of the wells emanated from the rectangular cut-outs in the Clamp Brace. When the wells and glass slide were assembled and placed in the Chamber Slide Holder, clamps

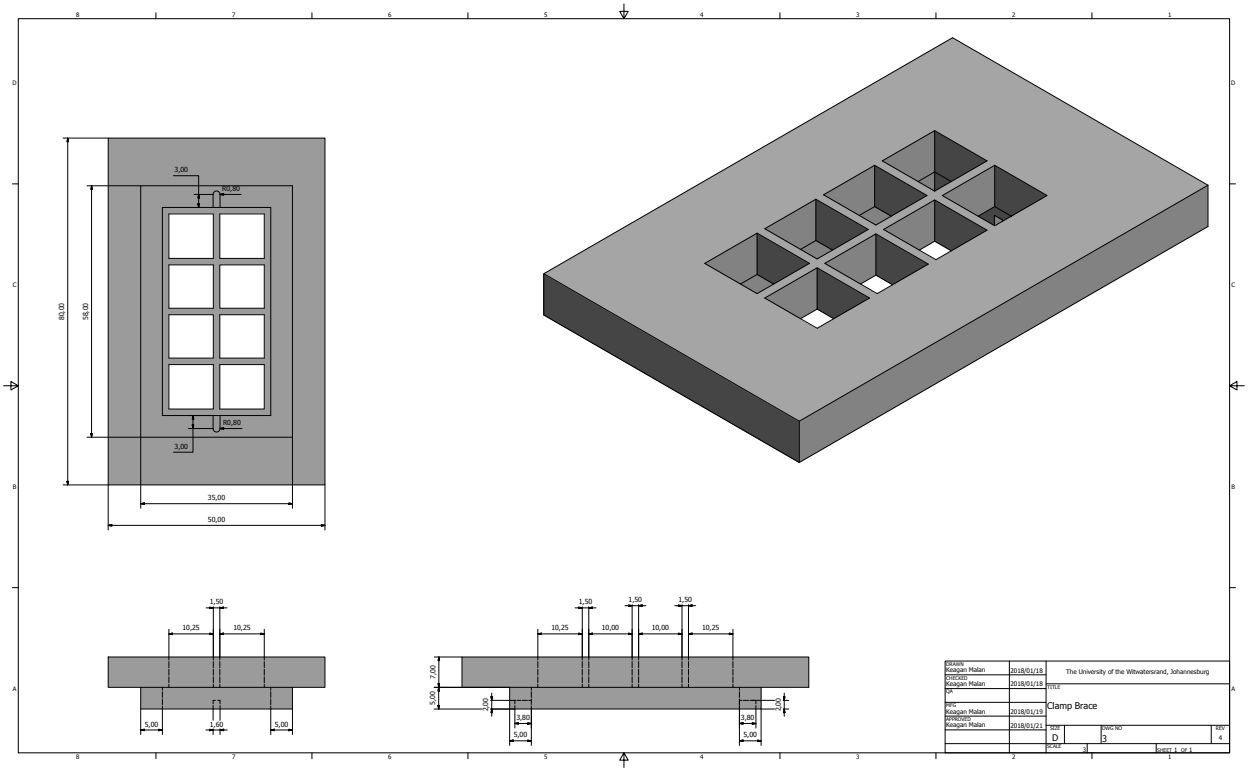


Figure 4.2.3: Clamp Brace.

could be used to hold the Clamp Brace and the Chamber Slide Holder together. The surface around the edge of the Clamp Brace provided the space for these clamps to be placed.

The thin sections between the rectangular cut-outs were designed to force down onto the small ribs between the wells, and the rectangular extrusion surrounding the rectangular cut-outs was designed to force down on the base of the well-assembly directly above the gasket that sealed the wells to the glass slide. The rectangular extrusion had small insets on its short sides because the base of the well-assembly had small protrusions on its corresponding sides, and the force would be concentrated on these protrusions if no insets existed.

4.2.4 Lid Spacer

The Lid Spacer depicted in Figure 4.2.4 was designed to be a spacer between the top surface of the well-assembly and the lid. This allowed clamps to be placed on top of the lid, if desired, without the lid cracking or breaking. The struts of the Lid Spacer were dimensioned so that their centre-lines passed over the centre-lines of the wells. This helped distribute the forces applied to the lid evenly whilst still allowing for the inside of each well to be seen with ease.

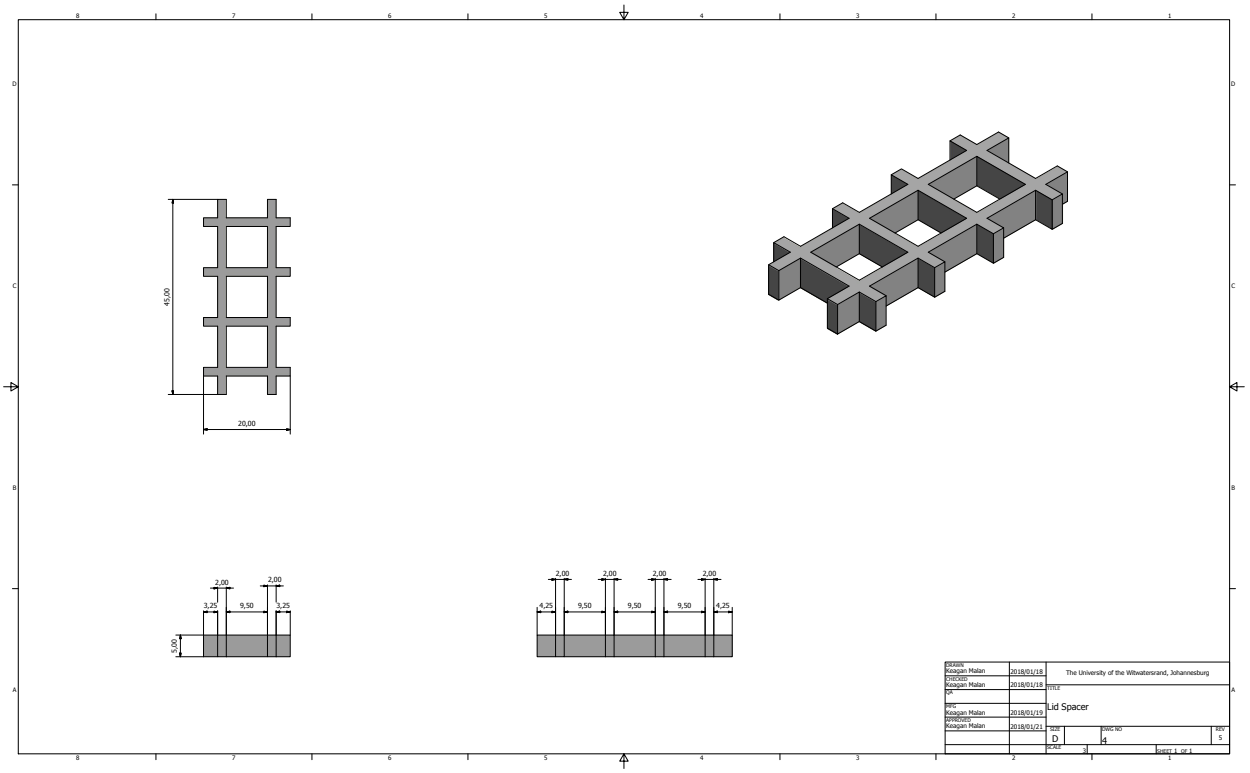


Figure 4.2.4: Lid Spacer.

4.3 Design of quantification technique

4.3.1 Choice of cell-line

The MCF-7 (ATCC HTB22) cell-line is an adherent, epithelial, adenocarcinoma line obtained from the breast tissue of a 69 year old female [45]. It was chosen because it has been used in numerous TTF treatment experiments which identified the optimal treatment-frequency to be 150 kHz [46, 47, 48] and it has a fairly fast doubling time of 29 hours [45, 48], which allows for results to be obtained with relatively short treatment periods.

In addition, it has been reported that MCF-7 cells become larger and more spread after mitotic slippage [46], which is useful if the morphology of the cells is to be analysed.

4.3.2 Choice of quantification technique

4.3.2.1 Alamar Blue identified as resazurin

Cell viability assays, which measure decreases in viable cell numbers, may be used as a direct measure of cytotoxicity [49]. Commonly used are the Trypan Blue dye (which is excluded by living cells but which stains dead cells), the Sulforhodamine B assay (which forms an electrostatic complex with the amino acid residues of proteins) and the Alamar Blue assay (which provides a redox indicator that exhibits both fluorescent and colourimetric changes) [49]. The advantage of the Alamar Blue assay over other assays is that it is easy to use, has a low toxicity, doesn't require the cells to be trypsinised before measurements, and it may be used on both adherent and suspension cell-lines [49].

Kirson *et al.* used an an XTT assay (a type of metabolic assay) to quantify the results for their *in vitro* experiments [8]. However, it was decided that a cell viability assay, such as Alamar Blue, was sufficient for this research as decreases in viable cell numbers (due to decreased cell proliferation, decreased cell survival, or increased cell death) could be used as a direct measure of treatment efficacy [49]. Furthermore, Alamar Blue is non-toxic, involves no cell lysis, and has been shown to be accurate, sensitive, and linear for time-course measurements [50].

Despite these advantages, however, the Alamar Blue assay uses a proprietary dye with unspecified composition. Using a proprietary product has associated risks such as a lack of assurance of the continuity of the composition, the inability to determine its mode of action, and the inability for other researchers to replicate the experiments without purchasing the proprietary product themselves [51]. Fortunately, the dye used in the Alamar Blue assay has been identified as resazurin [36].

In order to mitigate the risks associated with using a proprietary dye, and because of the significant financial benefit, it was decided that plain resazurin (in powder form) would be used to make the dye solution instead of using Alamar Blue, which comes in a pre-mixed liquid form to be used as a 10 % solution (e.g. 10 μL mixed in with 90 μL medium).

This stock solution of Alamar Blue was calculated to be equivalent to a resazurin concentration of 560 μM [52], which implies that the final concentration of resazurin to be used and added to cell cultures is 56 μM. This is marginally higher than the value reported by O' Brien *et al.* in which it was determined that the concentration of the stock solution of Alamar Blue was equivalent to a resazurin concentration of 440 μM, which would result in a final concentration of 44 μM [36]. However, because of the proprietary nature of the dye, these researchers have no assurance that they were in fact testing stock solutions of the same concentration and therefore it is frivolous to make comparisons of this nature.

The concentrations detailed above may be expressed in different units as follows. Using the molar mass of resazurin (251.173 g/mol), the molar concentration of 56 μM may be expressed as a mass concentration as shown in Equation 4.3.1.

$$\begin{aligned}\rho &= cM \\ &= (56\,\mu\text{M})\,(251.173\,\text{g/mol}) \\ &= \left(56 \times 10^{-6}\,\text{mol/L}\right)(251.17\,\text{g/mol}) \\ &= 0.0141\,\text{g/L} \\ &= 0.0141\,\text{mg/mL}\end{aligned} \tag{4.3.1}$$

where

ρ = mass concentration
c = molar concentration
M = molar mass

Assuming the solvent added to the resazurin powder has a density of 1000 mg/mL (similar to that of water), this concentration may be expressed as

$$\begin{aligned}\rho &= 0.0141\,\text{mg/mL} \\ &= 0.0141\,\frac{mg}{mL} \times \frac{1\,\text{mL}}{1000\,\text{mg}} \times 100\% \\ &= 0.00141\%\,\text{by mass}\end{aligned} \tag{4.3.2}$$

Assuming the calculations of [52] are correct, the result of Equations 4.3.1 and 4.3.2 is the concentration recommended by the Alamar Blue protocol [37]. However, a concentration appropriate to the incubation time of the dye and the doubling time of the cells should be chosen. This is particularly important as cells with long doubling times require long-term incubations to reduce the dye which, if long enough, may have toxic effects on the cells [53].

Fairly long incubation times have been used by other researchers, such as the 48 hours with a 0.02 % resazurin solution used by Chandra *et al.* [54]. However, it has also been demonstrated that incubation times in the order of days may have toxic effects on the cells [53], and the Alamar Blue protocol recommends incubating the cells with the dye for periods of less than eight hours [37].

4.3.2.2 Resazurin concentration for MCF-7 growth

In order to determine the optimal combination of cell plating density and resazurin concentration for the MCF-7 cells, a similar protocol to that specified in [37] was used.

Mimicking the procedure by Kirson *et al.* [8], it was decided that the cells would be allowed to grow for a control period of 24 hours before the 24 hours of treatment commenced. After the treatment, the resazurin solution would be added and allowed to reduce for 1 hour before aliquots were taken. The plating density and resazurin concentration chosen needed to ensure that the reduction of the resazurin solution:

1. Remained in the linear range (away from saturation).
2. Changed significantly in the 1 hour period before aliquots were taken.

Various combinations were tested and it was found that seeding 100 000 cells allowed for a reduction of close to 40 % in the time period before aliquots were taken, when used with 0.5 mL of a resazurin solution with a concentration of 0.141 mg/mL. This high concentration was used (10 times higher than recommended by the Alamar Blue protocol) because lower concentrations were found to be subject to more variance which produced indeterminate results. Note that the seeding of 100 000 cells to be used in 0.5 mL of dye corresponds to a plating density of 200 000 cells/mL.

Chapter 5

Simulations

This chapter contains the details and results of the simulations that were performed. The simulation results were crucial in determining the magnitude of the voltages that needed to be used in the experiments in order to ensure that the magnitude of the electric fields applied to the cell culture was sufficiently large to have a therapeutic effect.

The details of the simulation of the designed experiment are presented in Section 5.1, followed by the simulation results in Section 5.2. A comparison between the simulation results and analytical predictions is then presented in Section 5.3.

5.1 Simulation details

5.1.1 Software package and solver settings

The system was simulated on FEKO version 7.0.2, an electromagnetic simulation package provided by Altair. The electric fields in the region of interest were solved with the Method of Moments (MoM) solver using the Volume Equivalence Principle (VEP). As the FEKO software is generally used for higher frequency simulations, a "low frequency stabilisation" setting was enabled for the MoM solver.

5.1.2 Geometry

Simulations were performed for both a 2-wire set-up and an 8-wire set-up. The geometry for each of these set-ups is depicted in Figures 5.1.1 and 5.1.2 respectively. Note that, although

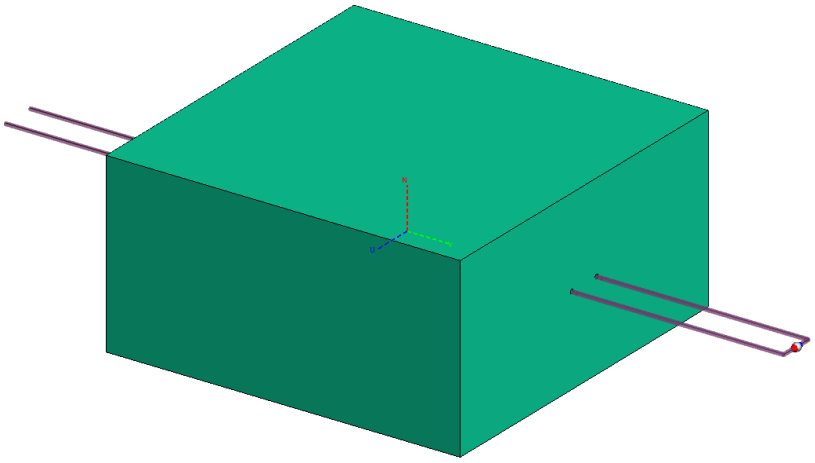


Figure 5.1.1: Geometry used for the 2-wire simulations.

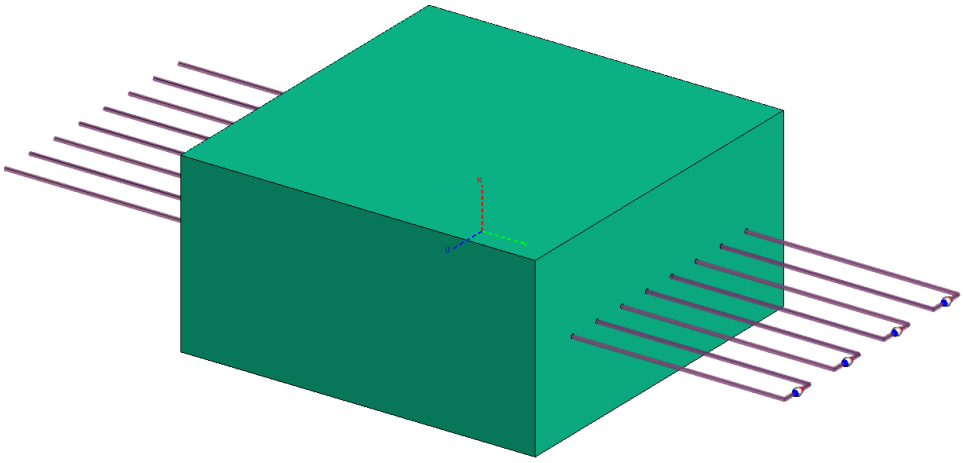


Figure 5.1.2: Geometry used for the 8-wire simulations.

not shown here, fine meshing was performed on the geometry before the simulations were run.

A close-up of the wire geometry is provided in Figure 5.1.3 and the dimensions used in all of the simulations are provided in Table 5.1. Note that the width is defined along U-dimension (on the axis between the wires), the depth is defined along the V-dimension (on the axis along the wires) and the height is defined along the N-dimension (the remaining orthogonal dimension).

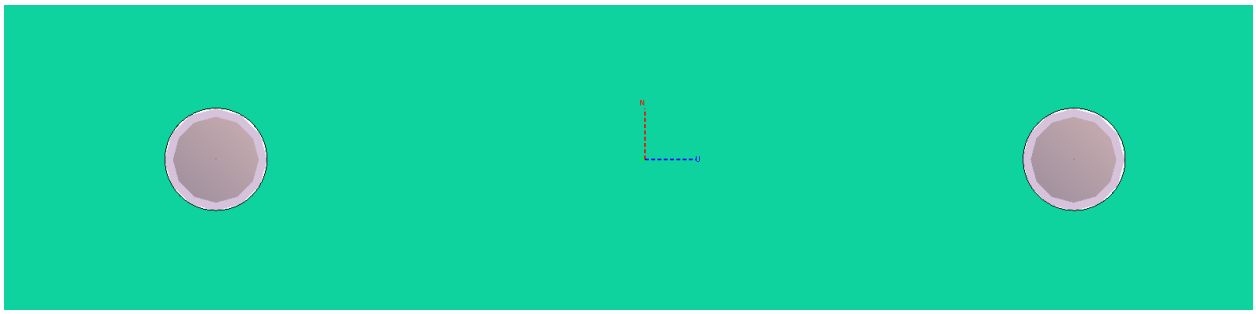


Figure 5.1.3: Close-up of the wire geometry.

Table 5.1: Geometry used for the simulations.

Parameter	**Value**	**Unit**
Wire bare diameter	0.100	mm
Wire outer diameter	0.119	mm
Wire insulation thickness	9.5	μm
Wire length	22	mm
Distance between wire centres	1	mm
Width of dielectric block (U-dimension)	10	mm
Depth of dielectric block (V-dimension)	10	mm
Height of dielectric block (N-dimension)	5	mm

5.1.3 Materials

The details of the materials used in the simulations are provided in Table 5.2. The values for the copper and polyethylene materials were taken from the FEKO Materials Library and the values for the culture medium was was taken from the paper by Kirson *et al.* [8].

Table 5.2: Materials used in the simulations.

Structure	**Material**	**Relative permittivity**	**Conductivity (S/m)**
Wire core	Copper	N/A	58.13×10^{6}
Wire insulation	Polyethylene	2.25	7.5104×10^{-9}
Culture medium	Custom	80	0.3

Note that the conductivity given for the polyethylene material in Table 5.2 was calculated from its loss tangent, $tan\,(\delta) = 0.0004$, using Equation 3.3.9 and a frequency of 150 kHz.

5.1.4 Excitations

In the experiments performed by Kirson *et al.* it was shown that the efficacy of TTF treatment increased with higher field intensities but also that different cell-lines required different field strengths in order to achieve the same treatment efficacy [8]. The aim of this research was not to find the threshold at which the electric field intensity yielded results, and so it was decided that the voltage used for excitation should be chosen such that it generated a field intensity of at least 3–4 V/cm throughout the cell-layer.

This field intensity is slightly higher than the 1–3 V/cm range that is normally used, but it was deemed to be justified given the scope of the research. It must be highlighted that, in previous *in vitro* experiments, the only effect observed with using higher field intensities, was increased treatment efficacy [8, 18, 7]. Analytical predictions further support this observation [22].

The parameters of the excitations used in the simulations are provided in Table 5.3. In all of the simulations, all of the wire ports (one for the 2-wire simulation and four for the 8-wire simulation) used voltage sources with these parameters. Note that the amplitude given is the peak amplitude which would result in a peak-to-peak amplitude of double the specified value.

Table 5.3: Excitations used in the simulations.

Parameter	**Value**	**Unit**
Frequency	150	kHz
Amplitude	2	V

It must also be emphasised that a frequency of 150 kHz was used as it had been identified as the optimal treatment-frequency for the MCF-7 cell-line [48].

5.1.5 Near-field request

The number of field points in the near-field request, along each dimension of the simulation, is detailed in Table 5.4.

Table 5.4: Number of points in the near-field request.

Parameter	**Value**
Number of field points along the width	10 000
Number of field points along the depth	3
Number of field points along the height	1

A large number of field points was used along the width as this was the dimension of interest where the electric field intensity was expected to vary significantly, especially over the very thin layers of wire-insulations where the permittivity was far less than that of the culture medium.

Three field points were used along the depth so that the electroquasistatic assumption could be confirmed. If all three sets of data along this dimension were similar, it could be said that the time-delays due to the propagation of the electromagnetic wave were unimportant. A single set of field points was used along the height as any additional information about the electric field intensity along this dimension was deemed to be futile due to the thinness of the cell-layer.

5.2 Simulation results

As one would expect of an electroquasistatic system, the profile of the electric field intensity was the same all along the depth dimension of the wires. Therefore, the results provided below are for the profile of the electric field intensity along the width dimension, $U \in (-5\,\text{mm}, 5\,\text{mm})$, but taken at the centres of the depth dimension ($V = 0$) and the height dimension ($N = 0$).

5.2.1 Two wires

The simulation results for a single pair of wires are depicted in Figures 5.2.1 to 5.2.3. Although Figure 5.2.1 shows the full profile of the electric field intensity, it is difficult to see the intensity that the cell layer would be exposed to, and so Figures 5.2.2 and 5.2.3 show the same data, but with different axes in order to allow for this data to be seen.

The electric field intensity at the centre-point between the wires was read off the graph as $0.333\,\text{kV/m}$ which equates to $3.33\,\text{V/cm}$ using the conversion of $0.1\,\text{kV/m} = 1\,\text{V/cm}$.

5.2.2 Eight wires

The simulation results for four pair of wires are depicted in Figures 5.2.4 to 5.2.6. Again, Figures 5.2.5 and 5.2.6 were provided so that the details of the electric field intensity in the culture medium could be seen.

The minimum field intensity was, once again, located at the centre-point, and was read off the graph as $0.364\,\text{kV/m}$ which equates to $3.64\,\text{V/cm}$.

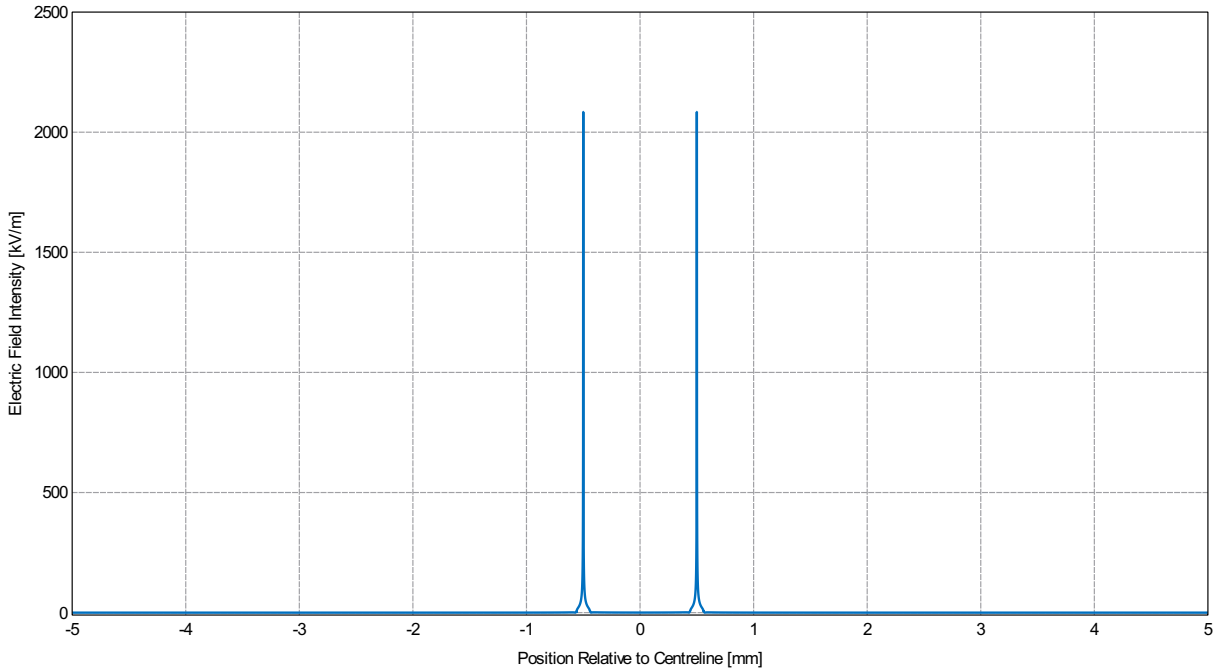


Figure 5.2.1: Simulation results for a single pair of insulated wires in culture medium.

5.3 Comparison with analytical predictions

5.3.1 Analytical predictions

The electric field predicted by Equation 3.4.1 and the electric potential predicted by Equation 3.4.3 are depicted in Figure 5.3.1 for two wires whose centre are separated by 1 mm. The magnitude of the excitation between the wires was set to be 2 V, the same as what was used to produce the simulation results. In order to achieve this magnitude, the line charge density, ρ_l, on the wires was set to be 505 pC/m and -505 pC/m respectively. Care was taken to ensure that the geometry and material parameters used for the analytical predictions matched those used in the simulations. The independent axis is scaled so that the centre of each wire is located on each extremity of the axis.

Note that the electric potential is continuous even though the electric field intensity is discontinuous. This is important as a discontinuity in the electric potential would imply an infinite electric field intensity at that point [25]. Also note that the electric potential is negative as a result of the negative sign in Equation 3.4.2. This negative sign is included in order to conform with the convention that in going against an electric field, the electric potential increases [25].

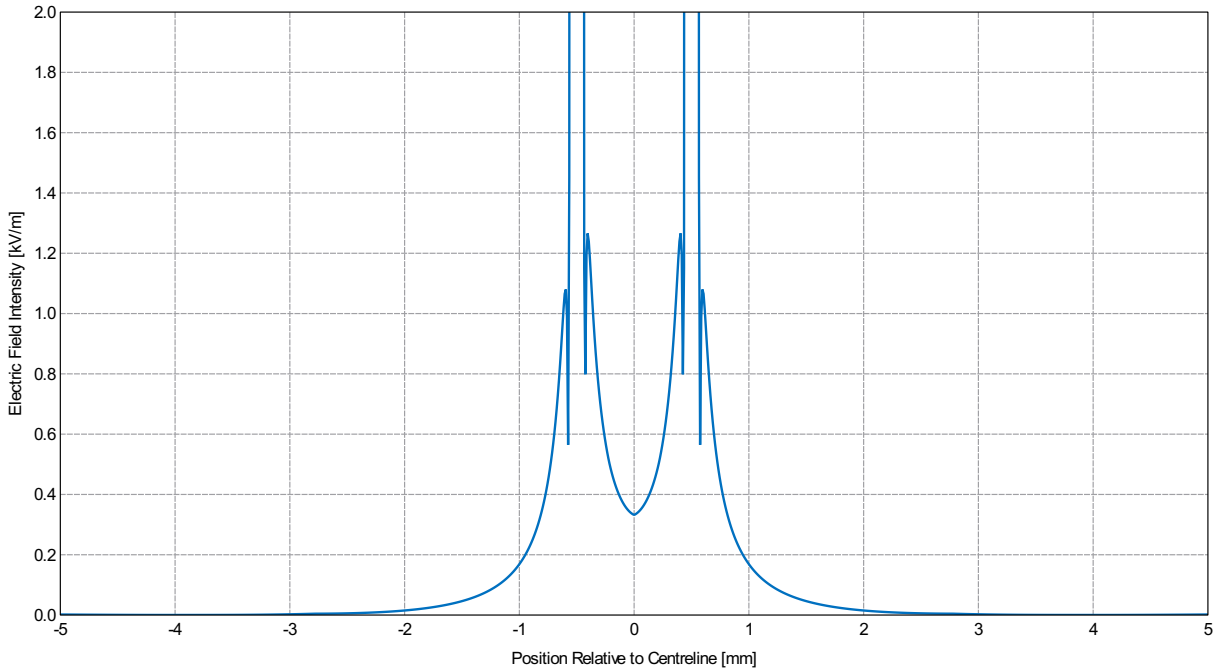


Figure 5.2.2: Simulation results for a single pair of insulated wires in culture medium (axes adapted).

Although it is difficult to see in the graphs, the decay of the electric field intensity is proportional to $\frac{1}{\epsilon r}$ whereas the decay of the electric potential is proportional to $-\frac{lnr}{\epsilon}$, as required by Equations 3.4.1 and 3.4.3.

An analysis of the electric potential showed that the total potential difference comprised three potential differences and, even though thin wire with a thin layer of insulation was modelled, the voltage drop across the two layers of insulation (one contributed by each wire) was still significant and accounted for approximately 69 % of the total voltage drop, as can be deduced from Equation 5.3.1.

$$\begin{aligned} V_{total} &= V_{insulation} + V_{medium} + V_{insulation} \\ &= (-0.69\,\mathrm{V}) + (-0.62\,\mathrm{V}) + (-0.69\,\mathrm{V}) \\ &= -2.00\,\mathrm{V} \end{aligned} \tag{5.3.1}$$

The axes for the electric field intensity were altered so that the intensity at the centre-line could be seen with more easily. The resulting graph is shown in Figure 5.3.2, and the electric field intensity at the centre-line was read off the graph as $0.454\,\mathrm{kV/m} = 4.54\,\mathrm{V/cm}$.

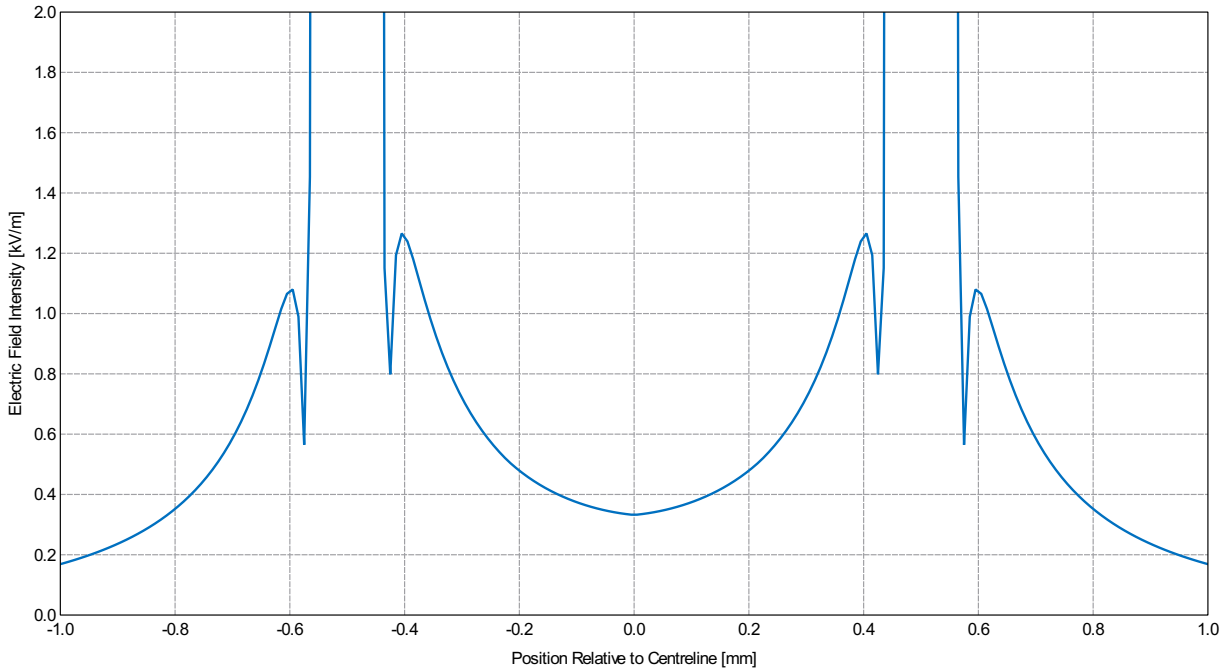


Figure 5.2.3: Simulation results for a single pair of insulated wires in culture medium (axes further adapted).

5.3.2 Comparison

Clearly, there are slight differences between the results from the simulations and the results predicted by analytical methods. There are numerous possible causes for these discrepancies:

- The analytical equations are for infinite line charges, not finite ones as was used in the simulations.
- The analytical equations are only valid for electrostatic analyses but the simulations modelled both the polarisation losses and the slight conduction losses that result from non-zero conductivities.
- Analytically, the electric field intensity in a conductor must equal zero (under static conditions) with all of the charge migrating to the surface of the conductor [25]. However, the simulations didn't model the conductors in that way but rather modelled them as line charge sources at the centre of the wires.

Using the values for the electric field intensity at the centre-point between the wires, the analytical predictions deviate from the simulations by 36 %. This is a relatively small deviation

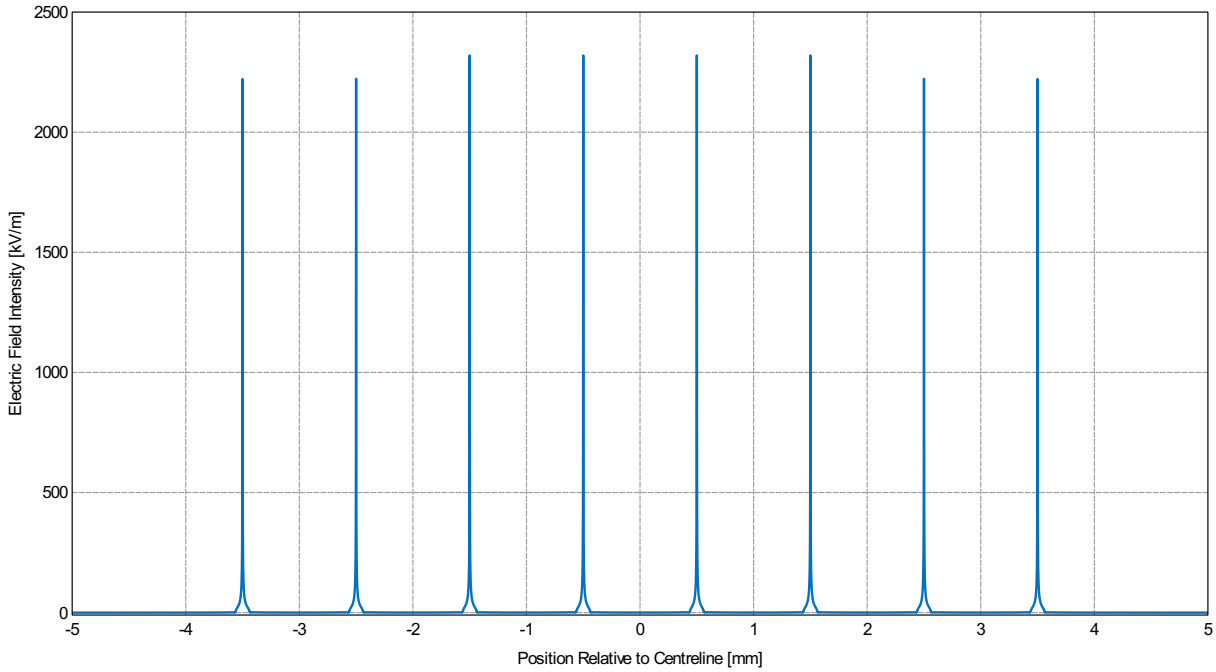


Figure 5.2.4: Simulation results for four pairs of insulated wires in culture medium.

given the assumptions, mentioned above, that were used for the analytical predictions.

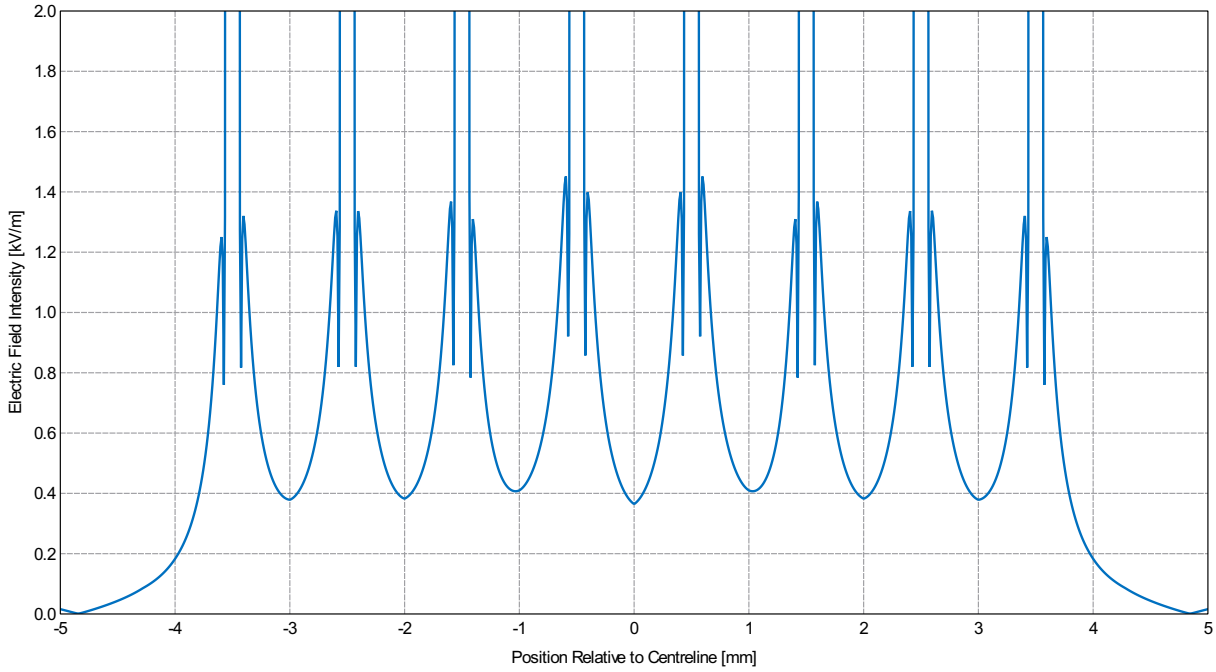


Figure 5.2.5: Simulation results for four pairs of insulated wires in culture medium (axes adapted).

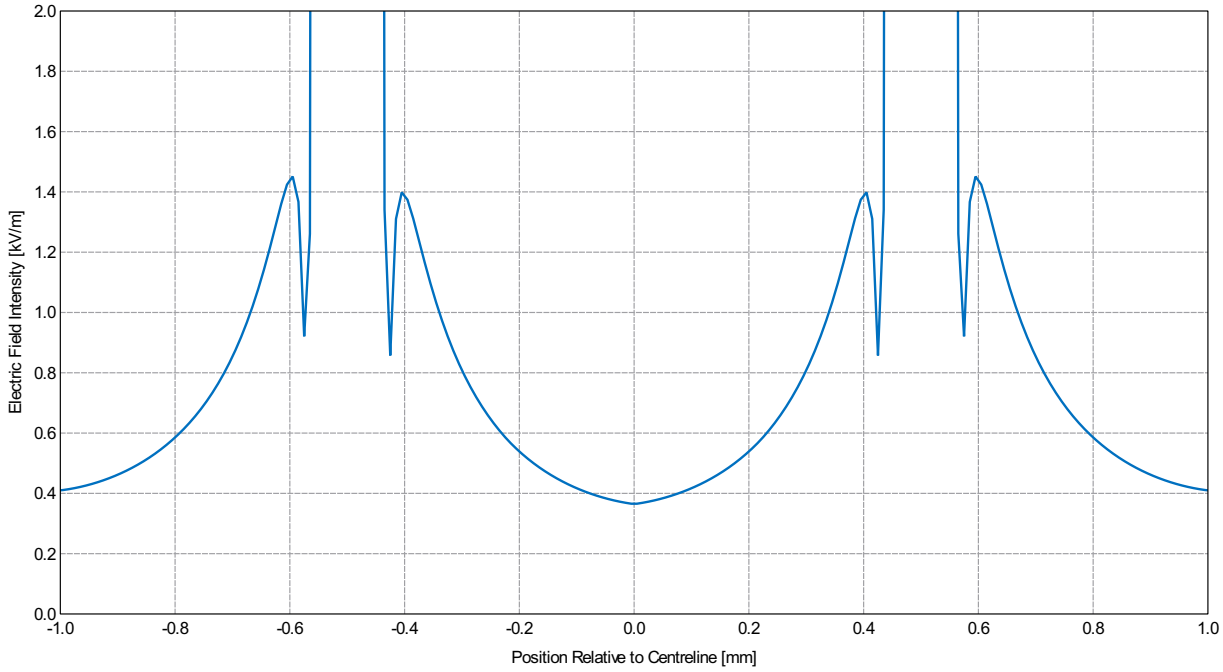


Figure 5.2.6: Simulation results for four pairs of insulated wires in culture medium (axes further adapted).

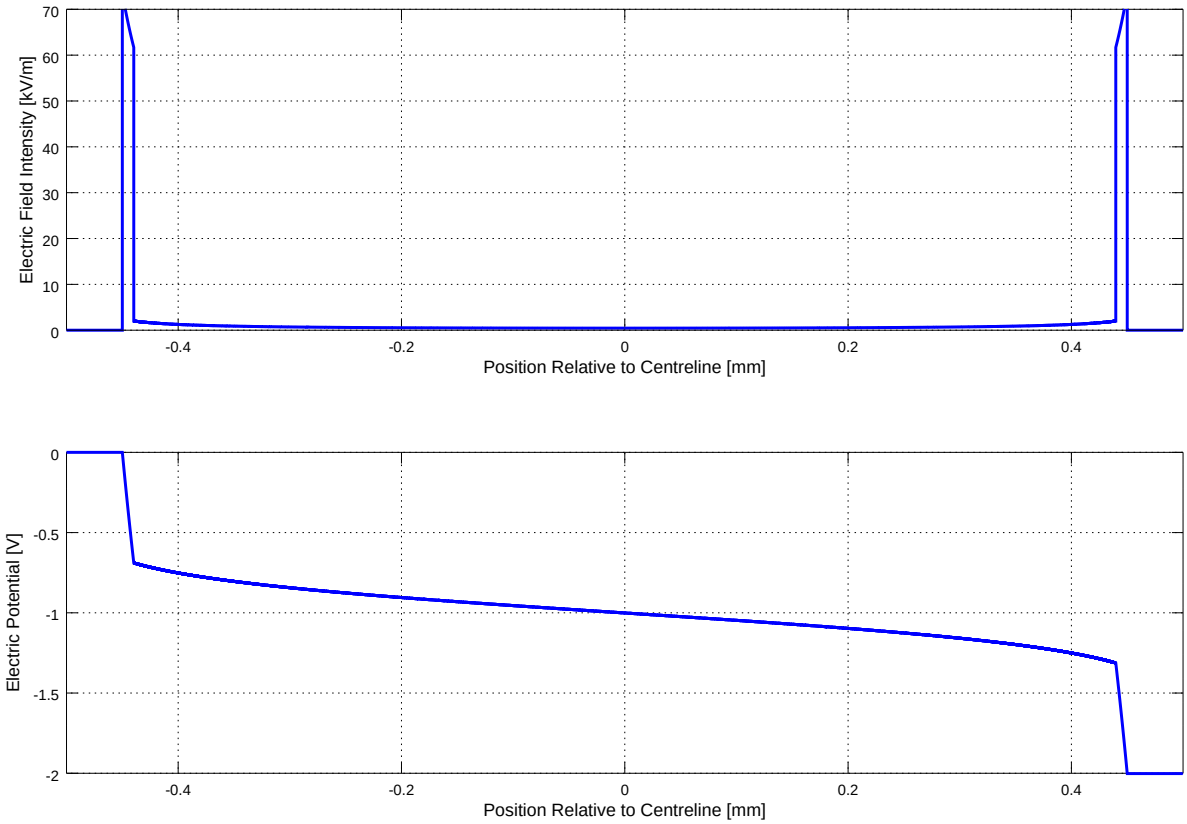


Figure 5.3.1: Analytical predictions for electric field intensity and electric potential.

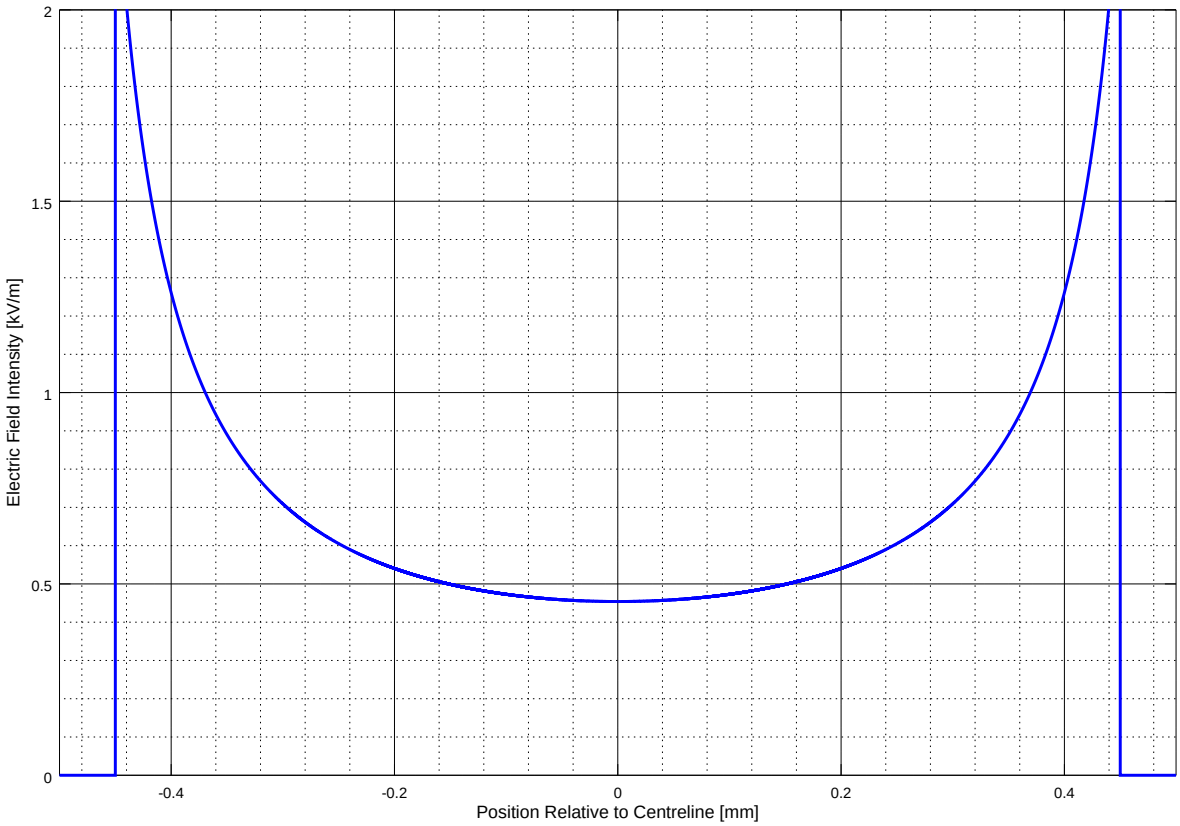


Figure 5.3.2: Analytical predictions for the electric field intensity (axes adapted).

Chapter 6

Methodology

This chapter details the methodology that was used in the experimental process. Section 6.1 details the preparation that was performed before experiments could be initiated, Section 6.2 describes the experimental procedure, and Section 6.3 details the techniques used to quantify the results.

6.1 Preparation for experiments

6.1.1 3D printed jig

The 3D-printed parts mentioned in Section 4.2 were printed on a Form 2 printer made by FormLabs. This printer uses stereolithography technology and is able to print with resolutions as small as 0.025 mm. However, this precision was not required for this research and so all of the parts were printed with a resolution of 0.1 mm.

Various resins were tested and it was found that the clear resin suited this research the best as it was strong and allowed for leaking culture medium to be easily identified. The parts were designed to be fairly thick (> 5 mm) so that they wouldn't flex with the stress induced by the clamping. The 3D-printed parts are shown in Figure 6.1.1.

6.1.2 Customised gasket

In the preliminary testing, it was found that the gaskets that were provided with the Nunc Lab-Tek Chamber Slides proved to be too thin to provide a good seal when the wires were

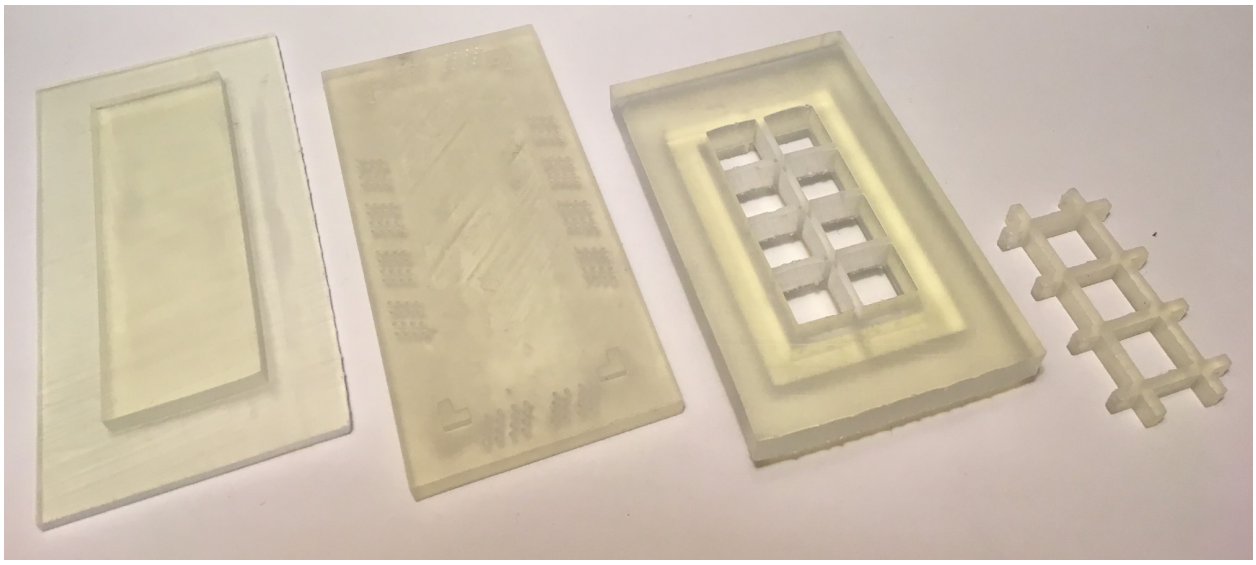


Figure 6.1.1: 3D-printed parts. From left to right: Slide Platform, Wire Guider, Clamp Brace and Lid Spacer.

incorporated into the system. Therefore, a thicker gasket was created by piping a silicone sealant (Bostik Clear Home Silicone Sealant) into the mould provided by the space in the Nunc Lab-Tek Chamber Slide where the original gasket lay. This allowed for thicker (and wider) gaskets to be made simply and cheaply to the exact dimensions required.

Excess silicone was removed from the gasket using a craft-knife so that the gasket didn't impose on the culture area. One of these customised gaskets is shown next to the original gasket in Figure 6.1.2.

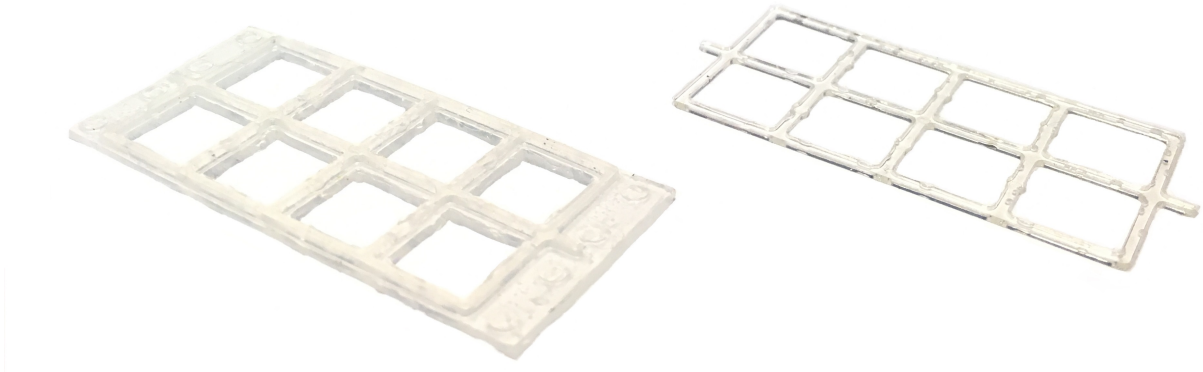


Figure 6.1.2: Customised gasket (left) next to original gasket (right).

6.1.3 Threading of wires

If the centre-line of the wells is taken to be at position zero, for the 2-wire set-up the wires were threaded through the wire holes at ± 0.5 mm so that they were 1 mm apart and symmetric about the centre-line of the wells. If the same coordinate system is used for the 8-wire set-up, the wires were threaded through the ± 0.5 mm, ± 1.5 mm, ± 2.5 mm and ± 3.5 mm wire-holes so that each wire was located 1 mm from the next one. This was done on both sides of the Wire Guider where corresponding hole-groups were located.

However, as there were sixteen holes in each hole-group, but only eight holes had been utilised, this left half of the wire-holes open. In a fashion similar to that done in sewing, these open holes were used to "double-thread" the wires in order to fasten them tightly in place. This also allowed the wires to be tightened so that they were stretched taught across the Wire Guider and didn't slip out of position. Note that this double-threading was also performed for the 2-wire set-up.

The enamel on the ends of each wire was stripped and these ends were soldered together onto a thicker wire that was less fragile. This was important as crocodile-clips and probes needed to be connected to the wires without damaging them. For the 8-wire set-up, it was ensured that adjacent wires were soldered together onto different wires. In other words, if the wires had been numbered from one to eight according to their position, all of the wires with even numbers would have been soldered together and all of the wires with odd numbers would have been soldered together. This was done to ensure that the polarities of adjacent wires were opposite. An example of the wire-threading is shown in Figure 6.1.3.

Although the dielectric strength of the insulation of the wires was far greater than the voltages to be used between the wires, insulation tape was wrapped between the layers of wires that had opposite polarity (on the ends of the Wire Guider) as an extra precaution in case any of the wires had defects in their insulation.

6.1.4 Clamping and sealing

The clamping and sealing required several steps which are listed below:

- A thin cotton-wool cushion was placed onto the Slide Platform, and the glass slide was placed onto the cushion. The cushion evened out the force on the glass slide and prevented it from cracking.
- The Slide Platform was then raised into the rectangular cut-out in the centre of the Wire Guider so that the wires were pressed up against the glass slide.

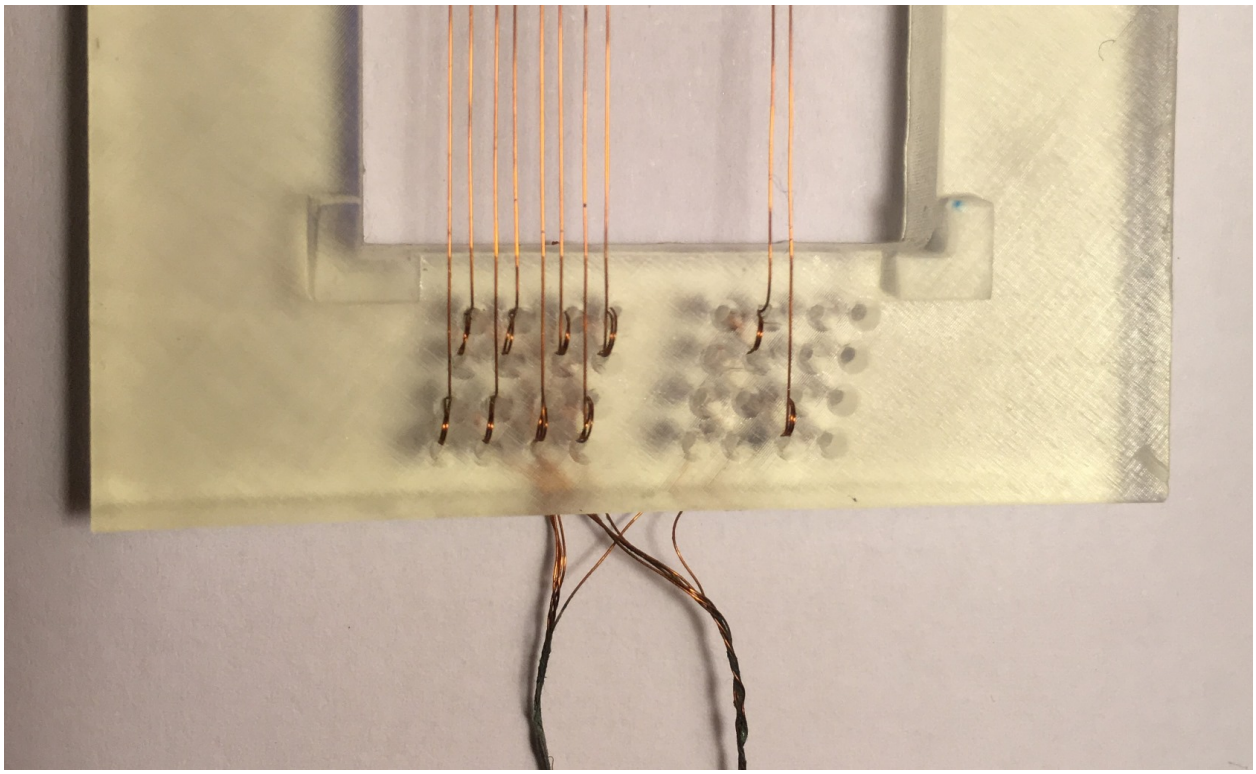


Figure 6.1.3: Threaded wires for a 8-wire set-up (left) and a 2-wire set-up (right).

- A thin layer or petroleum jelly (Vaseline BlueSeal Original) was applied to the underside of the customised gasket and the gasket was placed in position on the glass slide, on top of the wires.
- The well-assembly was placed onto the gasket such that the protrusions on the gasket fitted into the corresponding indent of the well-assembly.
- The Clamp Brace was placed on top of the well-assembly so that the tops of the eight wells protruded through the eight holes in the Clamp Brace.
- A single spring-clamp (Tork Craft 30 mm) was placed over the centre of the assembly in order to fix all of the components into place. It had its pads resting on the bottom of the Slide Platform and the top of the Clamp Brace.
- The remaining spring-clamps (Tork Craft 30 mm) were placed around the assembly in an alternating fashion to ensure that the forces applied to any one side were balanced. Six spring-clamps were used for this.
- The central spring-clamp was removed.

The wires were inspected through the holes in the Clamp Brace to ensure that wires were still parallel and located centrally across the culture surface of each well. The sealed assembly

with the lid on is shown in Figure 6.1.4 and the wires viewed through the sealed assembly are shown in Figure 6.1.5.

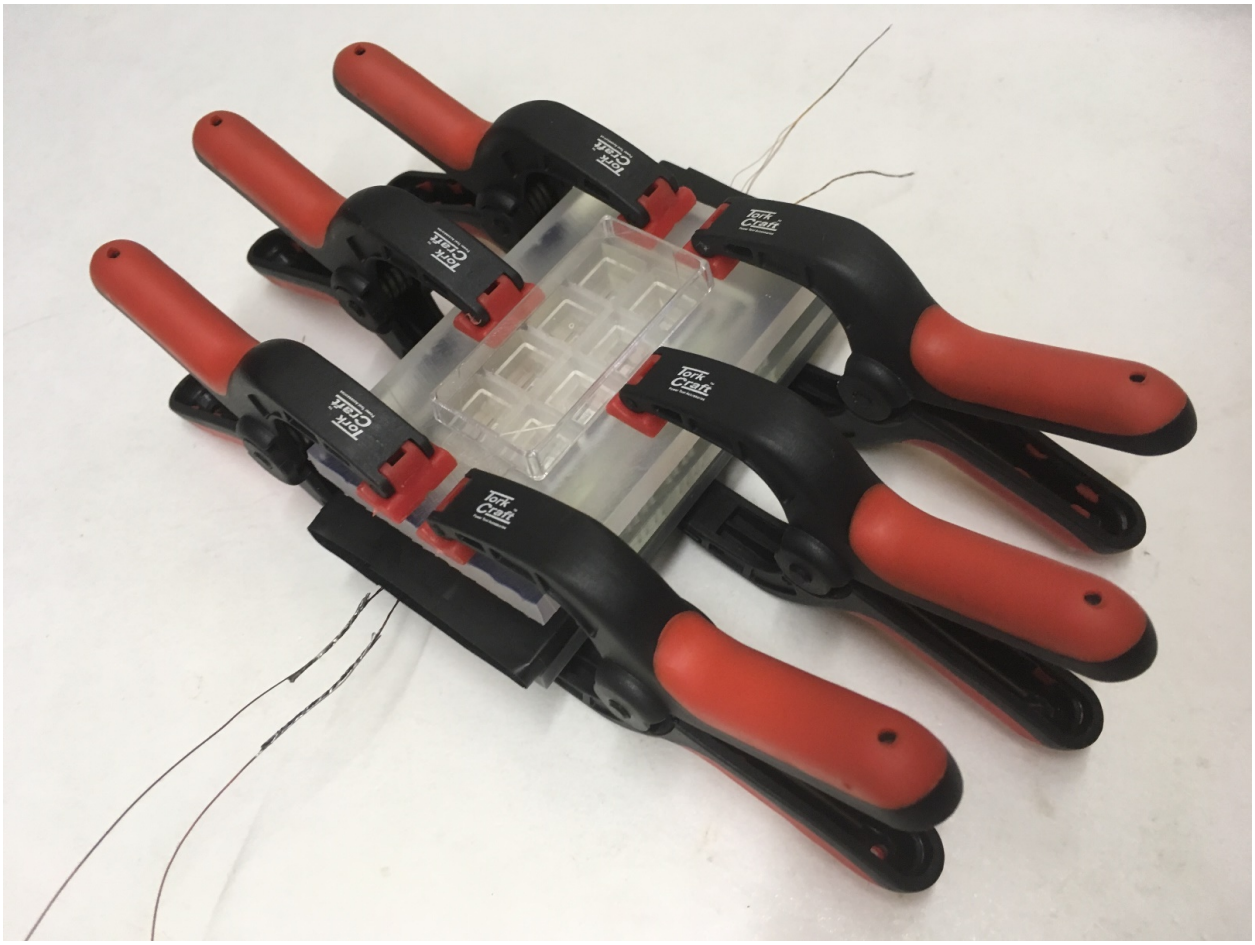


Figure 6.1.4: Sealed assembly.

6.1.5 Sterilisation

Working in a Labotec Level 2 sterile biohazard cabinet fitted with High Efficiency Particulate Air (HEPA) filters, the sealed assembly (along with the lid and the Lid Spacer) was sterilised using a 70 % ethanol solution. Excess petroleum jelly that had been squeezed out from under the gasket during the clamping was also removed by this ethanol solution. The components were then rinsed twice with sterile Phosphate Buffered Saline (PBS), pH 7.4, to remove any residual ethanol, and left to dry in the sterile biohazard cabinet.

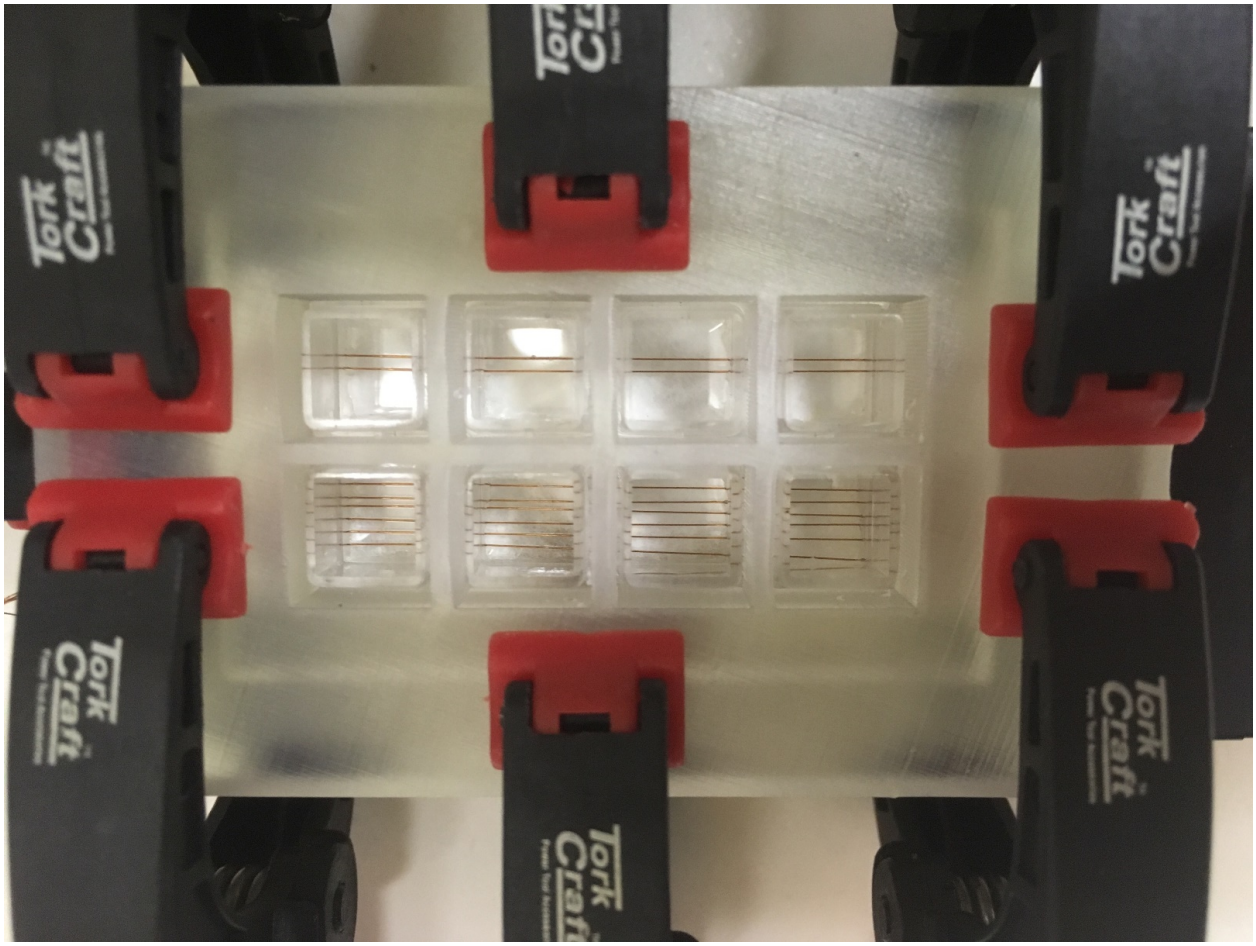


Figure 6.1.5: Wires visible in the sealed assembly.

6.1.6 Cell culture technique

A sterile, internal-thread-with-sealing-ring cryovial (Corning) of previously cryopreserved cells in 1 mL of freeze medium, was taken from the Liquid Nitrogen (-178 °C) tank (Afrox, SA) and rapidly thawed in sterile water at 40 °C. The freeze media consisted of sterile, neat Foetal Calf Serum (FCS) (Sigma) with 10 % (v/v) sterile, cell culture grade Dimethyl Sulphoxide (DMSO) (Sigma) added to it. The purpose of the DMSO was to prevent ice crystals from forming during the freezing process as the sharp edges of ice crystals damage the cell membranes and thus kill the cells.

Once thawed, the 1 mL cell solution was placed into a sterile 15 mL graduated polypropylene conical centrifuge tube (Corning). The tube was filled to the 12 mL mark with a pre-warmed (37 °C) cell culture media mixture composed of a 1:1 mix of standard Dulbecco's Modified Eagle Medium (DMEM) (Sigma) and Ham's F12 Nutrient Mixture (Sigma) supplemented with 10 % FCS (Sigma) and 1 % Penicillin-Streptomycin (P/S) (Sigma). The tube containing

the cells in the freeze media and culture media mixture was placed in a bench-top Beckman Coulter centrifuge and centrifuged at 1000 rpm for 2 minutes in order to wash the cells free from the DMSO of the freeze media, which can be toxic to cells at 37 °C.

Upon centrifugation, the cells formed a firm cell pellet at the bottom of the tube. The supernatant freeze media and culture media were poured off and the cell pellet was carefully resuspended by adding 1 mL of culture medium to it with a 1 mL pipette and slowly pipetting the cell solution up-and-down several times in order to form a single cell suspension.

This cell solution was then placed into a sterile 25 cm^2 cell culture flask with a vented lid, containing 25 mL of the described pre-warmed cell culture medium. The flask was gently swirled a few times to ensure an even distribution of the cells. The flask was then placed flat on a sterile shelf in a Forma Scientific water-jacketed incubator set at 37 °C and 8 % CO_2, with the CO_2 being supplied by an Afrox medical CO_2 cylinder which was located next to the incubator.

The flask of cells was checked every morning under an inverted microscope at 100 times magnification to establish the condition of the cells, and to estimate the percentage confluency. When the cells reached a confluency of approximately 80 % (in other words, the cells were in the log growth phase), the culture medium was poured off into a sterile glass beaker in the sterile biohazard cabinet. The flask was rinsed with 5 mL of sterile PBS, to remove any residual FCS which would inactivate the trypsin mixture (Sigma) used next for lifting the cells from the flask's culture surface.

Since the cells used in this research were adherent in nature, the enzymatic activity of 0.1 % trypsin mixed with 0.01 % ethylenediamine tetraacetic acid (EDTA) was needed to loosen the cells from the flask's culture surface and to loosen the cells from one another. The EDTA inhibits the cell-to-cell adherent effect of Ca^{2+} ions in the cell membranes and, together with the enzymatic activity of trypsin, the cells could be resuspended into a single cell-suspension in 1 mL of culture medium, to be counted.

The cells were counted manually using a standard haemocytometer and a bright-field microscope at 100 times magnification. The total cell count was noted and a calculation was performed to determine the number of cells/μL needed to result in 100 000 cells per 10 μL per well of the Nunc Lab-Tek Chamber Slide. This calculation was to ensure the plating density mentioned in Section 4.3.2.2 was achieved. After the calculation was confirmed, the cells were ready to be plated.

6.1.7 Cell proliferation dye preparation

The cell proliferation dye solution was prepared by adding 7.05 g of resazurin powder to 50 mL of the previously mentioned cell culture medium, thereby forming a solution with a concentration of 0.141 mg/mL. After the treatment, this dye solution was added directly to the empty wells and was not diluted any further.

6.1.8 Creation and loading of broadband signal

The broadband signal was created in Octave by summing sinusoids in the time domain. 201 sinusoids were summed (100 kHz to 300 kHz in 1 kHz increments) and the phases of each sinusoid was chosen so that the overall signal created had the lowest peak-to-peak value. This assignment of phase was automatically performed by a script which ran through a few million iterations of phase-assignments and chose the set of phases that minimised the peak-to-peak value. The signal that was used is shown in Figure 6.1.6, along with its one-sided FFT in Figure 6.1.7, and its power spectral density in Figure 6.1.8. Note that a uniform distribution was used for the amplitudes of the frequencies in the desired band.

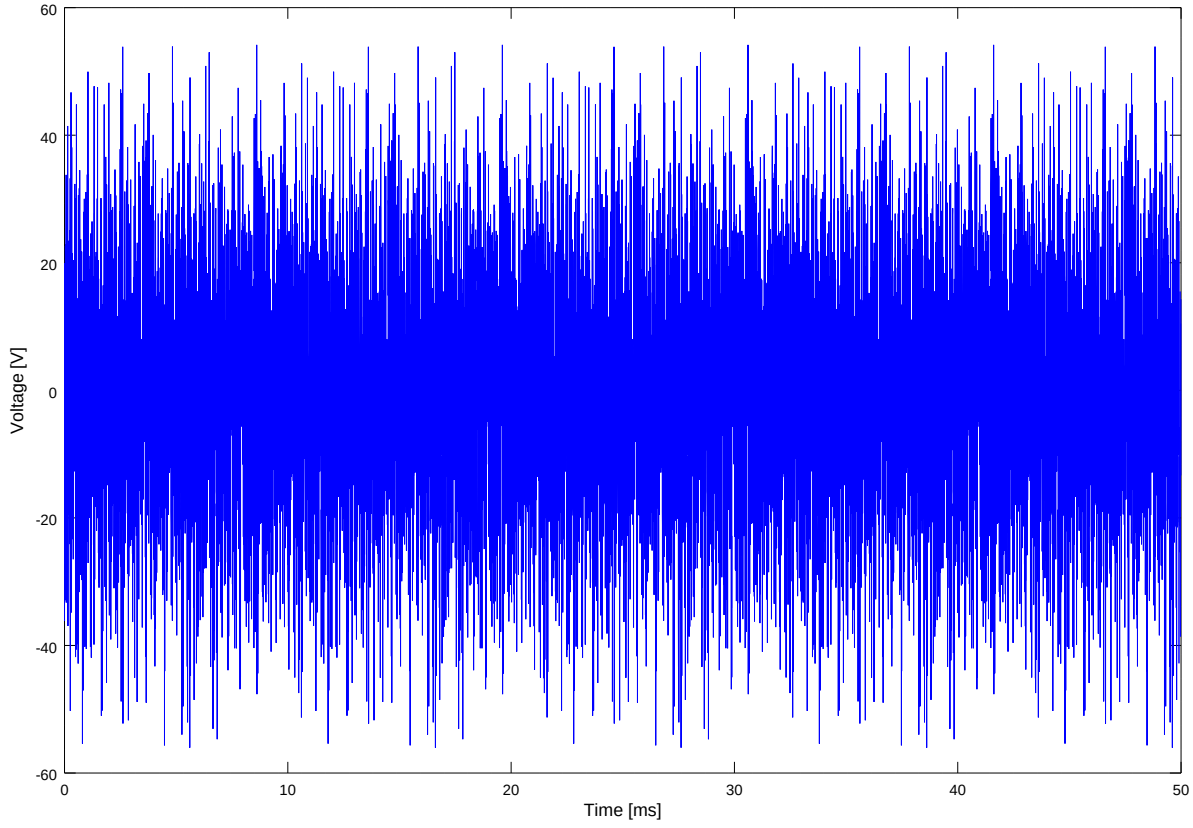


Figure 6.1.6: Time-domain of the broadband signal.

The parameters of the broadband signal are listed in Table 6.1 using the same nomenclature introduced in Section 2.2.

The signal created in Octave was saved as a *.csv* file, which was then converted to a *.tfw* format using Tektronix's ArbExpress software. The signal was then loaded onto an Arbitrary Function Generator (Tektronix AFG 3022B) and outputted using the Arbitrary Waveform

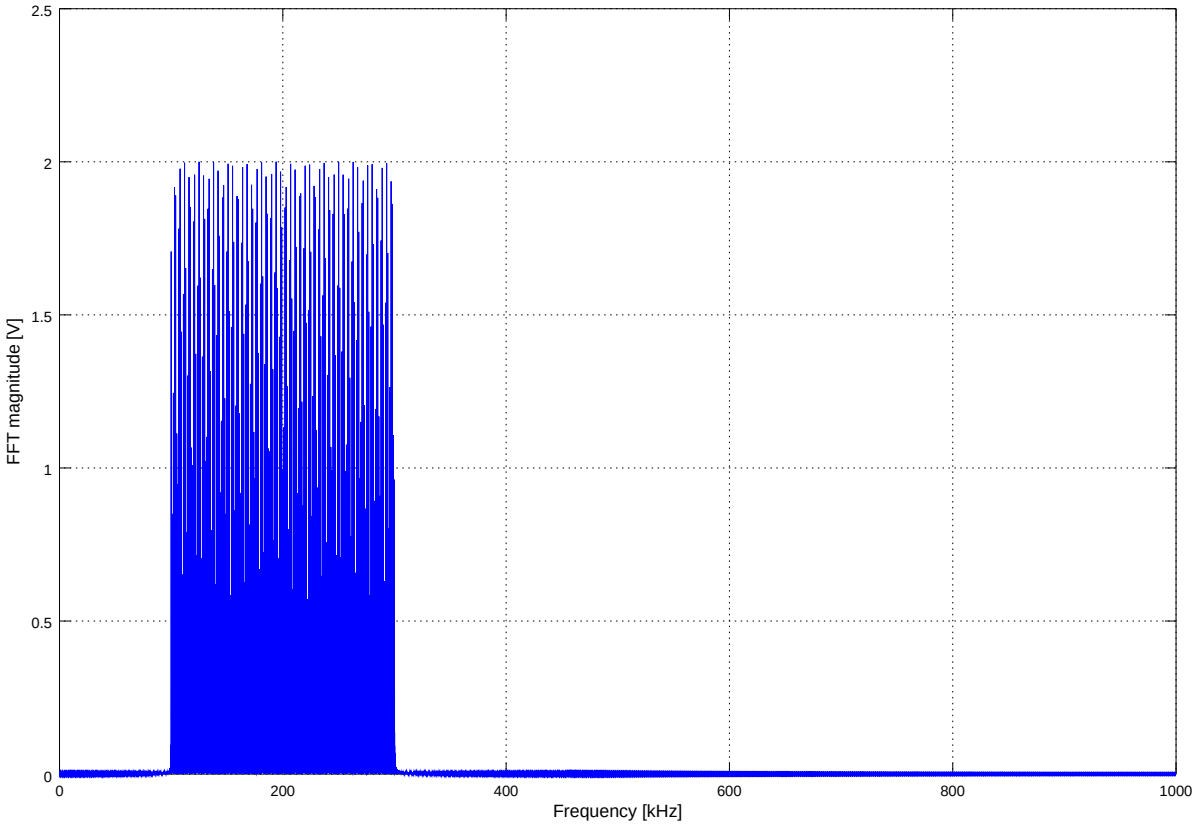


Figure 6.1.7: Single-sided FFT of the broadband signal.

Table 6.1: Parameters of the broadband signal.

Symbol	Description	Value	Units	Notes
Ω_0	First frequency included	$200\pi \times 10^3$	rad/sample	Corresponds to 100 kHz
Ω_{N-1}	Last frequency included	$600\pi \times 10^3$	rad/sample	Corresponds to 300 kHz
$\Delta\Omega$	Frequency resolution	$2\pi \times 10^3$	rad/sample	Corresponds to 1 kHz
N	Number of superimposed sinusoids	201	—	
A	Amplitude of each sinusoid	2	V	Peak amplitude
θ_i	Phase of the i^{th} sinusoid	$\theta_i \in [0, 2\pi)$	rad	Chosen to minimise the summed amplitude
F_s	Sampling frequency	2	MHz	
T_s	Sampling period	0.5	μs	
N_0	Number of samples in time-domain signal	100×10^3	samples	

option which loads the entire signal into memory and allows for the amplitude and frequency for the entire signal to be specified. The signal had 100 000 points sampled at a sampling frequency of 2 MHz and so the period of the whole signal was calculated as

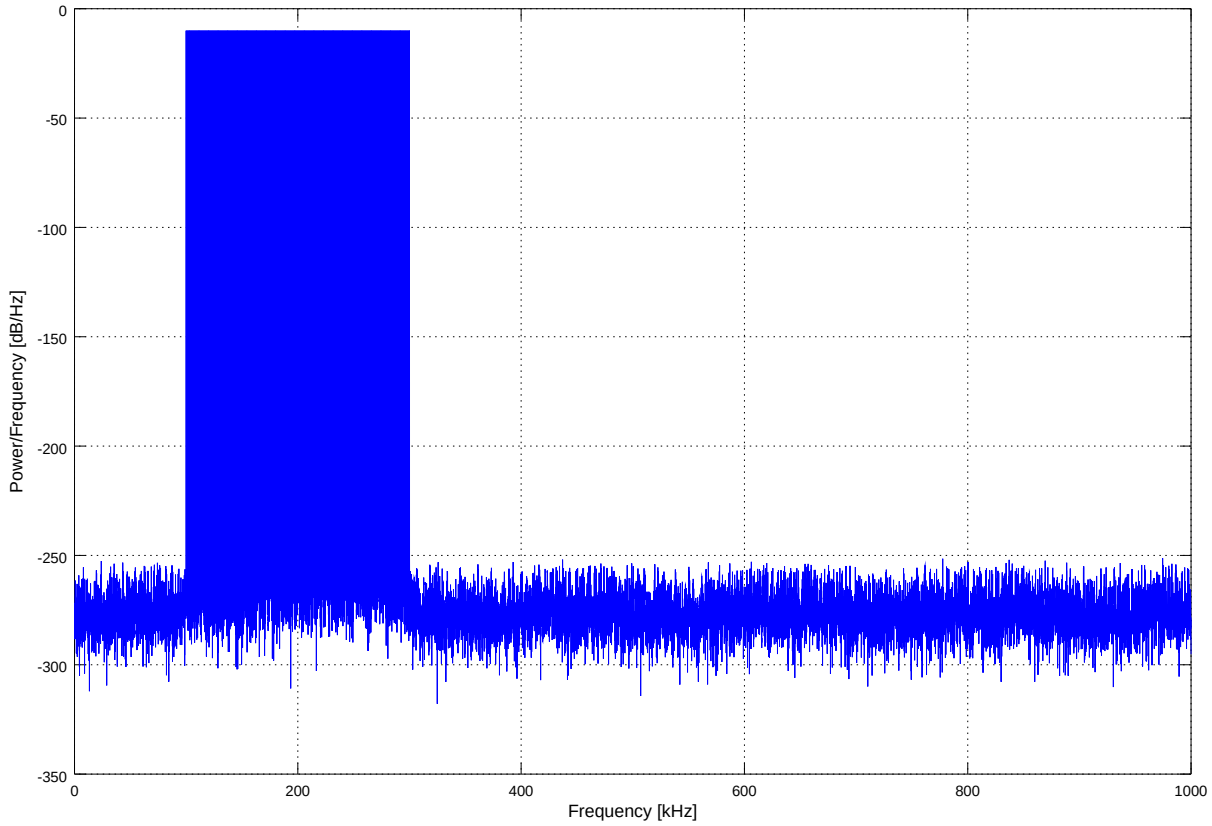


Figure 6.1.8: Power spectral density of the broadband signal.

$$\begin{aligned} T &= L \times T_s \\ &= 0.05\,\text{s} \\ &= 50\,\text{ms} \end{aligned}$$

where

T = period of whole signal
L = number of points in whole signal
T_s = sampling period

This period of 50 ms corresponds to a frequency of 20 Hz for the whole signal. The output impedance of the function generator was set to its high impedance setting and the amplitude of the signal was set to its maximum of $20\,\text{V}_{p-p}$ with a 0 V offset. This signal was then inputted into a Wideband Power Amplifier (Krohn-Hite Corporation Model 7500) which

amplified the signal to the required $110\,V_{p-p}$ with a 0 V offset. The $110\,V_{p-p}$ was calculated so that each of the 201 frequencies present had an amplitude of 2 V, as is evident in Figures 6.1.6 and 6.1.7.

6.2 Experimental procedure

The experimental procedure used was similar to that used by Kirson *et al.* for their *in vitro* experiments [8]. 100 000 cells in 10 μL of culture medium were plated in the centre of each well. The cells were left for one hour to settle and attach to the slide, before 490 μL of culture medium was added to make 500 μL of culture medium in total. Care was taken to ensure that the initial 10 μL did not evaporate.

The cells were then placed in an incubator at 37 °C with 8 % CO_2 and left to grow for a control period of 24 hours. After this period, the culture medium was replaced with fresh medium and the treatment signals were connected to the wires on the sealed assemblies. The cells were treated for 24 hours before the cell proliferation was quantified.

The electrical signals for the single-frequency treatment were created by an Arbitrary Function Generator (Tektronix AFG 3021B) which was set to output a signal of $4\,V_{p-p}$ with a 0 V offset at 150 kHz. Note that this voltage corresponded to an amplitude of 2 V. It must also be emphasised that a frequency of 150 kHz was used as it had been identified as the optimal treatment-frequency for the MCF-7 cell-line [48]. The output of the Arbitrary Function Generator was connected directly to the wires which were being used to deliver the single-frequency treatment.

As mentioned in Section 6.1.8, the broadband signal was loaded onto an Arbitrary Function Generator which then passed the signal through an amplifier to generate the required voltage of $110\,V_{p-p}$ with a 0 V offset. The output of the amplifier was connected directly to the wires which were being used to deliver the broadband treatment. The validity of all of the signals were confirmed on an oscilloscope (Tektronix DPO4034) which provided frequency, peak-to-peak amplitude, and FFT measurements.

The equipment that was used is labelled and shown in Figure 6.2.1, and the inside of the incubator is shown in Figure 6.2.2. There was a small hole in the rear of the incubator that allowed for the cables from the oscilloscope, signal generator and amplifier to pass through from the outside to the inside of the incubator.

6.3 Quantification of results

Once the treatment period was completed, the sealed assemblies were taken out of the incubator and the temperature of the wells was measured without delay using an infrared

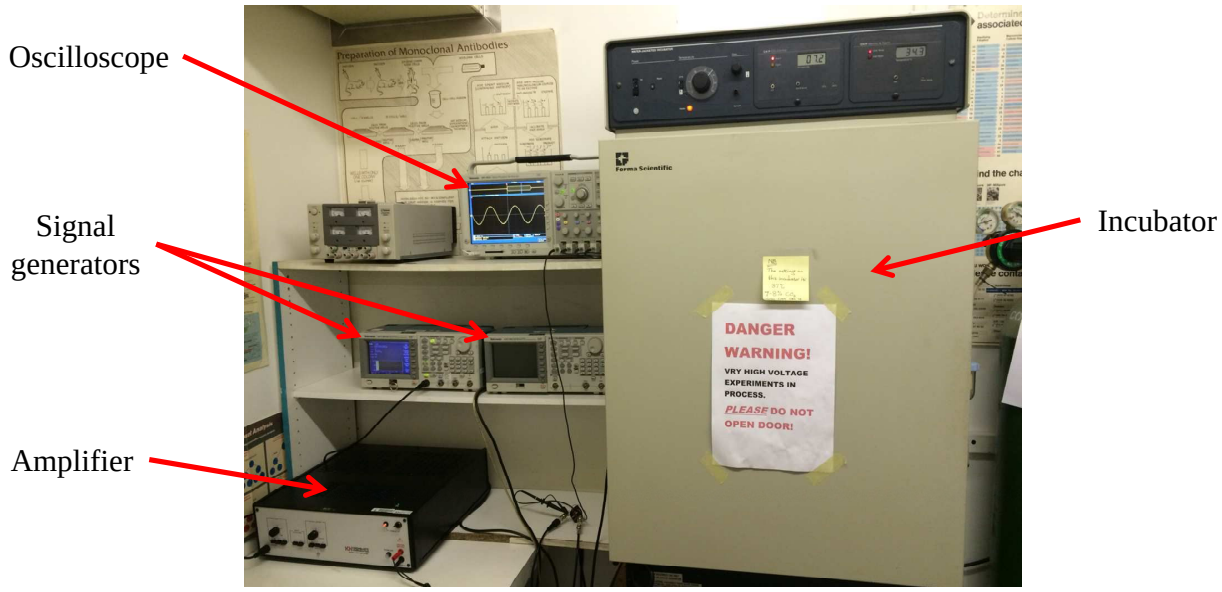


Figure 6.2.1: Laboratory set-up.

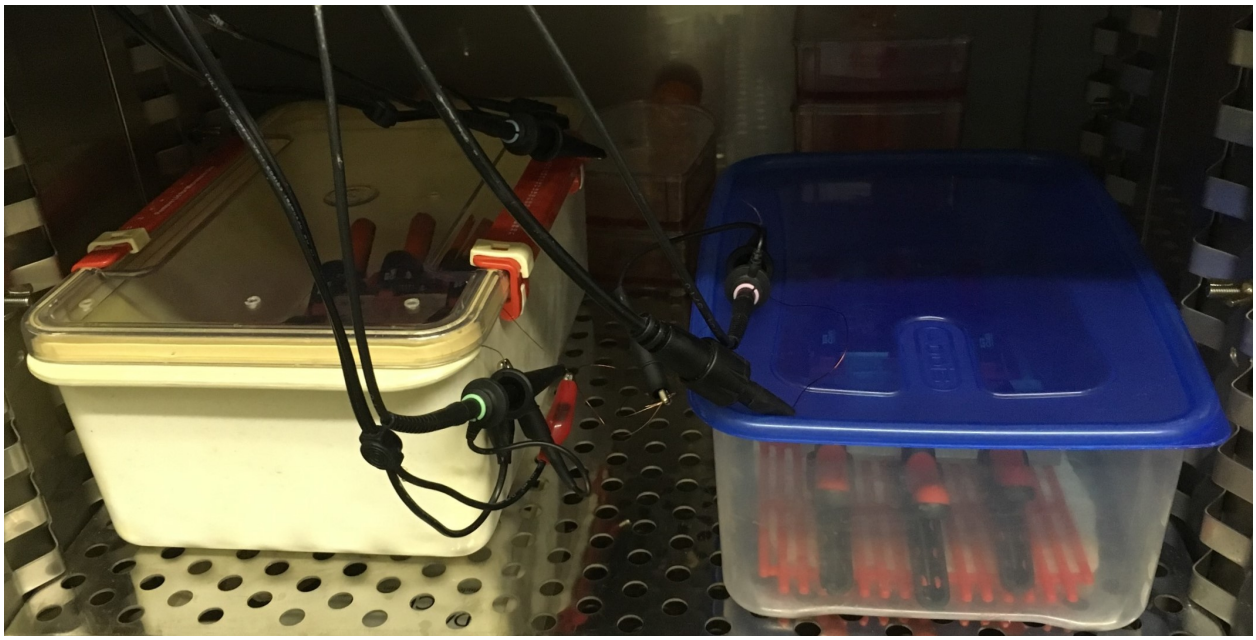
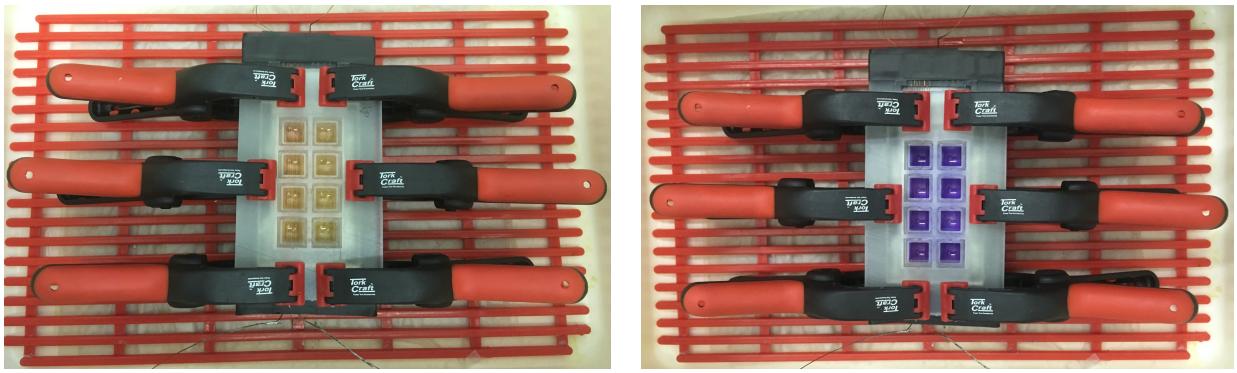


Figure 6.2.2: Inside of the incubator.

thermometer (EeziTemp DT-8806). The sealed assemblies were then placed inside the sterile biohazard cabinet and the culture medium in each well was sucked off using a pipette. The fluid was immediately replaced with 500 μL of dye solution. Figure 6.3.1 shows the sealed assembly with the wells containing culture medium (Figure 6.3.1a) and dye solution (Figure 6.3.1b).



(a) With culture medium in the wells.

(b) With dye in the wells.

Figure 6.3.1: Sealed assembly.

The sealed assemblies were then returned to the incubator and left for one hour to allow for the cells to reduce the dye solution. After this period, the sealed assemblies were taken out of the incubator and placed in the sterile biohazard cabinet once again.

Four 100 μL aliquots were taken from each well and pipetted into a sterile, flat-bottomed, 96-well cell culture plate using the reverse pipetting technique to ensure that no air bubbles were created. Each time that aliquots were taken from a different well, the pipette tip was replaced with a new one to ensure that no cross-contamination of the solutions occurred. As each test had four individual wells, four pipette tips were used and a total of 16 aliquots were taken per test. 16 blank aliquots (containing only the cell culture medium) and 16 aliquots for the negative control (containing only the dye solution) were also taken.

Figure 6.3.2 shows an example of a 96-well plate containing aliquots from one of the experiments. The first two columns contained the blank aliquots, the next two contained the aliquots from the negative control and the remaining columns contained aliquots from the sealed assemblies. Note that the eight empty wells seen in Figure 6.3.2 are as a result of two of the wells leaking, thereby deeming their contents invalid for that experiment. Although it is difficult to see in this figure, the aliquots from the sealed assemblies have reduced the dye slightly, turning it from the deep blue colour of the negative control, to a more purple hue.

The 96-well plates containing the aliquots were taken to a spectrophotometer (BioTek Synergy HT) and the absorbance of each well was read at wavelengths of 570 nm and 600 nm. The absorbance data was then analysed in accordance with the equations provided in [37]. The spectrophotometer that was used to obtain the absorbance readings is shown in Figure 6.3.3.

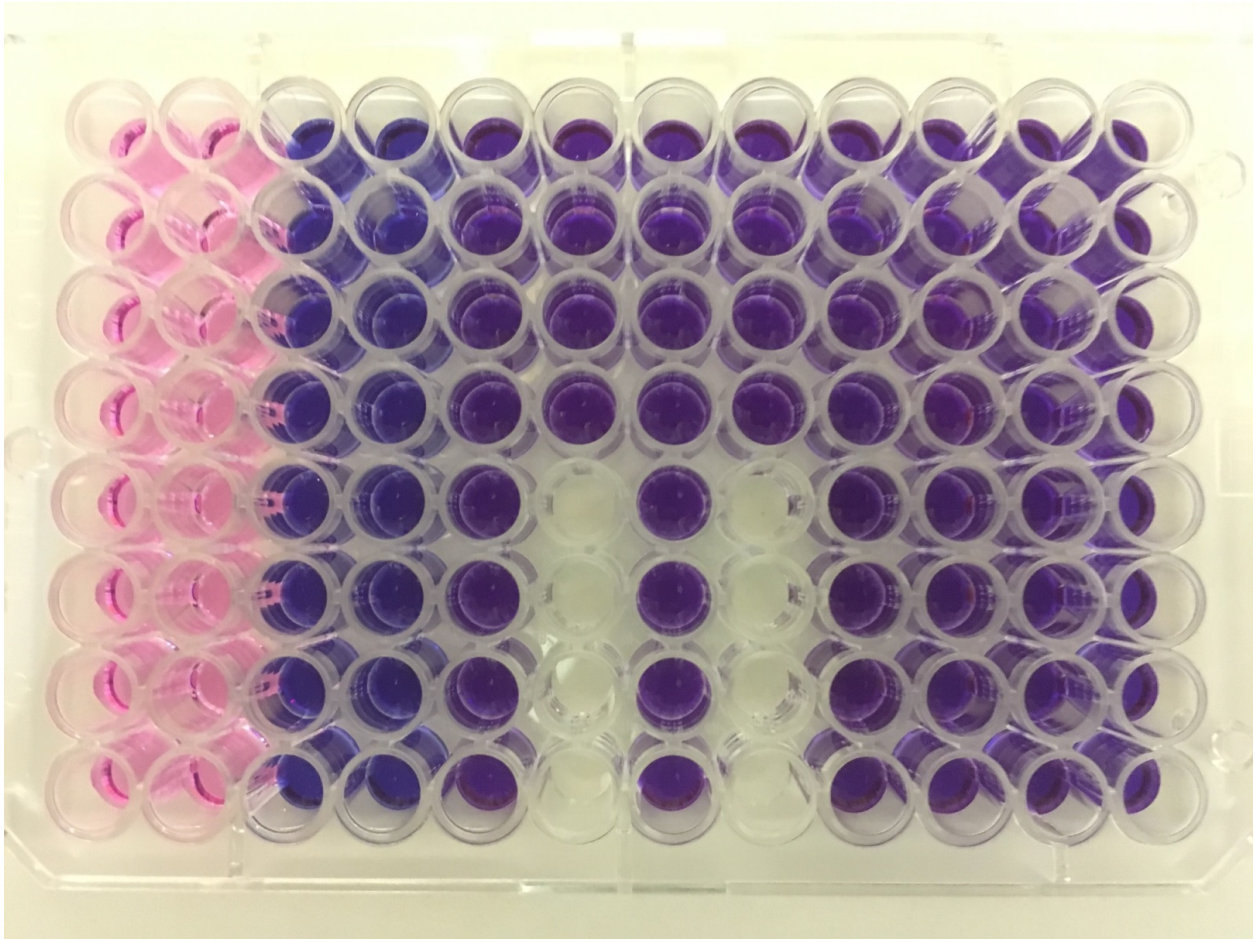


Figure 6.3.2: 96-well plate with aliquots.



Figure 6.3.3: The spectrophotometer that was used.

Chapter 7

Results

The experimental results are detailed in this chapter. Section 7.1 explains the nomenclature used in the presentation of the results, Section 7.2 presents various sets of results and Section 7.3 contains a summary and an analysis of the results.

7.1 Nomenclature

Before the results are presented, it is important to understand the nomenclature used for the controls. In these experiments, a positive control was defined as a set of untreated wells that had cells plated in them. This was different to a negative control, which was defined as a set of untreated wells that had no cells plated in them.

Positive controls contain cells that are growing without any inhibition, and they therefore dictate the maximum expected proliferation rate of the cells, and therefore the maximum expected reduction rate of the dye. When the calculations are performed, the percentage reduction of the dye for a set of wells is always reported with reference to the negative control, which has no cell proliferation and therefore no change in the reduction of the dye.

The inhibition of proliferation for a set of wells is normalised with reference to the positive control. In these experiments, the positive control chosen to normalise all the other data was the positive control that contained eight wires in the cell culture. The values were normalised such that this positive control had a 0 % inhibition of proliferation. Therefore, positive values for this measure indicated proliferation-inhibition, whilst negative values indicated proliferation-stimulation. For more information on this normalisation, the reader is advised to consult the Alamar Blue protocol [37]. Note that the term "inhibition of proliferation" used in this research is equivalent to the "therapeutic enhancement ratio" term used by Kirson *et al.* in [8].

In order to assess the validity and repeatability of the measurements, the experiments were performed in two independent batches. These batches are identified in subsequent sections as Experiment Set 1 and Experiment Set 2. It should be noted that the exact same set-up, methodology and equipment was used for both batches of experiments.

The error bars in the figures below represent a standard deviation of uncertainty on either side of the mean value.

7.2 Sets of results

7.2.1 Positive controls

Three positive controls were used with the aim of determining:

- Whether the inclusion of the wires in the cell culture would have an effect on cellular proliferation
- Whether positive controls on separate culture plates would yield different results

The reduction and proliferation data for each positive control is shown in Figures 7.2.1 and 7.2.2. For each of the positive controls, the temperature of the wells was measured to be 36.7 °C for Experiment Set 1 and 36.3 °C for Experiment Set 2.

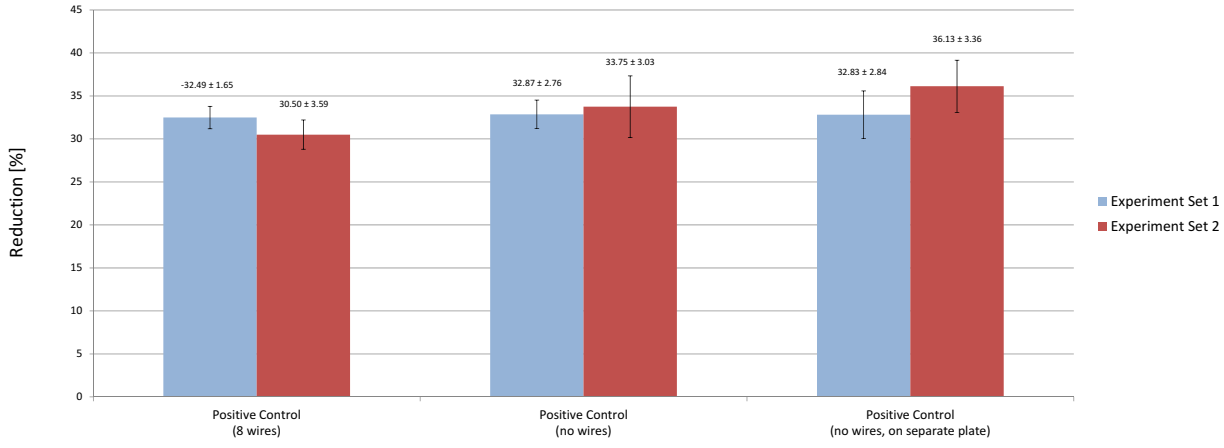


Figure 7.2.1: Reduction of the dye for the positive controls, where greater deviations between controls are evident for Experiment Set 2 when compared with Experiment Set 1.

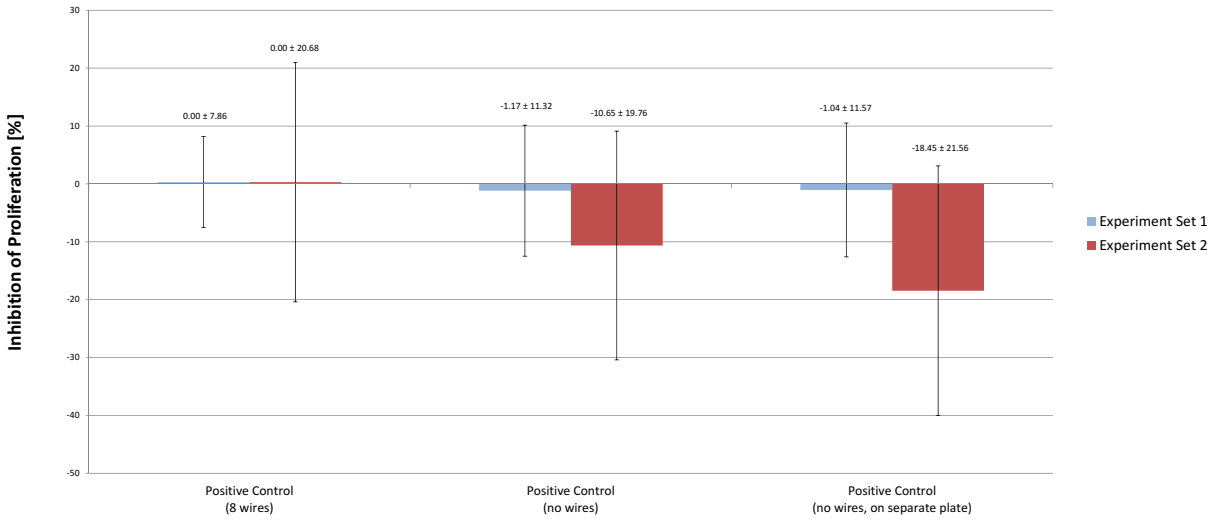


Figure 7.2.2: Normalised inhibition of proliferation for the positive controls, where Experiment Set 2 shows large uncertainties and large deviations between the various controls.

7.2.2 Multiple pairs of wires

In the experiments by Kirson *et al.*, two wires were used to deliver the electric fields, and the cells were cultured between the wires and allowed to adhere and settle before more culture medium was added [8]. In the experiments performed for this research, it was found that the cells spread out across the entire culture surface, even if they had been allowed to settle and adhere in the region only between the wires. Therefore, an experiment was initiated to determine whether using multiple pairs of wires to subject the entire culture surface to the treatment would yield better results.

The reduction and proliferation data for the wells undergoing treatment with two wires and with eight wires are shown in Figures 7.2.3 and 7.2.4. As mentioned in Chapter 6, the exact same voltages were used on each pair of wires in order to produce the same electric fields in the cell culture medium. Note that the voltages displayed in the figures are peak-to-peak voltages. For both the 2-wire and 8-wire treatments, the temperature of the wells was measured to be 36.7 °C for Experiment Set 1 and 36.3 °C for Experiment Set 2.

7.2.3 Broadband treatment

In this experiment, eight wires were used to deliver the electric fields for both the single-frequency treatment and the broadband treatment. The reduction and proliferation data

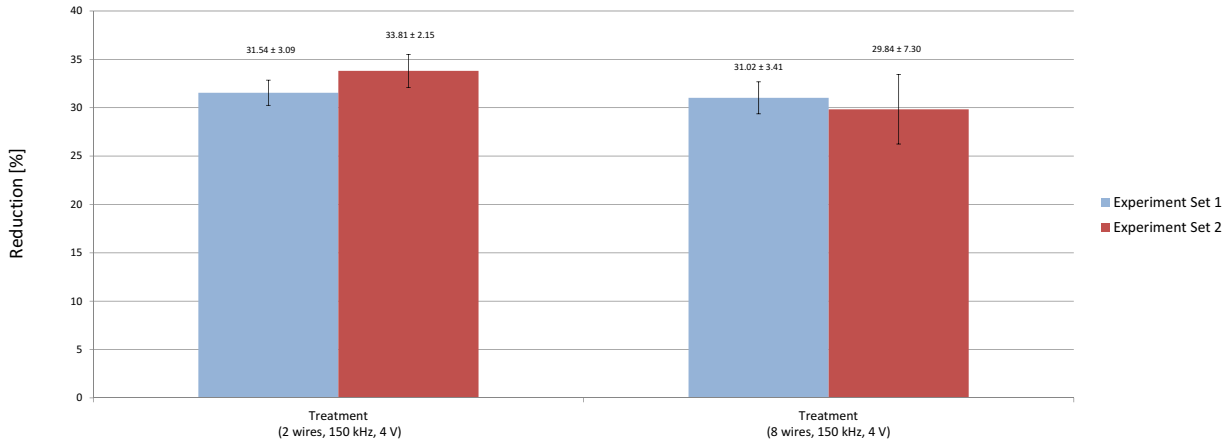


Figure 7.2.3: Reduction of the dye in the test comparing the efficacies of treatment using 2 wires and 8 wires, where Experiment Set 1 shows very similar reductions but Experiment Set 2 shows a lowered reduction for the 8-wire treatment.

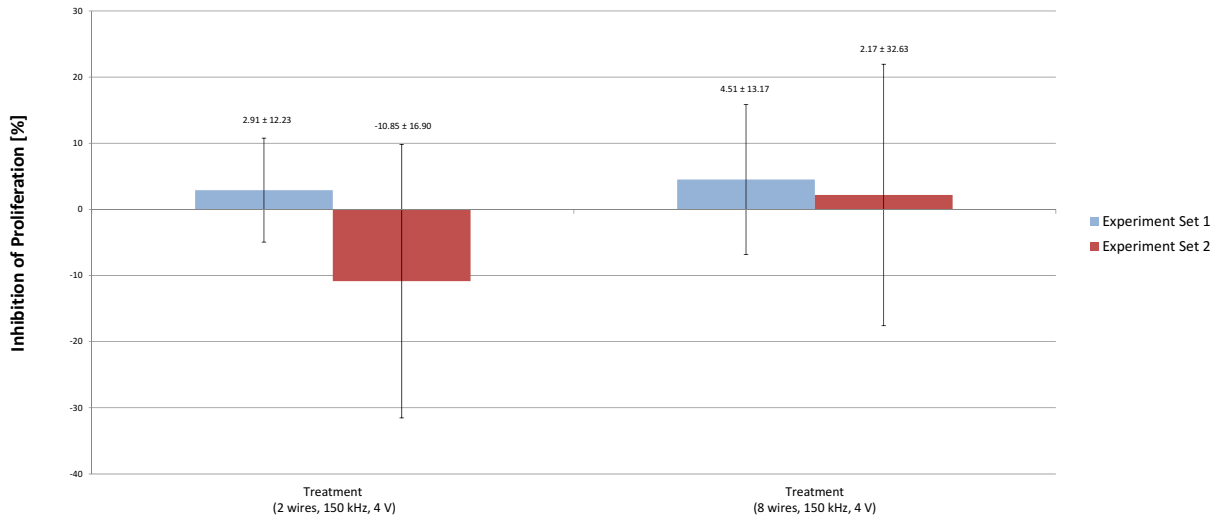


Figure 7.2.4: Normalised inhibition of proliferation for the cells undergoing treatment using 2 wires and 8 wires. The 2-wire treatment for Experiment Set 2 appears to stimulate cell proliferation instead of inhibiting it.

for the wells undergoing each type of treatment are presented in Figures 7.2.5 and 7.2.6. Note that the voltages displayed in the figures are peak-to-peak voltages. For both types of treatment, the temperature of the wells was measured to be 36.7 °C for Experiment Set 1 and 36.3 °C for Experiment Set 2.

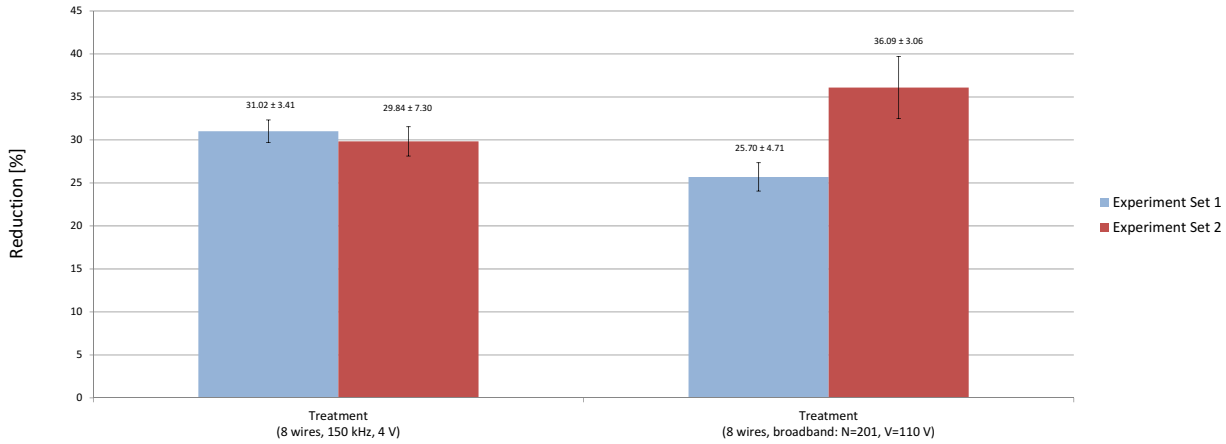


Figure 7.2.5: Reduction of the dye in the test comparing the efficacies of single-frequency treatment and broadband treatment. The experiment sets display opposite trends with Experiment Set 2 showing an increase in reduction for the broadband treatment.

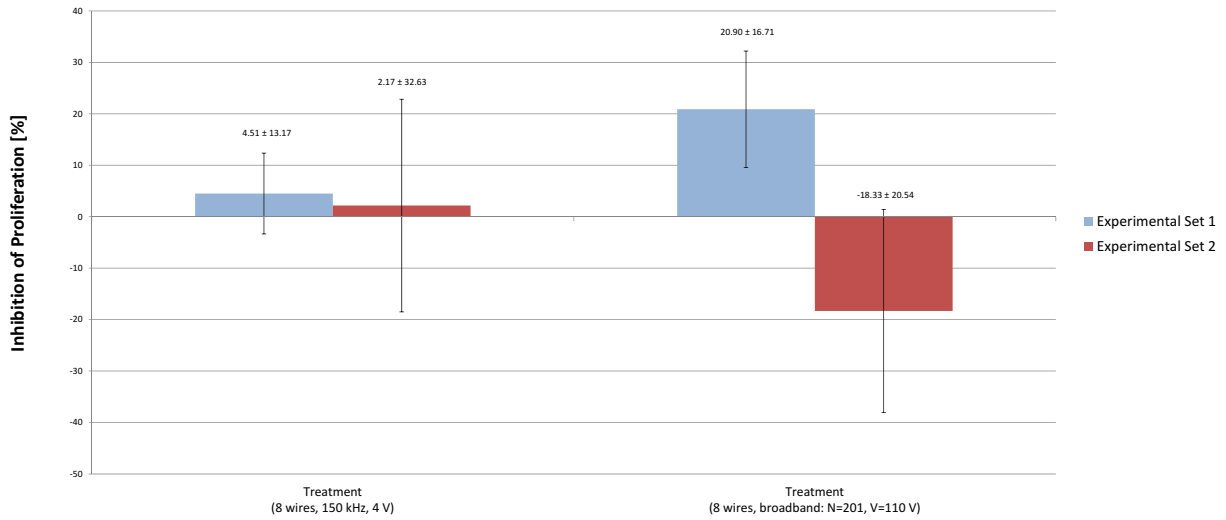


Figure 7.2.6: Normalised inhibition of proliferation for the cells undergoing single-frequency treatment and broadband treatment. The broadband treatment in Experiment Set 2 appears to be stimulating cell proliferation instead of inhibiting it.

7.3 Summary and analysis

The reduction and proliferation data for all of the experiments are superimposed and shown in Figures 7.3.1 and 7.3.2. Note that, although the single-frequency treatment was performed

using both an 8-wire and a 2-wire set-up, the broadband treatment was performed using only an 8-wire set-up and not a 2-wire set-up.

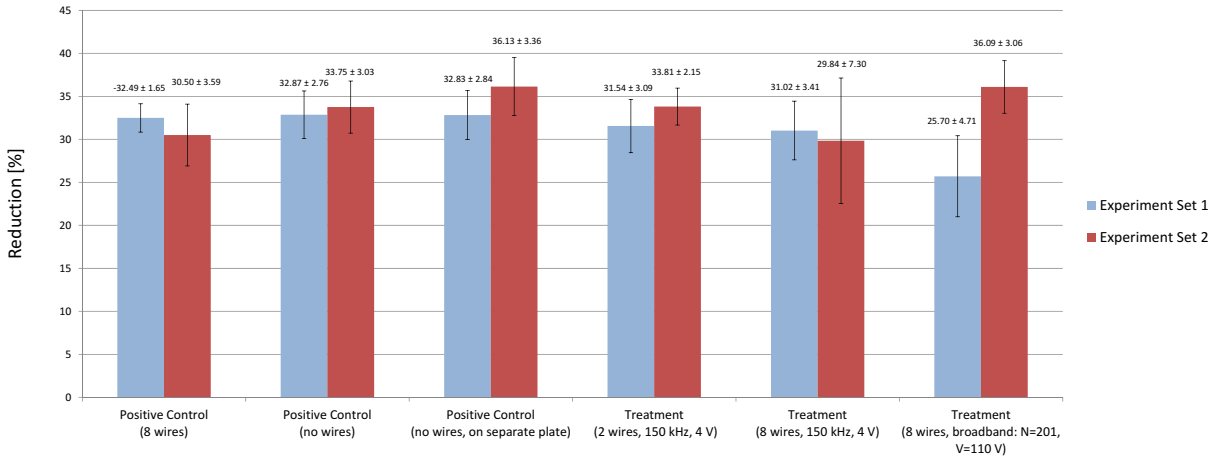


Figure 7.3.1: Percent reduction data showing large uncertainties in both experiment sets.

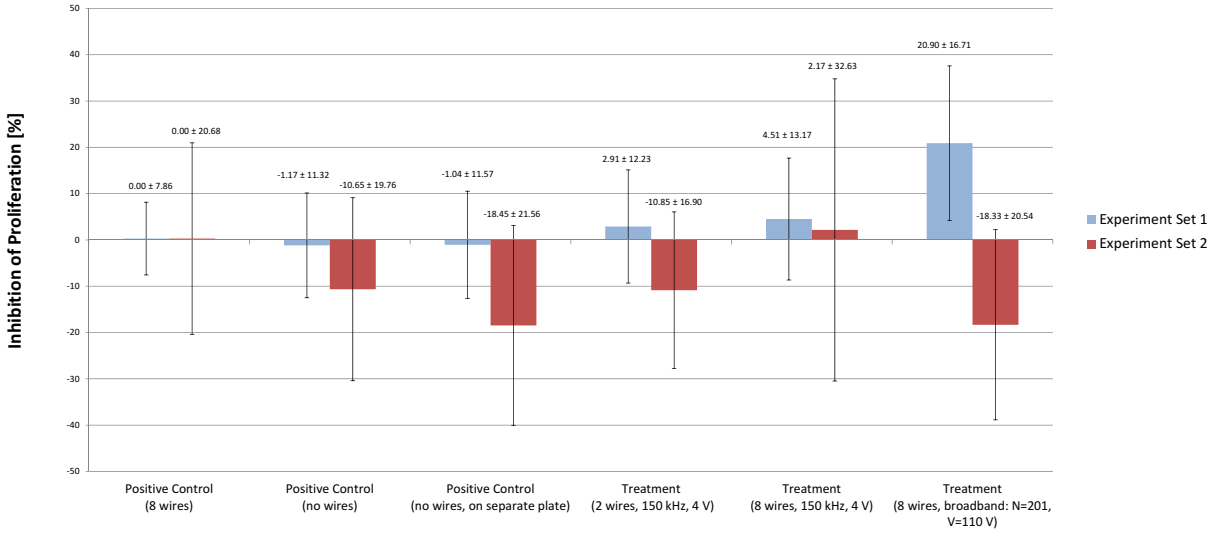


Figure 7.3.2: Normalised inhibition of proliferation data showing large uncertainties and no convincing trends between experiment sets.

In these figures, it can be seen that for Experiment Set 1:

- The positive controls are all fairly similar
- The treatment using eight wires is marginally better than the treatment using two wires

- The broadband treatment is significantly better than the single-frequency treatment

However, for Experiment Set 2, these trends are no longer apparent and it can be seen that:

- The controls vary greatly
- The treatment using eight wires is significantly better than the treatment using two wires
- The broadband treatment is significantly worse that the single-frequency treatment

This variation in results is worrying and attention must be drawn to the large uncertainties in the measurements. Despite the attempts to minimise these uncertainties by using a high dye concentration, ensuring aliquots were reverse pipetted, and using 16 samples per datum, analysis of the uncertainty propagation showed that the small measurement uncertainties resulted in surprisingly large uncertainties after all the calculations were performed. Each calculation required five scalar multiplications, two subtractions and one division. With each of these operations, the uncertainty increased.

Table 7.1 lists the mean values ($\bar{x}$) and the standard deviations (σ) for the reduction data for each series seen in Figure 7.3.1, and Table 7.2 lists the same statistical measures for the inhibition of proliferation data for each series seen in Figure 7.3.2. In these tables, the data for the negative controls (to which all the other values are normalised) are also included. It should be noted that there was a large difference between the mean values of the negative controls between the two experiment sets. The reason for this difference is unknown as the same dye, concentration of dye, and equipment were used for both experiment sets.

Table 7.1: Percent reduction data showing large uncertainties for the two experiment sets.

Series	**Experiment Set 1**		**Experiment Set 2**	
	$\bar{x}$	σ	$\bar{x}$	σ
Negative Control	10.17	1.30	20.74	1.70
Positive Control (8 wires)	32.49	1.65	30.50	3.59
Positive Control (no wires)	32.87	2.76	33.75	3.03
Positive Control (no wires, separate plate)	32.83	2.84	36.13	3.36
Treatment (2 wires, 150 kHz, 4 V)	31.54	3.09	33.81	2.15
Treatment (8 wires, 150 kHz, 4 V)	31.02	3.41	29.84	7.30
Treatment (8 wires, broadband: N=201, V=110 V)	25.70	4.71	36.09	3.06

The large uncertainties open up the question as to whether the results are statistically significant at all. Welch's t-tests were performed on the proliferation data so that comparisons could be drawn between the results in order to ascertain if they were significantly different.

Table 7.2: Normalised inhibition of proliferation data showing large uncertainties for the two experiment sets.

Series	**Experiment Set 1**		**Experiment Set 2**	
	$\bar{x}$	σ	$\bar{x}$	σ
Positive Control (8 wires)	0.00	7.86	0.00	20.68
Positive Control (no wires)	-1.17	11.32	-10.65	19.76
Positive Control (no wires, separate plate)	-1.04	11.57	-18.45	21.56
Treatment (2 wires, 150 kHz, 4 V)	2.91	12.23	-10.85	16.90
Treatment (8 wires, 150 kHz, 4 V)	4.51	13.17	2.17	32.63
Treatment (8 wires, broadband: N=201, V=110 V)	20.90	16.71	-18.33	20.54

Table 7.3: Welch's t-tests performed on Experiment Set 1, showing a significant difference between broadband versus single-frequency treatment.

Comparison	t**-statistic**	$d.f.$	p**-value**
8-wire positive control versus 0-wire positive control	0.3396	26.74	0.73681
8-wire treatment versus 2-wire treatment	0.3561	29.84	0.72427
Broadband versus single-frequency treatment	3.0814	28.45	0.00454

Table 7.4: Welch's t-tests performed on Experiment Set 2, showing no significant difference between any of the comparisons.

Comparison	t**-statistic**	$d.f.$	p**-value**
8-wire positive control versus 0-wire positive control	1.4894	29.938	0.14684
8-wire treatment versus 2-wire treatment	1.4173	22.507	0.17009
Broadband versus single-frequency treatment	-2.1267	25.274	0.04345

These tests were performed independently for each experiment set. The parameters and results for Experiment Set 1 and Experiment Set 2 are shown in Tables 7.3 and 7.4 respectively. In both tables, $d.f.$ refers to the degrees of freedom.

Using a significance level of 0.01, the p-values in Table 7.3 indicate that for Experiment Set 1:

- The positive controls are not significantly different from each other
- The treatment using eight wires is not significantly different from the treatment using two wires
- The broadband treatment is significantly different from the single-frequency treatment

Therefore, having confidence that the result is statistically significant, it can be said that the broadband treatment in Experiment Set 1 inhibited the proliferation of the MCF-7 cells

by 16.39 % more than the equivalent single-frequency treatment. This difference translates to a 363 % increase in treatment efficacy.

However, again using a significance level of 0.01, the p-values in Table 7.4 indicate that for Experiment Set 2:

- The positive controls are not significantly different from each other
- The treatment using eight wires is not significantly different from the treatment using two wires
- The broadband treatment is not significantly different from the single-frequency treatment

The significant result from Experiment Set 1 could not be repeated in Experiment Set 2. Therefore, the claim made therefrom (of broadband treatment yielding an improved treatment efficacy) must be abandoned. Consequently, it is concluded that the treatments performed in these experiment (both the single-frequency and broadband treatments, and both in a 2-wire and 8-wire set-up) do not inhibit the proliferation of MCF-7 cells at the electric field intensities used.

Chapter 8

Ultrasound

This chapter presents a brief description of the research that was performed using ultrasound. Its contents diverge slightly from the rest of the dissertation as it was an extension of the research performed for broadband electric field treatment. However, as discussed below, it was thought that ultrasound could be a possible, alternative means of delivering energy in order to achieve the same results of TTF therapy, through taking advantage of the same mechanisms of action.

A brief introduction is given in Section 8.1, followed by a description of the preliminary experiments and the results obtained therefrom in Sections 8.2 and 8.3 respectively. The chapter is concluded with a brief discussion in Section 8.4.

8.1 Introduction

The thermal ablation of cancerous tissue using ultrasound has been well researched and documented [55], however, the use of non-thermal ultrasound in cancer treatment has also attracted attention in recent years [56]. Of particular relevance is that non-thermal ultrasound at a frequency of 1 MHz was found to induce changes in the cytoskeleton in cancer cells [57].

Additionally, Naruse predicted that the chromosome system would have a mechanical resonance at frequencies of between 22 kHz to 50 kHz during metaphase [58]. This indicates that the resonance used for TTF treatment may, in fact, be mechanical in nature. If this is indeed the case, it may be possible to use ultrasound at the same frequencies to yield similar results.

As mentioned previously, biological materials generally have high permittivities and conductivities (see [13]) which makes it difficult to establish electric fields of significant intensities

inside of them. However, unlike electric fields, ultrasound can penetrate the body with ease and is not constrained by the electrical properties of biological materials [55, 59]. Therefore, the complications that arise due to the high voltages required to produce broadband electrical fields may be circumvented by using ultrasound. This makes ultrasound particularly attractive for broadband treatment, and hence its inclusion in this research.

8.2 Preliminary experiments

A set of preliminary experiments were performed using ultrasonic treatment at frequencies in the TTF therapy range. Cells were grown in standard 24-well cell culture plates, with the controls and treated cells located on separate plates so that there would be no significant mechanical coupling between them.

Initially, the transducers were clamped directly to the underside of the wells undergoing treatment as shown in Figure 8.2.1. However, in the case of the transducer shown, this had the disadvantage of only allowing for a single well to be treated.



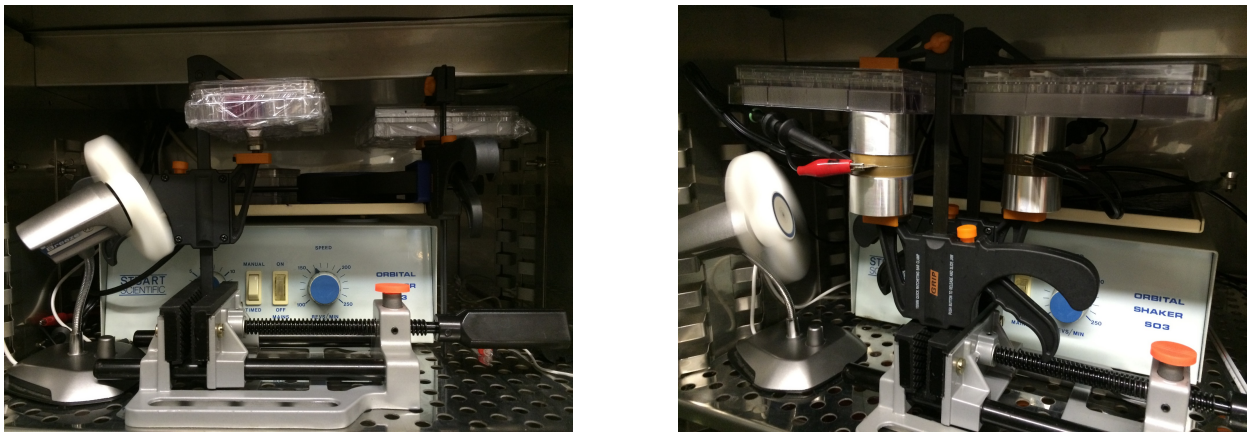
(a) Close-up view.

(b) Full view.

Figure 8.2.1: Transducer clamped to the underside of a 24-well cell culture plate.

Controlling the temperature of the transducer was also found to be difficult. In an attempt to mitigate temperature effects, a fan was used to circulate the air in the incubator, and higher-power transducers were tested. This set-up can be seen in Figure 8.2.2. However, the controlling of the temperatures of the transducers still remained an issue. Ultrasound gel was used to couple the transducers to the cell culture plates, but with the transducers heating up, the gel dried out.

A new experimental set-up was designed where the 24-well cell culture plates were suspended in a bath of pre-heated water such that the underside was completely submerged (with no



(a) Small transducer.

(b) Large transducers.

Figure 8.2.2: Ultrasonic treatment set-up with clamped transducers.

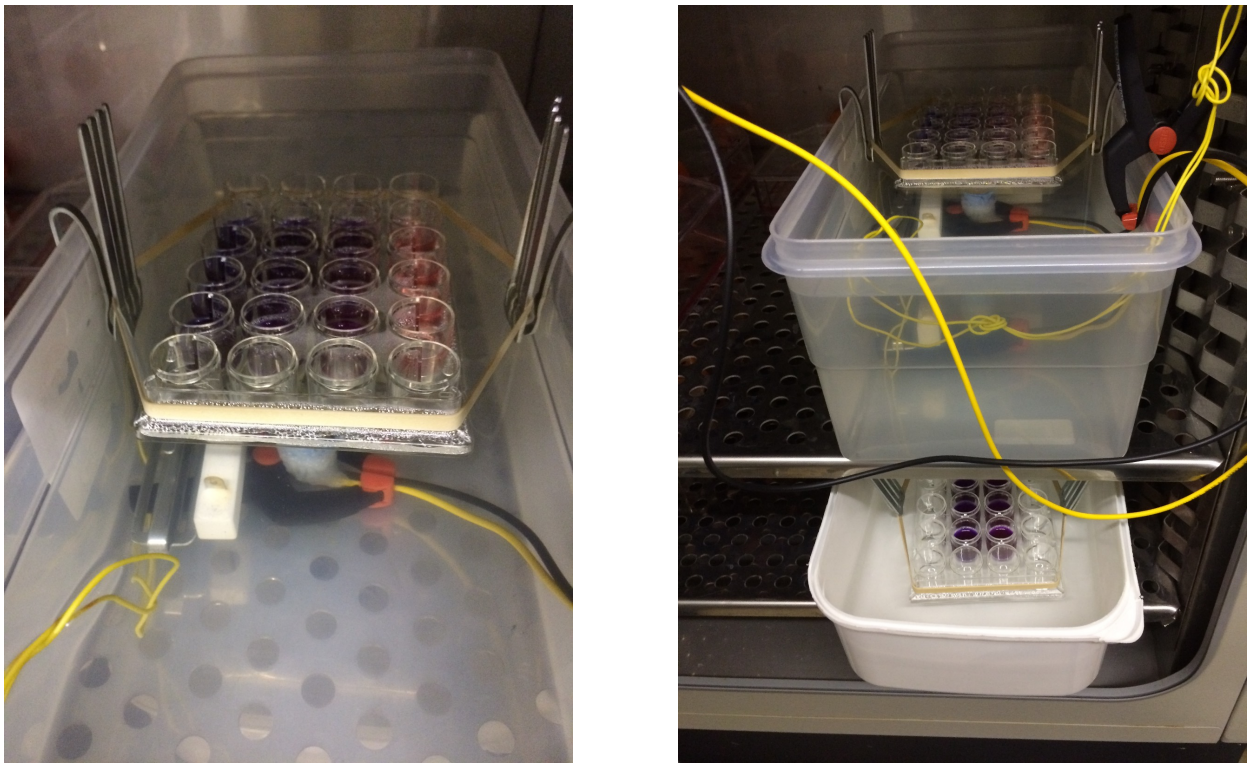
bubbles), but the well-openings were above the water level. This was implemented using standard curtain hooks, which connected to the sides of the water bath, and an elastic band which was wrapped around the cell culture plate and connected to the hooks on either side. The transducers delivering the ultrasound were placed in the water-bath which helped to cool them and circumvented the coupling issues mentioned previously. This set-up is depicted in Figure 8.2.3.

It was found that the distance between the transducers and the cell culture plate made very little difference to the intensity of the ultrasound in the wells of the cell culture plate. Therefore, the transducers were left at the bottom of the water-bath instead of being clamped to the cell culture plate, as they previously were. This had the added benefit of allowing more of the cell culture plate to be subjected to the ultrasound due to the spreading-out of the pressure waves as they travelled through the water.

The pressures inside the water-bath, and inside of the wells of the cell culture plates, were measured using an omnidirectional hydrophone (Onda HGL-0200 with Onda AH-2010 pre-amplifier) which was connected to an oscilloscope (Tektronix DPO4034) through a DC power supply (Onda AH-2010-DCBNS).

Another advantage of using a water-bath is that the acoustic impedances of water, poly-styrene (of which the cell culture plate was composed) and biological materials, are all fairly similar [59, 60]. This helps decrease the reflections at the change of interfaces, thereby allowing for a larger proportion of the initial wave intensity to reach the cell layer.

At their resonant frequency, the transducers had their impedances electrically matched to $50\,\Omega$, which was the output impedance of the signal generators and amplifiers. This allowed for maximum power transfer to the transducer to occur. The transducers were all capacitive



(a) Close-up view.

(b) Full view.

Figure 8.2.3: Ultrasonic treatment set-up in a water-bath.

in nature, and so the matching was performed by adding an inductance (using a custom-made inductor) to cancel out the capacitive impedance, before transforming the new, real impedance to 50 Ω (using a custom-made transformer). This matching was performed with the aid of a Vector Network Analyser (Rohde & Schwarz ZND).

The treatment signals used 100 cycles of the resonant frequency at a duty-cycle of 0.1. This low duty-cycle was used to ensure that the transducers didn't overheat. From this, the Pulse Repetition Frequency (PRF) of the signal was calculated, and the signal was loaded onto an Arbitrary Function Generator to be repeated at this PRF. Short ramp-functions were used to ramp the signal up to its full magnitude at the start of the "on" period, and to ramp it down to its zero magnitude at the start of the "off" period.

As an example of the PRF calculation, consider a transducer with a resonant frequency of 100 kHz. The period of this frequency is 10 μs and so the "on" period, consisting of 100 cycles, has a period of 1 ms. For a duty cycle of 0.1, the "off" period is nine times longer than the "on" period and so the total period of the signal is 10 ms. The PRF is calculated as the inverse of this total period, which evaluates to 100 Hz.

With the cooling provided by the water-bath, the voltages applied to the transducers could

be large without risking them heating up significantly. Voltages of up to $400\,V_{p-p}$ were applied to the large, 60 W transducers depicted in Figure 8.2.1. These transducers had a resonant frequency of 120 kHz and so were driven at a PRF of 120 Hz. This PRF is in the audible range and could be heard as a low humming-sound originating from the transducers.

8.3 Preliminary results

The results from the preliminary ultrasonic experiments were indeterminate, with some of the experiments demonstrating an inhibition of proliferation for the ultrasonically treated cells, but with other experiments demonstrating the opposite effect. The lack of repeatability in the experimental results meant that no conclusions could be drawn from them, and the results were hence deemed to be indeterminate.

8.4 Discussion

The causes that rendered the results to be indeterminate are unknown. A possible complication that was identified with the ultrasonic treatment is that the propagation of the ultrasonic waves was directed perpendicularly to the culture surface, meaning that the cells were subjected to waves which travelled along the axes of their height. This was different to the implementation of the electric field treatment, where the direction of the electric field was parallel with the culture surface. Logically, it makes sense that the cells would divide in the direction parallel to the culture surface, instead of perpendicular to it, as this parallel orientation would require less energy.

A possible means of avoiding this complication would be to use 3D cultures, in which the axes of mitosis are expected to be more randomly orientated in all three dimensions. A resazurin-based dye has previously been used successfully on 3D cultures [61], and so the same quantification technique presented in Section 4.3.2 could be used if experiments using 3D cultures were to be performed.

Another concern is that, because the electric field treatment takes advantage of a rotational resonance but the ultrasonic treatment takes advantage of a translational resonance, the resonant frequencies that cause the disruption of mitosis may be different. The resonant frequency of the rotational system would be a function of a moment of inertia whereas the resonant frequency of the translational system would be a function of a mass.

It is proposed, however, that any imperfection or misalignment of the intracellular structures would cause some component of the rotational resonance to be present, even when stimulated by a translational, planar wave.

Chapter 9

Discussion

Although some discussion is provided in previous chapters, this chapter contains additional discourse in key aspects of the research. Firstly, Section 9.1 examines whether the research aim and objectives were met. The complications that were encountered with the set-up are then detailed in Section 9.2, followed by a scrutiny of the methodology and results in Section 9.3. Finally, a description of possible extensions for the research is provided in Section 9.4.

9.1 Research aim and objectives

In Section 1.2.3, it was stated that the objectives of the research were to:

- Treat a cell-line with single-frequency TTF treatment at the optimal treatment-frequency for that cell-line
- Treat the same cell-line with a comparable form of broadband TTF treatment
- Compare the results obtained using these two treatment techniques

All of these objectives were achieved, and their validations are discussed briefly below.

It must be emphasized that the MCF-7 cell-line was chosen because its optimal treatment-frequency had been identified as 150 kHz [48]. Therefore, the single-frequency TTF treatment performed in this research was at the optimal treatment-frequency for the cell-line used in this research. This confirms that the first objective was achieved. Broadband TTF treatment was performed on the same MCF-7 cell-line, using the same electric field intensity per frequency as was used in the single-frequency treatment. This confirms that the second objective

was achieved. Lastly, the results from these two experiments were compared and discussed, thereby meeting the criteria of the final objective.

In Section 1.2.2, the research question was stated as:

> "Can the efficacy of TTF treatment be improved by using broadband electric fields?"

The results of this research showed that treatment using broadband electric fields did not significantly and repeatably improve the efficacy of TTF treatment. However, it must be emphasised that this was only shown to be true for the MCF-7 cell-line and only with the specific voltages used.

9.2 Complications with the experimental set-up

Although the set-up was carefully designed, various issues with it were exposed in the experimental process. The parts that were 3D-printed underwent several re-designs to overcome these problems, the most serious of which was getting the system to seal properly. With wires running through the system it proved to be impossible to obtain a good seal with the original gaskets. This lead to the creation of the customised gasket which was thicker, wider and made from a softer silicone than the original one. This improved gasket allowed for a larger contact surface with the glass slide and allowed for more compression around the wires.

However, slow leaks were still evident, even with the improved gasket. As the wires contacted the flat glass slide tangentially, small spaces on either side of the tangential contact remained. It seemed that the slow leaking was due to fluid running out along the underside of the wires, in these small spaces. This issue was solved by using a small amount of petroleum jelly on the gasket to seal off these spaces.

Another issue that was identified was that the wires seemed to stretch slightly over time and didn't remain parallel to each other due to this stretching. Although the wires could be re-tightened, a simpler solution was to raise the glass slide slightly in order to force the wires to be taught. This was one of the functions of the cotton-wool cushion that was placed between the glass slide and the Slide Platform. With this adjustment, experiments could be repeated without the set-up requiring any significant preparation.

It was also mentioned in Section 6.1.3 that insulation tape was used to separate wires of different polarities that lay on top of each other. This was introduced after an electrical fault occurred due to insulation defects and the leaking of a well: the conductive cell culture

medium electrically connected a defect in the insulation of one of the wires with a defect in the insulation of another wire with opposite polarity. In this incident, the wires were delivering broadband treatment at over 100 V and the electrical fault caused the wires to heat up and melt a portion of the 3D-printed parts, before burning out. All of the cells in the vicinity of these wires were found to be dead, most likely due to the overheating of the cell culture medium, and the results for that experiment were deemed to be invalid.

9.3 Scrutiny of the methodology and results

It was known that there would be natural variation with the cells and that this variation would result in measurement uncertainty. However, as seen in Section 7.3, the calculations required to determine the results from the resazurin-based assay greatly exacerbated the uncertainty. The use of a different assay that didn't have this intrinsic flaw should have been investigated. Additionally, other quantification techniques could have been used to confirm the proliferations results. Possible techniques include Trypan Blue cell counting methods, metabolic assays, protein assays, morphological analyses, and the use of molecular probes.

Another method of lowering the uncertainty would have been to average the raw data (for each series separately) across experiment sets. It follows on that, if several more experiment sets were performed, a large number of measurements could have been averaged together which could have been used to further lower the uncertainties. However, it must be emphasised that this averaging must be performed on raw data, before any calculations are performed.

It was thought that the efficacy of the treatment delivered using 8-wires would be vastly superior to the treatment delivered using 2-wires. As seen in Chapter 7, this was not the case. The motivation behind the belief that the 8-wire set-up would be superior was based on the fact that it provided a more consistent distribution of the electric field intensity across the culture surface, thereby allowing for a larger proportion of the cells to be subjected to electric field intensities above the therapeutic threshold.

Another criticism of the experimentation is that treatment was performed for only 24 hours, even though MCF-7 cells are reported to have a doubling time of 29 hours. Although a large proportion of the cells would have attempted to undergo mitosis after 24 hours, more accurate treatment results could have been obtained if the cells were subjected to longer treatment periods.

In the initial *in vitro* experiments performed by Kirson *et al.* [8], all of the cell-lines, except for one, had doubling times of less than 24 hours, which was also the treatment period that they used. It should also be noted that the "therapeutic enhancement ratio" calculated from their results ranged from approximately 30 % to 100 %, whereas, in this research, the same

metric never exceeded 21 %. In fact, for several of the treatments, this metric was reversed, implying a stimulation of cell proliferation instead of the expected inhibition. The source of this discrepancy is unknown but it is suspected that may be related to the mismatch between the treatment period and the doubling time of the MCF-7 cells.

In a 2007 publication by Kirson *et al.* [18], treatment efficacies (equivalent to the "therapeutic enhancement ratio" mentioned previously) of between 70 % and 90 % were observed after 24 hours of treatment at optimal frequencies. Although, the cell-lines used were different to that used in this research, it should be noted though that the cell-line that required the highest intensity electric field was a breast cancer cell-line (MDA-MB-231) [18]. The electric fields were also switched between two perpendicular directions, which was claimed to have improved the treatment efficacy by 20 % for some of the cell-lines used [18].

In a 2009 publication by Kirson *et al.* [7], treatment efficacies of around 50 % were observed, even with the switching of the electric fields. However, in these 24-hour experiments, a lower field intensity of 1.75 V/cm was used [7].

This insight leads to another possible explanation for the poor treatment efficacies observed in this research: despite the simulations and calculations performed, the voltages used may have been too low to generate the electric field intensities required to inhibit cell proliferation. This is a likely scenario given that neither the single-frequency, nor the broadband treatment generated results that differed significantly and repeatably from the controls. This theory may also explain why there was no significant difference between treatment delivered using 2-wires and 8-wires: if the electric field intensity was too low, it would not have made a difference how well distributed the intensity was across the culture surface.

With this in mind, it would have been useful to repeat the experiments using higher voltages to see if greater treatment efficacies could have been achieved. If an improvement was observed, this would have indicated a flaw in the simulations and analytical calculations that were used to predict the electric field intensities from the applied voltages.

A final criticism for the experiments is that the optimal treatment-frequency for the MCF-7 cell-line was not confirmed in this research. The assumption that the frequency of 150 kHz was optimal was based purely on the research by other authors. However, even cells from the same cell-line may behave differently under different conditions, and so this confirmation of the optimal treatment-frequency should have been performed.

9.4 Extensions

One of the concerns with broadband TTF treatment is that the treatment band may overlap with the sensitivity band of normal cells of the same tissue-type. Although the scope of

this research didn't allow for the characterisation of this possible overlap, it is an important concern that requires additional research.

Another concern was that, for *in vivo* treatment, the higher voltages required for broadband treatment may prove to be dangerous. For this *in vivo* treatment, the high-voltage electrodes would need to be fully insulated in order to deliver the electric fields, and so under normal operation, the high voltages would pose no concern to health and safety. However, defects in the insulation could result in harm if no current-limiting circuitry is implemented. Other possible methods of lowering the voltages required for broadband treatment include using a different amplitude distribution for the treatment band (for example, a Gaussian distribution), and using fewer frequencies in the treatment band. Both of these methods could significantly lower the voltages required, possibly without sacrificing any of the treatment efficacy.

Although in this research broadband treatment didn't yield increased treatment efficacies for the MCF-7 cell-line, there is reason to believe that broadband treatment may result in increased treatment efficacies with other cell-lines. This is supported by the fact that Kirson *et al.* showed that the B16F1 and F-98 cell-lines were each sensitive to their own band of frequencies [8]. The ability to characterise the frequency-sensitivity of cell-lines easily and quickly, would be extremely useful for broadband treatment. Although this characterisation was performed manually by Kirson *et al.* (through full experiments at each frequency), it may be possible to characterise the frequency-sensitivity using much faster impedance techniques. If there is some form of resonance occurring in the cell at a frequency where it is sensitive to the electric fields, there should be an impedance change around that frequency. It is hypothesised that if this change can be detected, a simple impedance-sweep of the cells may be enough characterise their frequency-sensitivity.

It was shown by Zhao *et al.* that a small DC electric field with a magnitude of $1.5\,\mathrm{V/cm}$ orientates the axis of mitosis [23]. It was also shown by Kirson *et al.* that TTF treatment is vastly more effective when mitosis is orientated such that the cleavage axis is aligned with the direction of the electric field. Therefore, it is proposed that it may be possible to align the axes of mitosis by using a superimposed DC field on the TTFs, thereby further increasing the treatment efficacy. Both of the above-mentioned studies were performed in *in vitro* environments, however, this proposed extension could possibly be applied in *in vivo* environments too.

Although the results from the preliminary ultrasonic experiments were indeterminate, it is believed that therapy using ultrasound is still plausible. In addition, it is interesting to note that the current state-of-the-art systems being used to deliver TTF treatment make use of high-permittivity ceramic insulators, such as lead magnesium niobate-lead titanate (PMN-PT) [42]. These ceramic insulators are piezoelectric in nature, implying that they may in fact be generating ultrasound, albeit at a low intensity.

Chapter 10

Conclusions and Future Work

10.1 Conclusions

The background and theory behind TTF treatment was investigated and it was found that the concept of using a customised, low-impedance experimental set-up to perform broadband TTF treatment in an *in vitro* environment was viable. Therefore, an experimental set-up of this nature was designed, simulated, constructed and used to implement broadband TTF treatment on cells cultured from the MCF-7 cell-line.

The results showed that, with the voltages used, there were no significant and repeatable differences between the broadband treatment and the optimal single-frequency TTF treatment. However, as the results from both the single-frequency and broadband treatment were similar to those of the untreated controls, it is suspected that the voltages used were too low to generate the electric field intensities required to inhibit the proliferation of the MCF-7 cells.

10.2 Recommendations for future work

There is much scope for future work derived from this dissertation, including:

- Repeating the experiments with higher voltages
- Repeating the experiments and averaging the raw data across experiments to lower the uncertainties
- Repeating the experiments with other cancer cell-lines

- Characterising the frequency-sensitivity for each cancer cell-line and comparing it to the frequency-sensitivity for normal cells of the same tissue type
- Determining the optimal amplitude distribution for the frequency band to be used in treatment
- Determining whether the broadband treatment is effective in 3D cultures and in *in vivo* environments
- Improving the experimental set-up so that it can be standardised and used by other researchers
- Determining whether profiles of frequency-sensitivity can be characterised using impedance-sweeps
- Determining whether improved treatment efficacy can be obtained by aligning the mitotic axes using a small DC electric field
- Determining whether similar results can be achieved with treatment that uses ultrasound instead of electric fields

References

[1] GBD 2015 Mortality and Causes of Death Collaborators, "Global, regional, and national life expectancy, all-cause mortality, and cause-specific mortality for 249 causes of death, 1980-2015: a systematic analysis for the Global Burden of Disease Study 2015," *Lancet*, vol. 388, no. 10053, pp. 1459–1544, Oct 2016.

[2] C. D. Mathers and D. Loncar, "Projections of global mortality and burden of disease from 2002 to 2030," *PLoS Medicine*, vol. 3, no. 11, pp. 2011–2030, Nov 2006.

[3] GBD 2015 Disease and Injury Incidence and Prevalence Collaborators, "Global, regional, and national incidence, prevalence, and years lived with disability for 310 diseases and injuries, 1990-2015: a systematic analysis for the Global Burden of Disease Study 2015," *Lancet*, vol. 388, no. 10053, pp. 1545–1602, Oct 2016.

[4] F. Bray and B. Møller, "Predicting the future burden of cancer," *Nature Reviews Cancer*, vol. 6, no. 1, pp. 63–74, Jan 2006.

[5] A. M. Davies, U. Weinberg and Y. Palti, "Tumor treating fields: a new frontier in cancer therapy," *Annals of the New York Academy of Sciences*, vol. 1291, pp. 86–95, Jul 2013.

[6] R. Stupp et al., "NovoTTF-100A versus physician's choice chemotherapy in recurrent glioblastoma: a randomised phase III trial of a novel treatment modality," *European Journal of Cancer*, vol. 48, no. 14, pp. 2192–2202, Sep 2012.

[7] E. D. Kirson et al., "Chemotherapeutic treatment efficacy and sensitivity are increased by adjuvant alternating electric fields (TTFields)," *BMC Medical Physics*, vol. 9, no. 1, pp. 1–13, Jan 2009.

[8] E. D. Kirson et al., "Disruption of cancer cell replication by alternating electric fields," *Cancer Research*, vol. 64, no. 9, pp. 3288–3295, May 2004.

[9] P. H. Gutin and E. T. Wong, "Noninvasive application of alternating electric fields in glioblastoma: a fourth cancer treatment modality," in *American Society of Clinical Oncology 2012 Educational Book* (R. Govindan, ed.), pp. 126–131, American Society of Clinical Oncology, Jun 2012.

[10] M. Pless et al., "A phase I/II trial of Tumor Treating Fields (TTFields) therapy in combination with pemetrexed for advanced non-small cell lung cancer," *Lung cancer*, vol. 81, no. 3, pp. 445–50, Sep 2013.

[11] R. Stupp et al., "Maintenance therapy with tumor-treating fields plus temozolomide vs temozolomide alone for glioblastoma: a randomized clinical trial," *Journal of the American Medical Association*, vol. 314, no. 23, pp. 2535–2543, Dec 2015.

[12] E. Hondroulis et al., "Electrical field manipulation of cancer cell behavior monitored by whole cell biosensing device," *Biomedical Microdevices*, vol. 15, no. 4, pp. 657–663, Aug 2013.

[13] C. Gabriel, S. Gabriel and E. Corthout, "The dielectric properties of biological tissues: I. Literature survey," *Physics in Medicine and Biology*, vol. 41, no. 11, pp. 2231–2249, Nov 1996.

[14] B. Alberts et al., *Molecular Biology of the Cell*, ch. 8, 18, pp. 440–444, 524, 539, 1021. Garland Science, 6th ed., 2015.

[15] R. A. Serway and J. W. Jewett (Jr), *Physics for Scientists and Engineers with Modern Physics*, ch. 18, 26, 35, pp. 564–565, 810–816, 1109–1111. Brooks/Cole – Thomson Learning, 6th ed., 2004.

[16] N. A. Campbell and J. B. Reece, *Biology*, ch. 12, pp. 218–235. Benjamin Cummings, 7th ed., 2005.

[17] J. A. Tuszynski et al., "An overview of sub-cellular mechanisms involved in the action of TTFields," *International Journal of Environmental Research and Public Health*, vol. 13, no. 11, pp. 1–23, Nov 2016.

[18] E. D. Kirson et al., "Alternating electric fields arrest cell proliferation in animal tumor models and human brain tumors," *Proceedings of the National Academy of Sciences of the United States of America*, vol. 104, no. 24, pp. 10152–10157, Jun 2007.

[19] I. Ermolina et al., "Study of normal and malignant white blood cells by time domain dielectric spectroscopy," *IEEE Transactions on Dielectrics and Electrical Insulation*, vol. 8, no. 2, pp. 253–261, Apr 2001.

[20] V. Gowri Sree, K. Udayakumar and R. Sundararajan, "Electric field-mediated inactivation of tumor cells," in *Electrostatics Joint Conference*, (Boston), pp. 1–7, Jun 2009.

[21] A. Bajaj et al., "Detection and differentiation of normal, cancerous, and metastatic cells using nanoparticle-polymer sensor arrays," *Proc. Nail. Acad. Sci. USA*, vol. 106, no. 27, pp. 10912–10916, Jul 2009.

[22] C. Wenger et al., "Modeling Tumor Treating Fields (TTFields) application in single cells during metaphase and telophase," in *Proceedings of the Annual International Conference of the IEEE Engineering in Medicine and Biology Society, EMBC*, (Milan), pp. 6892–6895, Nov 2015.

[23] M. Zhao, J. V. Forrester and C. D. McCaig, "A small , physiological electric field orients cell division," *Proceedings of the National Academy of Sciences of the United States of America*, vol. 96, no. 9, pp. 4942–4946, Apr 1999.

[24] E. Wang et al., "Physiological electric fields control the G1/S phase cell cycle checkpoint to inhibit endothelial cell proliferation," *The FASEB journal: official publication of the Federation of American Societies for Experimental Biology*, vol. 17, no. 3, pp. 458–460, Jan 2003.

[25] D. K. Cheng, *Field and Wave Electromagnetics*, ch. 3, 5, 6, 7, pp. 77, 87–110, 203, 225–226, 307–308, 341–345. Addison-Wesley, 2nd ed., 1989.

[26] A. L. S. Chang et al., "Rejuvenation of gene expression pattern of aged human skin by broadband light treatment: a pilot study," *The Journal of Investigative Dermatology*, vol. 133, no. 2, pp. 394–402, Feb 2013.

[27] B. P. Lathi, *Signal Processing and Linear Systems*, ch. 4, 5, 8, pp. 245–252, 290–296, 338–343, 546. Oxford University Press, int. ed., 2010.

[28] S. W. Smith, *The Scientist and Engineer's Guide to Digital Signal Processing*, ch. 9, 11, 17, pp. 172–173, 212–215, 307–310. California Technical Publishing, 2nd ed., 1999.

[29] C. Waymouth, "Cell, tissue, and organ culture," in *Biology of the Laboratory Mouse* (E. L. Green, ed.), ch. 25, pp. 493–510, McGraw-Hill, 2nd ed., 1966.

[30] H. R. Chang et al., "Improving gastric cancer preclinical studies using diverse in vitro and in vivo model systems," *BMC Cancer*, vol. 16, no. 200, pp. 1–13, Mar 2016.

[31] U.S. Food and Drug Administration. 2018. "The drug development process — step 3: clinical research." [ONLINE] Available at: `http://www.fda.gov/ForPatients/Approvals/Drugs/ucm405622.htm#Clinical_Research_Phase_Studies`. [Accessed 2018-02-25].

[32] American Type Culture Collection (ATCC). 2016. "Cell lines." [ONLINE] Available at: `https://www.lgcstandards-atcc.org/Products/Cells_and_Microorganisms/Cell_Lines.aspx`. [Accessed 2018-02-25].

[33] T. L. Brown et al., *Chemistry the Central Science*, ch. 14, p. 581. Pearson Education, 10th ed., 2006.

[34] G. S. Sittampalam et al. 2004. "Assay Guidance Manual." [ONLINE] Available at: https://www.ncbi.nlm.nih.gov/books/NBK53196/pdf/Bookshelf_NBK53196.pdf. [Accessed 2018-02-25].

[35] T. A. Trumbo et al., "Applied spectrophotometry: analysis of a biochemical mixture," *Biochemistry and Molecular Biology Education*, vol. 41, no. 4, pp. 242–250, Jul 2013.

[36] J. O'Brien et al., "Investigation of the Alamar Blue (resazurin) fluorescent dye for the assessment of mammalian cell cytotoxicity," *European Journal of Biochemistry*, vol. 267, no. 17, pp. 5421–5426, Sep 2000.

[37] Bio-Rad Laboratories. 2016. "alamarBlue Technical Datasheet." [ONLINE] Available at: https://www.bio-rad-antibodies.com/static/uploads/ifu/buf012a.pdf. [Accessed 2018-02-25].

[38] H. A. Haus and J. R. Melcher, "Introduction to Electroquasistatics and Magnetoquasistatics," in *Electromagnetic Fields and Energy*, ch. 3, pp. 1–22, Massachusetts Institute of Technology: MIT OpenCourseWare, 1989.

[39] G. S. Smith and J. D. Nordgard, "Measurement of the electrical constitutive parameters of materials using antennas," *IEEE Transactions on Antennas and Propagation*, vol. 33, no. 7, pp. 783–792, Jul 1985.

[40] A. Walzl et al., "A simple and cost efficient method to avoid unequal evaporation in cellular screening assays, which restores cellular metabolic activity," *International Journal of Applied Science of Technology*, vol. 2, no. 6, pp. 17–22, Jun 2012.

[41] A. Pavesi et al., "Engineering a 3D microfluidic culture platform for tumor-treating field application," *Scientific Reports*, vol. 6, no. 26584, pp. 1–10, May 2016.

[42] Y. Porat et al., "Determining the optimal inhibitory frequency for cancerous cells using Tumor Treating Fields (TTFields)," *Journal of Visualized Experiments*, no. 123, pp. 1–8, May 2017.

[43] P. P. Banada et al., "Performance evaluation of a low conductive growth medium (LCGM) for growth of healthy and stressed Listeria monocytogenes and other common bacterial species," *International Journal of Food Microbiology*, vol. 111, no. 1, pp. 12–20, Aug 2006.

[44] S. V. Puttaswamy et al., "Enhanced cell viability and cell adhesion using low conductivity medium for negative dielectrophoretic cell patterning," *Biotechnology Journal*, vol. 5, no. 10, pp. 1005–1015, Oct 2010.

[45] American Type Culture Collection. "MCF7 (ATCC HTB-22)." [ONLINE] Available at: https://www.atcc.org/products/all/HTB-22.aspx. [Accessed 2018-02-25].

[46] N. Gera et al., "Tumor treating fields perturb the localization of septins and cause aberrant mitotic exit," *PLoS ONE*, vol. 10, no. 5, pp. 1–20, May 2015.

[47] R. S. Schneiderman et al., "TTFields alone and in combination with chemotherapeutic agents effectively reduce the viability of MDR cell sub-lines that over-express ABC transporters," *BMC cancer*, vol. 10, no. 229, pp. 1–7, May 2010.

[48] M. Giladi et al., "Mitotic spindle disruption by alternating electric fields leads to improper chromosome segregation and mitotic catastrophe in cancer cells," *Scientific reports*, vol. 5, no. 18046, pp. 1–16, Dec 2015.

[49] I. A. Cree, *Cancer Cell Culture Methods and Protocols*, ch. 19-21, pp. 219–258. Humana Press, 2nd ed., 2011.

[50] S. N. Rampersad, "Multiple applications of alamar blue as an indicator of metabolic function and cellular health in cell viability bioassays," *Sensors*, vol. 12, no. 9, pp. 12347–12360, Sep 2012.

[51] R. Horobin, "The problem of proprietary dyes, with special reference to alamar blue, a proprietary dye revealed," *Biotechnic & Histochemistry*, vol. 76, no. 4, pp. 163–164, Jul 2001.

[52] R. C. Borra et al., "A simple method to measure cell viability in proliferation and cytotoxicity assays," *Brazilian Oral Research*, vol. 23, no. 3, pp. 255–262, Jul 2009.

[53] R. T. Pace and K. J. L. Burg, "Toxic effects of resazurin on cell cultures," *Cytotechnology*, vol. 67, no. 1, pp. 13–17, Jan 2015.

[54] H. Chandra et al., "Glutamine synthetase encoded by glnA-1 is necessary for cell wall resistance and pathogenicity of Mycobacterium bovis," *Microbiology*, vol. 156, no. 12, pp. 3669–3677, Dec 2010.

[55] O. Al-Bataineh, J. Jenne and P. Huber, "Clinical and future applications of high intensity focused ultrasound in cancer," *Cancer Treatment Reviews*, vol. 38, no. 5, pp. 346–353, Aug 2012.

[56] J. Tang, C. Guha and W. A. Tomé, "Biological effects induced by non-thermal ultrasound and implications for cancer therapy: a review of the current literature," *Technology in Cancer Research and Treatment*, vol. 14, no. 2, pp. 221–235, Apr 2015.

[57] J. Škorpíková et al., "Changes in microtubules and microfilaments due to a combined effect of ultrasound and cytostatics in HeLa cells," *Folia Biologica (Praha)*, vol. 47, no. 4, pp. 143–147, Feb 2001.

[58] Y. Naruse, "Mechanical vibration model for chromosomes in metaphase of mitosis and possible application to the interruption of cell division," *BioSystems*, vol. 66, no. 1, pp. 55–63, Jun 2002.

[59] H. Azhari, "Appendix A: typical acoustic properties of tissues," in *Basics of Biomedical Ultrasound for Engineers*, pp. 313–314, John Wiley & Sons, Inc., 2010.

[60] J. Lochab and V. R. Singh, "Acoustic behaviour of plastics for medical applications," *Indian Journal of Pure and Applied Physics*, vol. 42, no. 8, pp. 595–599, Aug 2004.

[61] F. Bonnier et al., "Cell viability assessment using the Alamar blue assay: a comparison of 2D and 3D cell culture models," *Toxicology in Vitro*, vol. 29, no. 1, pp. 124–131, Feb 2015.